Ecole Polytechnique de l'Université de Nantes

Civil Engineering Department
Campus de Gavy Océanis

Boulevard de l'Université,
44600 Saint-Nazaire
France

Université catholique de Louvain (UCL)
Ecole Polytechnique de Louvain

Institute of Mechanics, Materials and Civil Engineering (iMMC);
Pôle Génie Civil et Environnement (GCE)
Place du Levant 1, Vinci Building
1348 Louvain-la-Neuve
Belgium

CONTRIBUTION TO THE DYNAMIC CHARACTERIZATION OF ROCK USING AN INSTRUMENTED DROP-WEIGHT TEST SYSTEM

IMPACT COMPRESSIVE STRENGTH OF ROCK

A Report Presented to the Engineering School

of

University of Nantes (Polytech Nantes)

In Partial Fulfillment of the Requirement for the Degree of Engineering Diploma in Civil Engineering

By

Mustafa Jafari

Supervised by:

Professor Alain Holeyman

08/2016

Table of Contents

Acknowledgements

First of all, I would like to thank my advisor, Professor Alain Holeyman, at Université catholique de Louvain for giving me the opportunity to follow my internship at Institute of Mechanics, Materials, and Civil Engineering (iMMC). He had the kindness to accept me in his team and guide me through my internship with advice, feedback, tips and support despite his busy schedule.

Taking this opportunity, I appreciate the valuable suggestions received from Ms. Catherine Doneux, research engineer at UCL. She helped me to get acquainted with the Instron drop-weight test system.

In addition, I am grateful to Mr. Karl Henry Victor, Mr. Sami Hamdi, Mr. Haythem Gharsallaoui who are PhD students at UCL. They helped me through my internship period so that I could integrate in the best possible way with the new environment. Their kind suggestions and help together with their sense of humor was an unforgettable part of my internship.

My sincere thanks also go to Mr. Fateh Bendahmane, professor at Polytech Nantes, and Mr. Ouali AMIRI, who is president of civil engineering graduate program at Polytech Nantes. I would like to thank them for helping me discover my potentials and guiding me with the process of finding a suitable internship by which I can now better set my academic and professional objectives.

I would like to thank all the fellow labmates and interns for their help. In particular, I am grateful to, Stavy Duchêne Stephane, Gorski, and Quentin Mestrez for their assistance in laboratory.

List of figures

List of tables

Abstract

In recent years, offshore wind turbines are emerging in seas. Most of offshore wind turbines are founded on monopiles, which are driven into sea bed. In such projects, soil resistance to driving (SRD) is a key technical, schedule and financial constraint in planning operations of foundation installation.

Driving pile foundations in indurated formations has become a major challenge of the industry since not much is known about their behavior to dynamic efforts. Pile driving involves high strain rates comparing to those of quasi-static strength tests. In order to characterize dynamic resistance of rock and its intrinsic response to dynamic efforts, an instrumented drop-weight test system is investigated using a synthetic rock. This testing system is usually used for puncture test on composite materials. Use of this machine for dynamic characterization of rock requires an experiment design involving a study of its applicability, some modifications to the machine in addition to developing consistent testing procedures.

Firstly, a mechanical model is developed for the impact loading of a specimen made of synthetic rock with an arbitrary geometry and dimensions behaving according to a material model proposed by European Committee for Structural Concrete (CEB 1990). This mechanical model is used to ensure that impact testing can reveal the true constitutive behavior of the specimen material. Furthermore, it is utilized to obtain the necessary impact testing parameters such as necessary striker impact velocity and mass. Next, specimen geometry is varied considering multiple scenarios in order to account for machine limitations such as available impactor masses, measurable load and striker impact velocity limits.

Impact compressive strength tests were conducted using the assumed mass-velocity combinations that would result in specimen failure if the synthetic rock behaved similar to concrete.

The obtained force time-histories were normalized by cross-sectional areas of specimens and treated with signal processing techniques such as FFT.

A linear relationship between impact strength and stress-rate is observed. The results are compared with those of CEB (1990).

The results are carefully studied from several perspectives in order to account for effects of various factors, which may lead to false interpretations. These factors include inertial effects, possible limitation of system frequency response, system ringing and equilibrium of stresses. Based on this analysis, bending resonance of test system is, primarily, suspected for resulting in sharp spikes in the signal causing higher strain rates and peaks. Besides, it is doubted if stress equilibrium is achieved since impact durations are very short.

Finally, some recommendations are made for improving the experiment design in order to avoid resonance, to ensure equilibrium of stresses and minimize the experiment errors associated with the fabrication and preparations of specimens.

Presentation of iMMC[1]

The Institute of Mechanics, Materials, and Civil Engineering (iMMC) at the Louvain School of Engineering (EPL) of the Université catholique de Louvain (UCL) is a leading international center for research in engineering. It is located in Louvain-la-Neuve, Belgium.

Its core strengths span several of the major engineering disciplines, and are grouped into five inter-related topics:

- Energy, thermodynamics, and chemical engineering
- Mechatronics and biomechanics
- Processing, materials, assembly, and structures
- Fluid mechanics, environmental engineering, and geomechanics
- Numerical and computational methods

The institute has five divisions that are:

- Génie civil et environnemental (GCE)
- Materials and process engineering (IMAP)
- Mechatronic, electrical energy, and dynamic systems (MEED), formerly: Mechatronics (MCTR)
- Applied mechanics and mathematics (MEMA)
- Thermodynamics and fluid mechanics (TFL)

The Civil Engineering and Environmental Division addresses different research areas as hydraulic sectors, soil mechanics, rock mechanics and structural engineering.

Basic research in hydraulics is part of the more general themes of land and control of natural hazards for the well-being and safety of people. The theme is especially flood control especially in the case of sudden events: Breaking dike or dam. The flood waves are studied both in from a hydrodynamic perspective as well as their sedimentary aspects.

The soil/rock mechanics research elaborates the study of the thermo-hydro-mechanical behavior of natural and artificial materials under various loads and monitoring their damage through non-destructive techniques. The fundamental theme in the field of geodynamics is the change in behavior of soil under cyclic and dynamic loads. The application related to this fundamental theme is the dynamic behavior of foundations under extreme solicitations. The fundamental theme in the field of geo-environment is that of kinetic dispersion of contaminants dissolved in the soil. The application related to this fundamental theme is the in situ remediation of contaminated subsurface environments.

The research in structural engineering is oriented toward in multiple directions in collaboration with the LEMSC laboratory which has many facilities and testing machines of all sizes. Their research focuses on the optimization of structures, behavior of concrete bridge deck of bowstring type, reinforced concrete structures subjected to significant fatigue efforts (wind turbine foundations), characterization of the wood material elements and tensegrity structures.

[1] https://www.uclouvain.be/en-immc.html

Introduction

1.1 Context

Climate change, threatening the present and future of humanity, has led the world to acknowledge the urgent need for renewable energy resources for the sake of reconciliation with the great forces of nature.

By 2030, 20-31% of European Union electricity demand is expected to be fulfilled by wind energy. Out of which, 25% is approximated to be the share of offshore wind turbines (OWT) (European wind energy association). In the meantime, the prospect of offshore wind farm markets seems promising owing to higher turbine capacity, shorter tower and stronger wind in the sea as long as economic and reliable substructures and foundation are ensured. Figure 1 depicts an offshore wind turbine with its components.

Figure 1, Wind Turbine system components

Nevertheless, foundation Installation in indurated formations such as rock, cemented layers and etc. has become one of the recent challenges of the industry about which not much is known. The majority of offshore wind turbines are founded on monopiles (driven into sea bed) imputable to their ease in transportation, construction and on-site quality control. Monopile foundation can have a diameter up to 8 meters and a thickness up to 60 mm (Board, 2011).

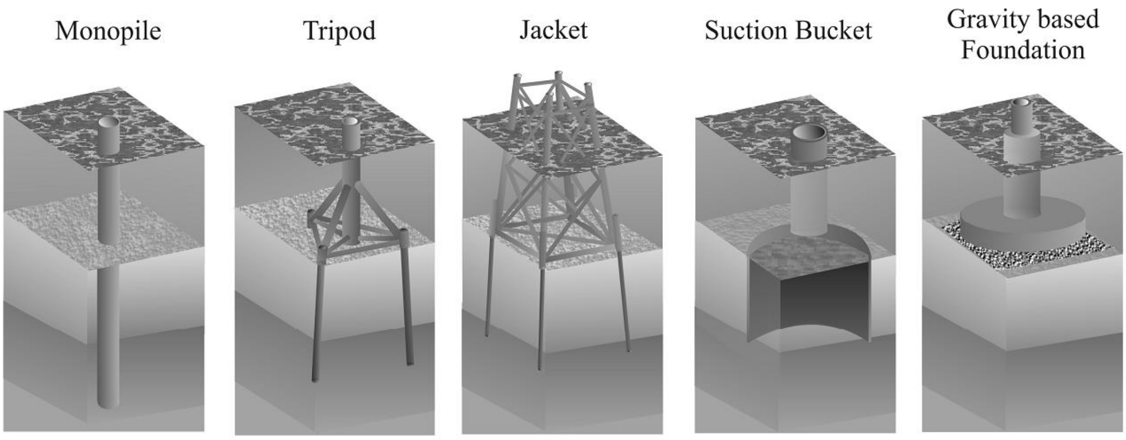

Figure 2, Foundation concepts for offshore wind energy converters

Pile premature refusal and collapse during installation are the troubles associated with pile driving in indurated formations ascribable to high uncertainty in predicting soil resistance to driving (SRD)(Aldridge et al., 2010).

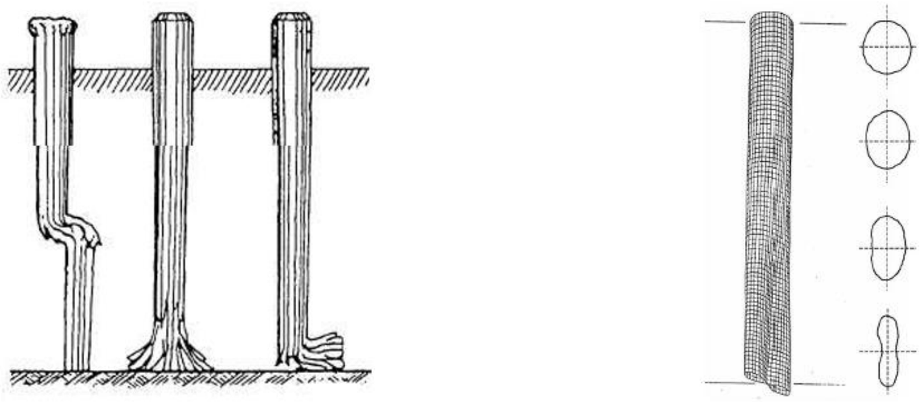

Figure 3 Pile refusal and collapse details

To illustrate the complexity of the task, it is noteworthy that monopiles are driven to depths up to 30 m by hydraulic hammers with impact energy of equivalent to 180 ton falling through 1.7 m. The installation and services vessels carry up to 500,000 gallons of diesel to fuel driving operations (Board, 2011).

This end-of-studies project contributes to characterization of indurated formations, which is necessary for estimating soil resistance to driving (SRD).

1.2 Research significance

Dynamic resistance of rock has recently become a subject of interest in pipe pile driving in off-shore foundation systems. The objective of this study is to contribute to enhancement of the understanding the dynamic properties of rock by employing an instrumented drop-weight test system. The applicability of such a testing system and strain rate dependency of the compressive strength of a synthetic rock are investigated.

1.3 Outline of study

In an attempt to shed light on the behavior of rocks at high strain rates, experiments are designed and conducted to measure the uniaxial impact compressive strength of rock.

First, some insight is gained into mechanical behavior of rock and available material models.

Second, a literature review of experimental techniques for different strain regimes is performed. Then, drop-weight test systems are investigated together with common problems and difficulties. Similar literature concerning explosive safety and impact response of concrete structures, which involve dynamic testing of concrete prove of great help for this purpose.

Third, the experiment is designed. The objective is to find out the optimal specimen dimensions, impactor mass and striker impact velocity. For this purpose, impact loading is characterized. Then, the specimen resistance is approximated by a material model proposed by European Committee for Structural Concrete (CEB, 1990). Knowing the evolution of impact stresses and specimen resistance, appropriate mass and velocity combinations, and specimen geometry were selected.

Fourth, impact tests are performed in laboratory with Instron drop-weight impact machine (Model HV 2500) based on the designed mass-velocity combinations. Similarly, quasi-static tests are performed in order to obtain quasi-static properties of materials.

Fifth, the obtained results are treated with signal processing techniques such as Fast Fourier Transform (FFT) in order to remove noise. The stress time-history and stress-strain diagrams are studied in order to observe probable strain rate effects. In order to ensure validity of the obtained results, various sources of noise and their probable effects are investigated.

Finally, some recommendations are made for improving the experiment design for future experiments.

In the text, dynamic strength and impact strength are used interchangeably.

Mechanical behavior of rock

Dynamic resistance of rock has recently become subject of interest in pipe pile driving in off-shore foundation installations. The strain rates encountered in pile driving in rocks ranges from 1 s^{-1} to as high as 100 s^{-1} (Hamdi and others, 2016). It is a known fact that the rock strength increases as the loading rate/strain rate increases (Lajtai et al., 1991). Similar behavior is observed in concrete-like materials (Grote et al., 2001).

The cause of strength enhancement at high strain rates is highly debated. Numerous attempts have been made in order to elucidate the dynamic behavior of rock and concrete-like materials.

Some consider it as an inherent material property originating from viscoelasticity, time dependent nature of crack growth, interaction of induced tensile micro-cracks while others attribute it to inertial and frictional effects due to specimen geometry and testing system limitations respectively.

(Cho et al., 2003) have stated, based on experiments and their numerical model that the increase in dynamic tensile strength of rocks is due to generation of crack arrests and depends on homogeneity of the rock mass. (Cotsovos and Pavlović, 2008)) have concluded that that the apparent gain in dynamic strength of concrete specimens at high strain rates is due to their inertia by comparing results from a finite element model (various mass distributions and DOF) and data from previous experiments i.e. the quasi-static strength of concrete suffice for its characterization if inertia effects are well incorporated in any model.

(joo Kim et al., 2010) performed a numerical simulation of Split Hopkinson Pressure Bar (SHPB) technique for concrete under compression using pressure-independent and pressure dependent constitutive material models (J2 and Drucker-Prager), which didn't account for rate-enhancement. His numerical simulation results matched with those of SHPB technique. He finally concluded that strength increase associated with strain rate, strongly but not fully, relies on the confinement introduced due to ends friction and lateral inertial effects of the specimen.

This strength enhancement asks for a plausible model taking into account strain rate sensitivity which can have a significant impact on the mechanical behavior of a material. Figure 4 and Figure 5 depict dynamic behavior of a high strength mortar tested in SHPB Test under different strain rates (Grote et al., 2001).

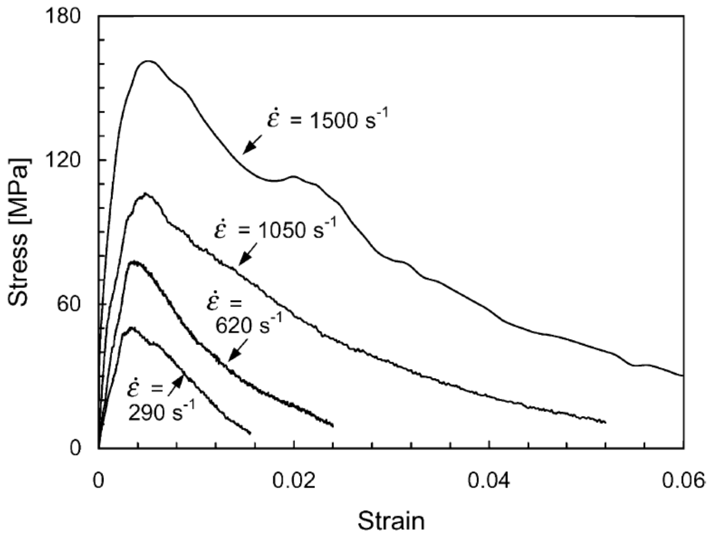

Figure 4, (a) Stress-strain behavior of mortar at different strain rates (Grote et al., 2001)

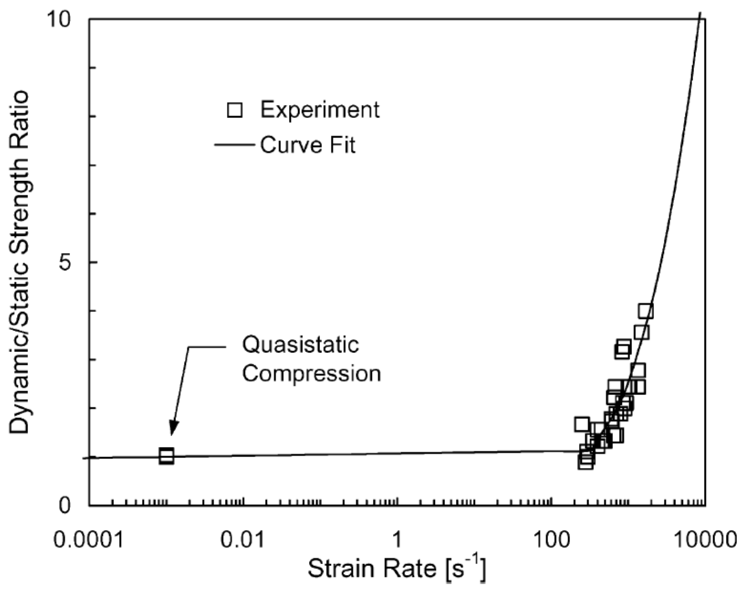

Figure 5, Strain rate dependency of the compressive strength of mortar (Grote et al., 2001)

In order to describe load carrying capacity of material under different stress conditions, several failure theories are used considering material properties.

For ductile materials, maximum-shearing-stress criterion (Tresca) and maximum-distortion-energy criterion (von Mises criterion) are used.

However, Mohr's criterion is used for brittle materials owing to their different compressive and tensile strengths.

An extension of Mohr's criterion is usually used in soil mechanics as Mohr-Coulomb failure criterion, for which the key input parameters are soil internal angle of friction, and cohesion.

Efforts to adapt Mohr-Coulomb failure criterion to rock masses has led to Hoek-Brown failure criterion. Hoek-Brown criterion (Hoek and Marinos, 2007) is a commonly accepted material model for behavior of rock under quasi-static loading. It establishes a non-linear relationship between the major and minor effective principal stresses through input parameters of geological strength index (GSI) and a material constant. The failure envelope corresponds to the stress state, where maximum principal stress in reached.

$$\sigma_1' = \sigma_3' + \sigma_{ci}\left(m_b \frac{\sigma_3'}{\sigma_{ci}} + s\right)^a$$

where m_b is a reduced value of the intact rock parameter m_i, which also depends on the Geological Strength Index (GSI) and the Disturbance Factor (D).

$$m_b = m_i \exp(\frac{GSI - 100}{28 - 14D})$$

s and a are auxiliary material constants for the rock mass, that can be expressed as:

$$s = \exp\left(\frac{GSI - 100}{9 - 3D}\right), \qquad s = 1\ for\ intact\ rock$$

$$a = \frac{1}{2} + \frac{1}{6}\left[\exp\left(-\frac{GSI}{15}\right) - \exp\left(-\frac{20}{3}\right)\right]$$

σ_{ci} is the uniaxial compressive strength of the intact rock material (defined as a positive value). From this value, the uniaxial compressive strength of the specified rock under consideration, σ_c can be obtained by setting $\sigma_3' = 0$:

$$\sigma_c = \sigma_{ci}\, s^a$$

The tensile strength of the specific rock under consideration, σ_t can be obtained by setting $\sigma_1' = \sigma_3' = \sigma_t$ (Hoek showed that for brittle materials, the uniaxial tensile strength is equal to the biaxial tensile strength).

$$\sigma_t = -\frac{s}{m_b}\ \sigma_{ci}$$

Hoek-Brown failure criterion together with Mohr-Coulomb failure criterion are illustrated in Figure 6.

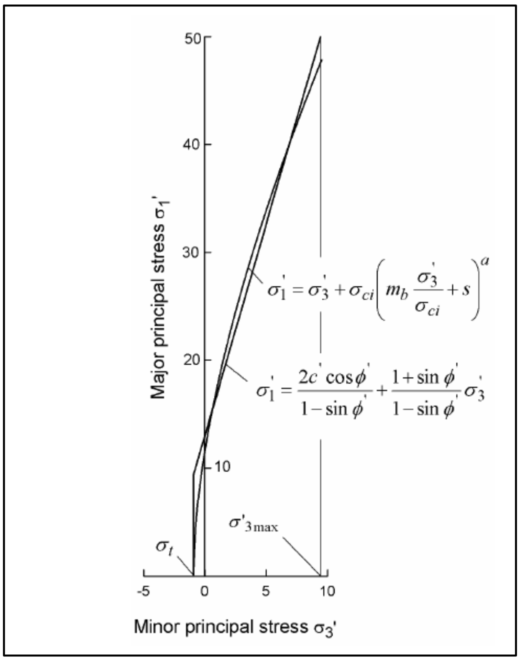

Figure 6, Hoek-Brown and Mohr-Coulomb failure criterion (Plaxis manual, 2015).

For an undisturbed intact sedimentary rock with a fine texture ($m_i = 9, GSI = 80 - 90, D = 0, \ , \sigma_{ci} = 8\ MPa$).

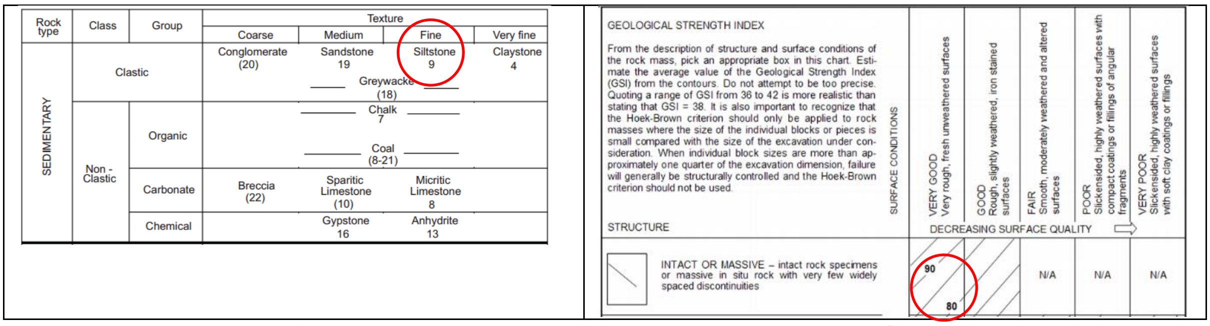

(a) (b)

Figure 7, Hoek-Brown parameters: mᵢ (a) and GSI (b) for a typical undisturbed sedimentary rock

The necessary parameters are calculated as follows:

$$s = 1$$

$$a = \frac{1}{2} + \frac{1}{6}\left[\exp\left(-\frac{GSI}{15}\right) - \exp\left(-\frac{20}{3}\right)\right] = \frac{1}{2} + \frac{1}{6}\left[\exp\left(-\frac{90}{15}\right) - \exp\left(-\frac{20}{3}\right)\right] = 0.500$$

$$m_b = m_i \exp\left(\frac{GSI - 100}{28 - 14D}\right) = 9 \exp\left(\frac{90 - 100}{28 - 0}\right) = 6.3$$

$$\sigma_1' = \sigma_3' + 8\left(6.3\,\frac{\sigma_3'}{8} + 1\right)^{0.5} \rightarrow \sigma_1' = \sigma_3' + 8 * (0.78\,\sigma_3' + 1)^{0.5}$$

Hoek et al. (2002) emphasize that Hoek-Brown failure criterion should be applied to rock masses where the size of the individual blocks or pieces is small compared with the size of the excavation under consideration. When individual block sizes are more than approximately one quarter of the excavation dimension, failure will generally be structurally controlled and the Hoek-Brown criterion should not be used.

It is noteworthy that all these material models do not incorporate loading rate effects and their input parameters are obtained through quasi-static loading tests. Quasi-static uniaxial compressive and tensile strengths can be measured according to ISRM 1979a and ISRM 1978c respectively.

Experimental techniques for low to high strain regimes

Different types of experiments exist for observing behavior of materials at various strain regimes starting from quasi-static to very high strain rates.

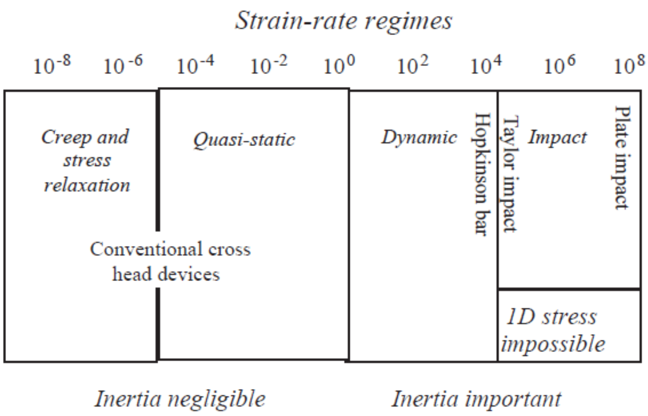

Figure 8, Strain rate regimes [s^{-1}] and techniques developed for obtaining them (Field et al., 2004)

At high strain rates, inertial effects, mechanical resonance in specimen and the apparatus can be important (Meyers, 1994). Split Hopkinson Pressure Bar (SHPB) test is used for dynamic characterization for strain rates 10^0 to 10^3 s^{-1} as depicted in Figure 8. It is usually the preferred choice of researchers. However, its dimensions (directly related to specimen cross section) renders it difficult to have in laboratories.

Initially developed for measuring energy absorption of materials, instrumented drop-weight impact machines have turned to be valuable devices in dynamic characterization of materials such as composites because of their ease of use. These two testing systems are briefly presented in the following sections.

3.1 Split Hopkinson pressure bar test (Kolsky bar test)

In SHPB test system, the specimen is sandwiched between two interfaces, which move relative to each other and squeeze the specimen. The specimen fails before release waves can reflect from the far ends of the interfaces.

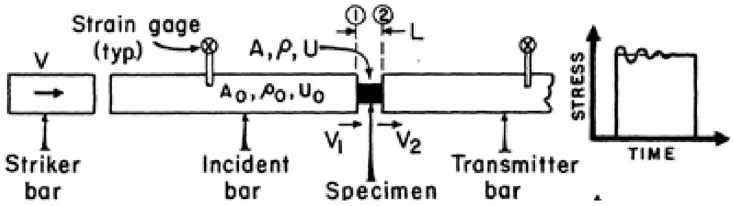

Figure 9, Split Hopkinson pressure bar for ductile material with stress pulse shape (Meyers, 1994)

$$\dot{\varepsilon} = \frac{d\epsilon}{dt} = \frac{V_1(t) - V_2(2)}{L} = \frac{C_0}{L}\,(\,\varepsilon_I - \,\varepsilon_R - \,\varepsilon_T), \qquad \varepsilon = \int_0^t \dot{\varepsilon}\; dt$$

$$\sigma = \frac{P_1(t) + P_2(t)}{2A} = \frac{A_0E_0\,(\,\varepsilon_I + \,\varepsilon_R) - A_0E_0\,(\,\varepsilon_T)}{2A}$$

Where

$\dot{\varepsilon}$: strain rate of the specimen

ε: strain of the specimen

$V_1(t) - V_2(2)$: relative velocity of the incident and transmitter bar interfaces with specimen

$\varepsilon_I, \varepsilon_R, \varepsilon_T$: incident, reflected and transmitted strains measured by strain gauges placed on the incident and transmitter bar.

σ: stress in the specimen, measured by averaging the end forces P1 and P2 in the incident bar and transmitter bar respectively divided by cross-sectional area of specimen (A).

E_0A_0: axial stiffness of the incident and transmitter bar

3.2 Drop-weight impact test

In these testing systems, an adjustable falling weight (drop-weight) can be dropped from a controllable height or fired with the assistance of springs in order to attain a desired impact energy (Figure 10).

The impact velocity is measured through a flag placed on the falling weight passing thorough photo-diode emitter/detector assemblies. The specimen is clamped to a base or placed on a platen which supports the specimen during impact.

The falling weight is equipped with an instrumented striker (tup). The striker contains a force transducer that is the heart of the machine, and measures the variation of impact force between the falling weight and specimen.

One of the advantages of drop-weight impact test is that it measures force time-history from which other vital information such as deformation and energy absorption time histories of the specimen can be calculated using Newtonian mechanics without instrumenting the specimen itself. The standard way of analyzing the output of a drop-weight machine assumes the falling weight behaves as a rigid body (Field et al., 2004).

This also turns out to be a pitfall since it must be ensured that striker measurements represent the required specimen properties.

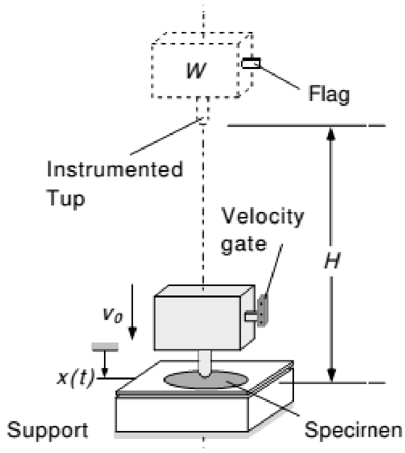

Figure 10, Example of the operation of a drop-weight impact test machine (Kessler, 2004)

The main difficulties associated with drop-weight experiments have been listed as bad reputation of accuracy related to poor signal-to-noise ratio and complexity of characterizing the loading pulse (Aymerich et al., 1970).

The force measurements of transducers attached to the falling weight can be strongly distorted. This is because the falling weight is excited below its resonant frequency. As a result, the loading time is long, being defined by the time taken to produce a net reversal of the falling weight momentum bringing it to rest or causing it to rebound. The reversal of momenta is caused by multiple wave reflections within the impactor leading to distortion of signal (Field et al., 2004).

This problem does not exist in SHPB for which specimen fails before release waves come back to the specimen, hence, leading to popularity of the experiment.

In order to obtain better measurements from drop-weight machines, it is recommended to utilize a momentum trap in the falling weight if it needs to be instrumented or design a separate force transducer placed below the specimen (Radford et al., 2003).

Swallowe and Lee (2003) used a momentum trap in their drop-weight system depicted in Figure 11(a). It is an additional cylindrical metal piece whose height is close to half that of the falling weight. It is attached to the weight by a layer of grease and reduces the vibrations of the drop-weight results as shown in Figure 11(b).

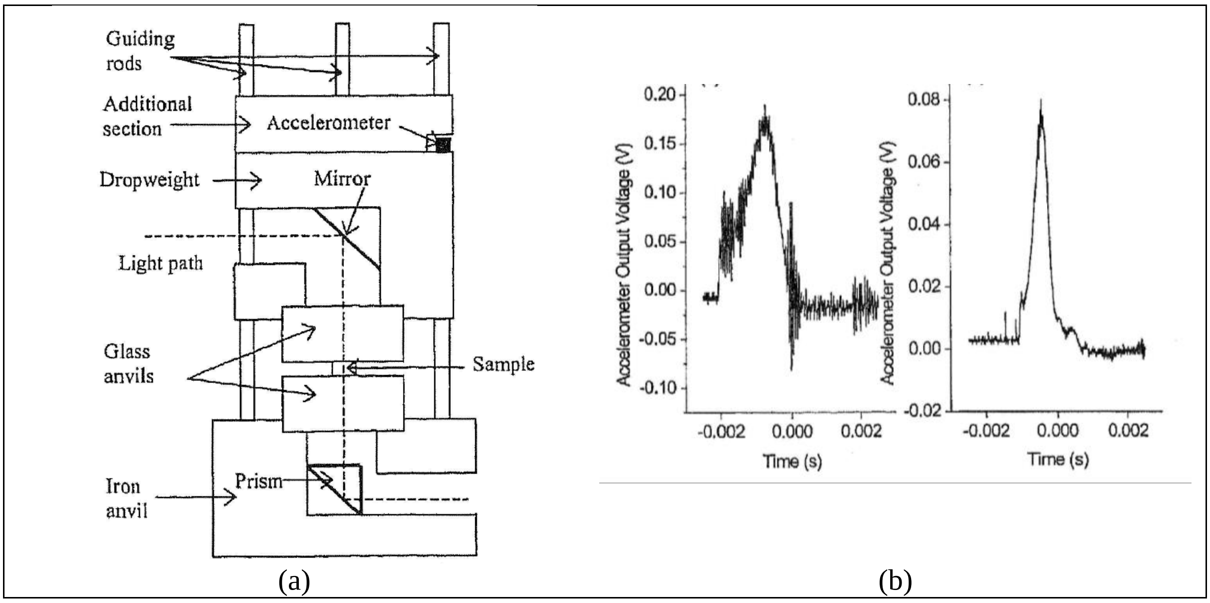

Figure 11, Use of a momentum trap in a drop-weight test system by Swallowe and Lee (2003)

Experiment design

The ensuing experiments are done for observing dynamic strength variations as a function of strain rate and the quasi-static strength.

First, an analysis of impact event has been performed in order to develop a mechanical model capable of predicting the stresses developed in the specimen due to impact loading.

Second, the rock strength at different strain rates is approximated by a concrete model code from European Committee for Structural Concrete (CEB 1990). Third, combining the evolution of stresses during impact and rock strength, possible failure points during impact were identified. Appropriate geometries, striker impact velocities and impactor masses are proposed.

4.1 Modeling of impact dynamics

Understanding the stresses developed in the specimen during the impact event is essential to interpreting drop-weight impact tests. The falling weight on the specimen can be interpreted in several ways such as:

1. treating the impact event as a one-dimensional dynamic wave propagation problem,
2. treating the impact machine and specimen as an oscillating spring mass system,
3. treating the falling weight as an accelerating and decelerating rigid body,

Each approach is elaborated in the following sections.

4.1.1 One-dimensional dynamic wave propagation analysis

Jr, Weaver et al. (1990) have presented a solution by S. Venant and J. Boussinesq for a bar of height (H) and mass (m) fixed at one end while being struck at the other free end by a mass (M). This solution addresses the problem of planar impact on a prismatic bar with parallel and smooth surface of contact via a one-dimensional wave propagation analysis. This solution approaches reality as ratio of bar height and bar wave velocity (H/C) increases.

Their solution indicates that impact ceases in the second reverberation of the stress wave in the bar when the mass ratio (μ) is equal to 1.73. Mass ratio (μ) is the ratio of the falling mass to the specimen mass.

A larger mass ratio ensures presence of multiple reverberations in the specimen before impact ends. Jr, Weaver et al. (1990) provide several approximate relations for calculating the maximum stress in the specimen.

$$\mu > 24 \qquad \sigma_{max} = \rho C v_0(\sqrt{\mu} + 1)$$

$$5 < \mu < 24 \qquad \sigma_{max} = \rho C v_0\left(\sqrt{\mu} + 1.1\right)$$

$$\mu < 5 \qquad \sigma_{max} = \rho C v_0(2 + 2e^{-\frac{2}{\mu}})$$

Where

ρ: $specimen\ density\ (kg/m^3)$

C: $bar\ wave\ velocity\ (m/s)$

v_0: $impact\ velocity\ (m/s)$

Let E and ρ be the bar modulus of elasticity and density respectively, the bar wave velocity will be $C = \sqrt{E/\rho}$. Then, the number of stress wave reverberations in the bar during the impact is $N = C\ t_{impact}/2H$.

A quasi-static state of stress can be assumed if the impact duration is sufficiently large such that stress waves can bounce back and forth in the specimen (at least three reverberations). Under superposition of multiple incident and reflected waves, the stress distribution will appear similar to a statically loaded specimen which means that the stress at both ends of the specimen become equal and the specimen is in stress equilibrium. In such as case, which is considered in Section 4.1.2, the specimen can be treated as a light spring which is struck by a heavy mass M.

4.1.2 Quasi-static approximation of impact loading

As discussed earlier, drop-weight test has the advantage of providing information about properties of impacted material by an instrumented striker, which measures the excitation force without instrumenting the specimen itself. *Therefore, it is vital to make sure that striker measurement (excitation force) represents the force developed in the specimen.*

The falling weight and specimen can be assumed as an oscillating SDOF system under the conditions discussed in Section 4.1.1. The response of this mass-spring system to an impact loading has two parts: (1) transient response and (2) steady state response.

In order to evaluate transient response of system, shock spectrum (response spectrum) is used. Shock spectrum is a plot of the maximum response of a SDOF for a specified excitation (kx_{max}/F_0) as a function of a non-dimensional time ratio (t_0/T).

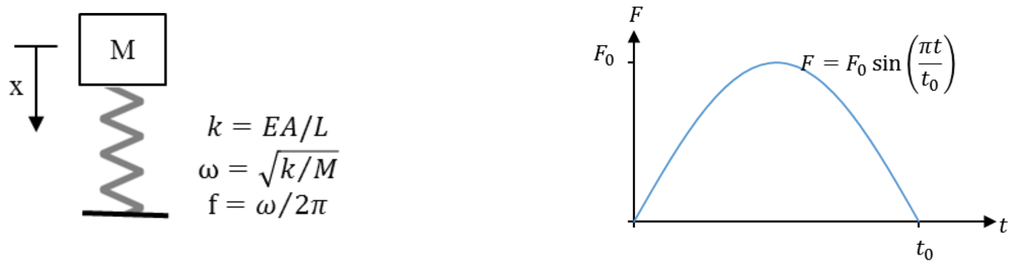

(a) (b)

Figure 12, (a) Single Degree of Freedom System for modeling impact dynamics and (b) half sine excitation pulse

Maximum value of the force developed in the SDOF system (kx_{max}) divided by the maximum of the excitation force (F_0) is plotted against the ratio of the duration of impact (t_0) divided by the natural period of SDOF system (T). Impact excitation can be modelled as sinusoidal pulse as shown in Figure 12. For impact durations greater than 3 times the natural period of the SDOF system, the force developed in the SDOF system is very close to the excitation force. This approximation improves with presence of a slight amount of damping as shown in Figure 13.

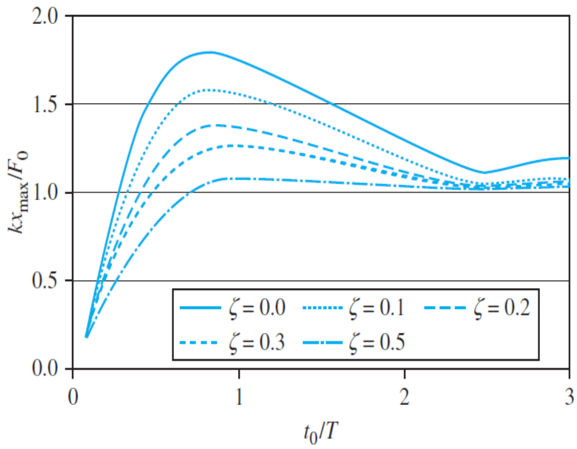

Figure 13, Response spectrum of SDOF system to a sinusoidal pulse (Kelly, 2012)

A quasi-static state of stress in the specimen means that the force in the specimen is at all times equal to the applied force (striker measurement). Figure 14 depicts the time response of a SDOF system to a half sine pulse excitation for different ratios of impact duration (t0) and system period (T). The time responses are plotted according to relations provided in Harris's handbook of vibrations (Harris and Piersol, 2002) as detailed below:

$$F = F_0 \frac{\sin \pi t}{t_0}$$

$$kx_{max} = \frac{F_0}{1 - T^2/4t_0^2} \left(\frac{\sin \pi t}{t_0} - \frac{T}{2t_0} sin\omega_n t\right) \qquad 0 \le t \le t_0$$

$$F = 0$$

$$kx_{max} = F_0 \frac{(T/t_0)\cos(\pi t_0/T)}{(T^2/4t_0^2) - 1} \sin \omega_n \left(t - \frac{t_0}{2}\right) \qquad t_0 \le t$$

Therefore, a quasi-static analysis can be applied to an impact event provided that the impact duration is more than three times the fundamental natural period of a structure. Lowest natural period of the specimen and natural period of impact can be obtained by the ensuing equations in which equivalent mass of specimen is equal to 1/3 of specimen mass (Reid and Zhou, 2000).

$$T_{imp} > 3\,T_n,$$

where,

$$T_n = \frac{2\pi}{\omega_n}, \qquad \omega_n \approx \sqrt{\frac{K_{structure}}{m_{eq}}}, and \qquad\qquad T_{imp} = \frac{2\pi}{\omega_i}, \qquad \omega_i \approx \sqrt{\frac{K_{structure}}{m_{eq}+M}}$$

Applying the inequality $T_{imp} > 3T_n$, one finds the minimum impactor mass for quasi-static analysis to be valid.

$$M \geq 8m_{eq} \approx 10m_{eq}$$

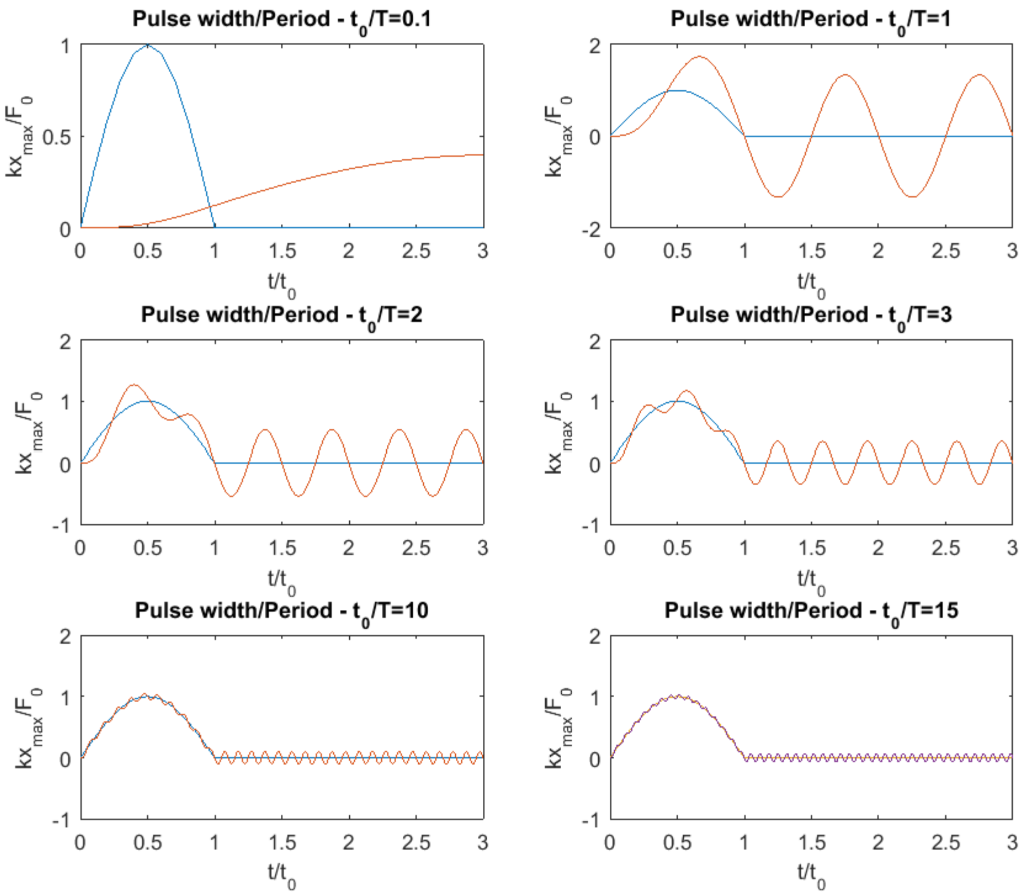

Figure 14, Time response of SDOF system (red) to a half sine pulse excitation (blue) without damping

Writing the fundamental equation of mechanics for the SDOF system in Figure 12, one obtains:

$$M\ddot{x} + \mathrm{b}\dot{x} + \mathrm{kx} = 0 \xrightarrow{b=0} M\ddot{x} + \mathrm{kx} = 0$$

$$x(t) = \frac{v_0}{\omega} sin(\omega t),$$

$\dot{x}(\omega t) = v_0 \cos(\omega t)$, $\ddot{x}(\omega t) = -v_0\omega \sin(\omega t)$, $F(\omega t) = Mv_0\omega \sin(\omega t)$

$x_{max} = \frac{v_0}{\omega}\ at\ t = t_c = \pi/2\omega$, $F_{max} = Mv_0\omega\ \ at\ t = t_c = \pi/2\omega$

$t_{imp} = 2t_c$

In order to find the maximum stress in the specimen, the maximum force (F_{max}) is divided by the specimen cross-sectional.

$$\sigma_{max} = \frac{Mv_0\omega}{A}$$

Introducing mass ratio $\mu = M/m$ and wave speed $C = \sqrt{E/\rho}$ in the maximum stress equation for comparison purposes, one would obtain:

$$\sigma_{max} = \frac{Mv_0\omega}{A} = \rho C v_0\sqrt{\mu}$$

For $\mu \geq 24$, the solution of mass-spring and Jr, Weaver et al. (1990) approximations differ less than 17%.

The strain rate of the applied loading can be calculated as striker impact velocity $\dot{x}(\omega t)$ over specimen height (H).

$$\dot{\varepsilon}(t) = \frac{\dot{x}(\omega t)}{H} = \frac{v_0}{H}\cos\omega t$$

4.1.3 Rigid body impact (Warnet and Reed, 1999)

The falling weight can be treated as rigid body which decelerates upon contact. Falling weight velocity and displacement at time t can be calculated using well-known momentum-impulse relationship in Newtonian mechanics. The falling weight can be treated as an accelerating and decelerating rigid body undergoing deformation and restitution periods as shown in Figure 15.

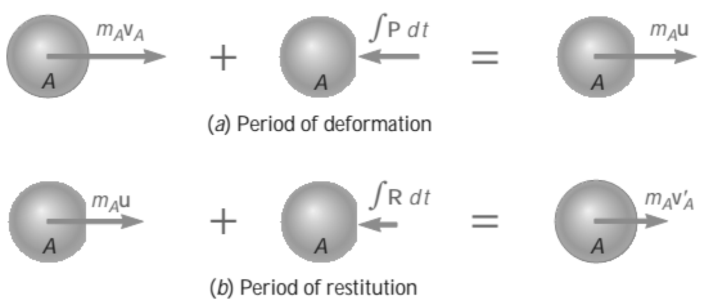

Figure 15, Deformation and restitution during an impact (Beer, 2016)

If the materials remain elastic during deformation, the impact force P(t) increases from zero to P_{max}, the striker impact velocity decreases from V_{imp} to zero as the specimen continues to deform to a maximum value. During restitution, P_{max} will decease at the same rate to zero.

However, if one of the materials yields, the impact force will decrease after the material has reached its yield point and there is little or no restitution. A rapid drop in the impact reaction rate can be expected.

The striker is connected to a force transducer which measures the impact force P(t) during the impact period. The resultant force acting on the striker is $F(t) = Mg - p(t)$, where M is the mass of the striker.

$$\frac{dp}{dt} = \boldsymbol{F(t)}$$

$$mv_f - mv_{imp} = \int_0^t \boldsymbol{F(t)}\, dt$$

$$v_f = v_{imp} + \frac{1}{m}\int_0^t \boldsymbol{F(t)}\, dt$$

$$v_f = v_{imp} + \frac{1}{m}\int_0^t [mg - P(t)]\, dt = v_{imp} + gt - \frac{1}{m}\int_0^t P(t)\, dt$$

$$v_f(t) = v_{imp} + gt - \frac{1}{m}\int_0^t P(t)\, dt\,, \qquad x(t) = v_{imp}t + \frac{1}{2}g\, t^2 - \frac{1}{m}\iint_0^t P(t)\, dt$$

Where,

$v_f(t)$: velocity of falling weight at time t

v_{imp}: velocity of falling weight upon impact

$x(t)$: displacement of falling weight at time t

Furthermore, one can calculate the strain energy (absorbed energy) at time t by applying the principal of conservation of energy to the striker from the moment it strikes the specimen.

$$V(t) + K(t) + E_a(t) = C$$

V (t): Potential energy of the striker at time t

K (t): Kinetic energy of the striker at time t

Ea (t): Strain Energy at time t

C: Constant which is $C = V(0) + K(0) + E_a(0) = 0 + \frac{1}{2}mv_{imp}^2 + 0 \ \rightarrow C = \frac{1}{2}mv_{imp}^2$

$$E_a(t) = \frac{1}{2}m\left(v^2 - v_{imp}^2\right) + mgx(t)$$

Assuming that the striker displacement equals that of the specimen vertical deformation, the strain rate equals:

$$\dot{\varepsilon}(t) = \frac{d}{dt}\left(\left(\frac{dx}{L}\right)\right) = \frac{\frac{dx}{dt}}{L} = \frac{v_f}{H}$$

, $where\ v_f$ is striker velocity at time t after impact.

4.2 Rock strength approximation for different strain rates

Since applicable data are not available regarding dynamic strength of rock at the intended strain rates, a concrete model developed by European Committee for Structural Concrete (CEB, 1990) is used assuming that our synthetic rock behaves like structural concrete.

CEB (1990) model code provides constitutive relations for stress and strain rate effects on compressive and tensile strength of concrete and the modulus of elasticity. These models are valid for normal and light weight concrete with compressive strengths starting from 12 MPa and 8 MPa respectively.

4.2.1 Impact compressive strength

CEB (1990) model provides relations for estimating the compressive strength at different strain rates by referring to a mean value of compressive strength f_{cm}.

For the synthetic rock used in this study, mean values of compressive strength are provided (Section 6.1). The relations are valid for monotonically increasing compressive strains at a range of approximately $30\,.\,10^{-6}s^{-1} < |\dot{\varepsilon}_c| < 3\,.\,10^{2}s^{-1}$.

$$DIF_{1990}^{+} = \frac{f_{c,imp}}{f_{cm}} = \begin{cases} \left(\dfrac{\dot{\varepsilon}_c}{\dot{\varepsilon}_{c0}}\right)^{1.026\alpha_s} & \dot{\varepsilon}_c \ \le 30\ s^{-1} \\ \gamma_s \left(\dfrac{\dot{\varepsilon}_c}{\dot{\varepsilon}_{c0}}\right)^{1/3} & \dot{\varepsilon}_c \ \ge 30\ s^{-1} \end{cases}$$

where

$f_{c,imp}$	= Impact compressive strength at $\dot{\varepsilon}$
f_{cm}	= Mean compressive strength at $30\,.\,10^{-6}s^{-1}$
DIF	= Compressive strength dynamic increase factor (DIF)
$\dot{\varepsilon}_c$	= Compressive strain rate in the range of $30 \times 10^{-6}$to $300\ s^{-1}$
$\dot{\varepsilon}_{c0}$	= $30 \times 10^{-6}\ s^{-1}$ (static strain rate)
$\log \gamma_s$	= $6.156\,\alpha - 2$
α_s	= $1/(5 + 9f_{cm}/f_{c0})$
f_{c0}	= 10 MPa

The compression dynamic increase factors are calculated for a synthetic rock of compressive strength of 8 MPa. Figure 16 depicts DIF from $10^{-1}s^{-1}$ to $300\ s^{-1}$. Based on CEB 1990 model code, the compressive DIF increase from 2 to 7.5 in this interval.

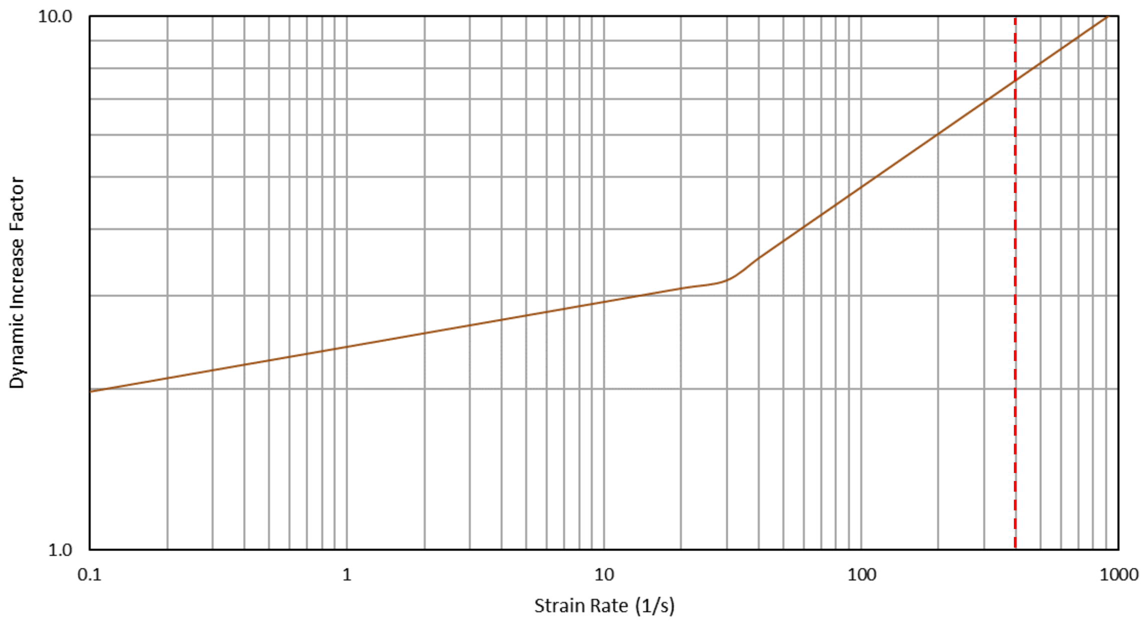

Figure 16, Dynamic increase factor versus strain rate for fcm=8 MPa (CEB, 1990)

4.2.2 Elastic modulus of elasticity

The effect of strain rate on the modulus of elasticity may be estimated by (CEB, 1990):

$$\frac{E_{c,imp}}{E_{ci}} = \left(\frac{\dot{\varepsilon}_c}{\dot{\varepsilon}_{c0}}\right)^{0.026}$$

$\dot{\varepsilon}_{c0} = 30\,.\,10^{-6}\,s^{-1}$ for compression

E_{ci}, quasi-static modulus of elasticity

$E_{c,imp}$, impact modulus of elasticity

The evolution of ratio of impact to quasi-static compressive strength against strain rate is depicted in Figure 17.

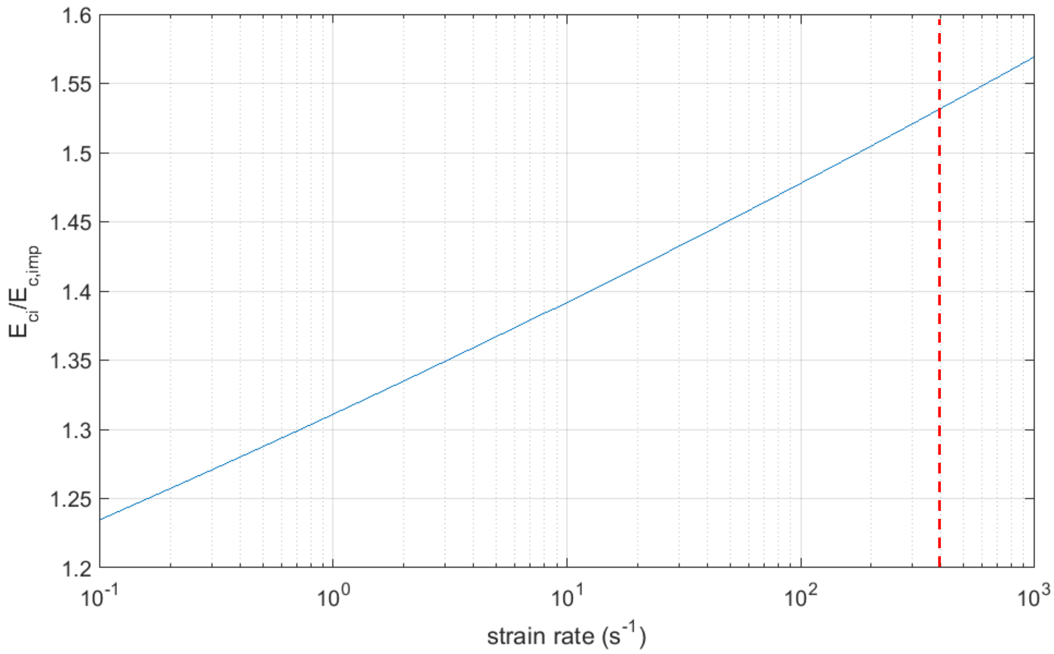

Figure 17, Evolution of ratio of impact to quasi-static modulus of elasticity with strain rate (CEB, 1990)

4.3 Experiment configuration

4.3.1 Preliminary specimen geometries and sizes

Various specimen geometries and dimensions are used for the purpose of characterizing rock or similar material such as concrete. The size and geometry of the specimen is governed by both the specimen material properties and the experimental limitations.

International Society for Rock Mechanics (ISRM) 1979a recommends a height-to-diameter ratio (H/D) of two for quasi-static tests. This H/D ratio minimizes the strength increase due to friction between specimen's end faces and the platens in the static compressive strength tests (Figure 18).

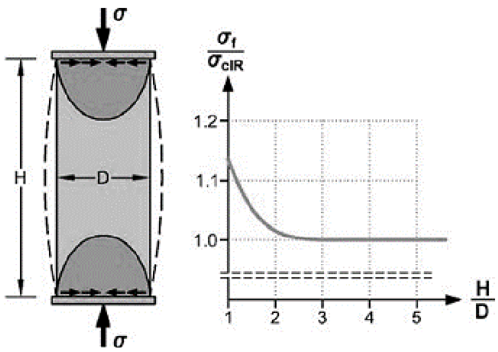

Figure 18, Influence of height-to-diameter ratio (H/D) on uniaxial compressive strength of intact rock (Wittke 1990)

For dynamic tests such as SHPB, height-to-diameters ratios (H/D) of 0.5 to 1.5 are used in order avoid inertial effects. In such cases, lubricants such as MoS_2 and lithium greases are used at the end faces of specimen (Ramesh, 2008).

Table 1 lists some geometries and their dimension used for static and dynamic strength of rock.

Table 1, Specimen geometries and dimensions used for rock compressive and tensile strength

Geometry	Type	Apparatus	Dimensions (mm)	Reference
Cylinder	Static-Compression	Servo Controlled Hydraulic Stiff Testing Compression Machine	D=29, L/D ~ 1.8-2	Prasad, 1994
Cylinder	Static-Compression	Servo Controlled Hydraulic Stiff Testing Compression Machine	D=9, L/D ~ 1.7-1.9	Prasad, 1994
Cylinder	Static-Tension	Brazilian	D=28, D/L ~ 0.3-1	Prasad, 1994
Cylinder	Dynamic-Compression	Hopkinson Pressure Bar Apparatus	D=9, L/D ~ 1.2-1.5	Prasad, 1994
Cylinder	Static and Dynamic Compression	Gear Controlled Loading System	D=29, L=60	Lajtai et al., 1991
Cylinder	Dynamic-Compression	Gear Controlled Loading System	D=54, L=110	Lajtai et al., 1991
Cylinder	Dynamic-Compression	Hopkinson Pressure Bar Apparatus	D=60, L=29-37	(Cho et al., 2003)
Cylinder	Dynamic-Tension	SHPB with Spalling phenomena: End Impact-Detonation	D=20, L=240-280	(Cho et al., 2003)

Table 2 provides specimen sizes and the apparatus used for dynamic characterization of concrete.

Table 2, Specimen geometries and dimensions used for concrete compressive and tensile strength

Geometry	Type	Apparatus	Dimensions (mm)	Reference
Cylinder	Dynamic-Tension	-	D=50, L=889	Birkimer, 1968
Cylinder	Dynamic-Tension	SHPB, Brazilian	D=19-52 L=45-51	Ross, 1995
Cylinder	Dynamic-Tension	SHPB	D=12.7, 25.4, 50.8 L=6.4, 12.7	John et al.,

Moreover, prismatic molds of size 40 mm x 40 mm x 160 mm are available at iMMC laboratory. These molds are used to cast prismatic specimen for three-point bending tests. It is possible to cut 40-mm cubes from these prismatic specimens. For higher H/D ratios, it is observed that smooth base faces cannot be ensured after cutting.

Based on the available literature and laboratory constraints, it is decided to study the possibility of using the specimen geometries and dimensions listed in Table 3. The final geometry is selected based a parametric study in Section 4.3.2.

Table 3, Preliminary specimen geometries and dimensions

Specimen Geometry #	Dimensions
Cylinder 1	D=0.06. H=0.12
Cylinder 2	D=0.05, H=0.075
Cylinder 3	D=0.05, H=0.05
Cylinder 4	D=0.04, H=0.04

Cube 1	L=0.04, W=0.04, H=0.04

4.3.2 Parametric study of dynamic model for determining test inputs

A parametric study is performed to determine optimal impactor mass (M), striker impact velocity (v0) and specimen size (A, H) so as to achieve failure of specimen at different strain rates.

A relationship should be established between the parameters of impact event and specimen strength to find the strain rate at which the impact stress exceeds the specimen dynamic strength. For given specimen dimensions (A, H), stiffness (k), impactor mass (M), and quasi-static compressive resistance (f_{cm}), it is necessary to find the strain rates for which:

$$\sigma_{imp} - f_{c,imp} = 0$$

where

$\sigma_{imp}(\dot{\varepsilon}_c, t) = \frac{M \times v_0\,(\dot{\varepsilon}_c) \times \omega\,(\dot{\varepsilon}_c)}{A} \sin(\omega t)$, impact stress developed in the specimen at time t

$f_{c,imp}(\dot{\varepsilon}_c) = \begin{cases} \left(\frac{\dot{\varepsilon}_c}{\dot{\varepsilon}_{c0}}\right)^{1.026\alpha_s}, & \dot{\varepsilon}_c \leq 30\ s^{-1} \\ \gamma_s \left(\frac{\dot{\varepsilon}_c}{\dot{\varepsilon}_{c0}}\right)^{\frac{1}{3}}, & \dot{\varepsilon}_c \geq 30\ s^{-1} \end{cases}$, impact resistance of the specimen

In order for the specimen to achieve rupture ($\sigma_{imp} = f_{c,imp}$), a failure moment should be selected before solving for failure strain rate ($\dot{\varepsilon}_c$) and calculating striker impact velocity ($v_0 = \dot{\varepsilon}_c H / cos\omega t$).

Failure moment is defined as the time when the impact stress developed in the specimen is equal to impact strength of the material, which is estimated by CEB (1990).

A failure moment of $t = \pi/2\omega$ corresponds to a striker velocity slow-down of 100% ($v = v_0 \cos(\pi/2) = 0$), thus zero strain rate ($\dot{\varepsilon}_c = v_0 \cos(\pi/2)/H = 0$) at failure. Therefore, a failure moment $0 < t < \pi/2\omega$ should be selected so as to ensure rupture of specimen at sufficient strain rates. Failure moments close to $t = \pi/2\omega$ result in high striker velocity-slow down and low strain rates while the opposite is true for those close to $t = 0$ (Figure 19).

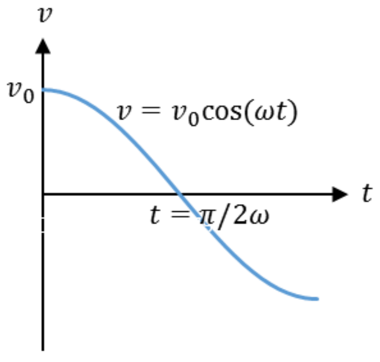

Figure 19, Striker velocity as a function of time

A typical failure moment of $t = \pi/3\omega$ corresponding to a striker velocity slow-down of 50% (non-zero strain rate) is selected and used to solve for the required strain rate at failure for a typical f_{cm}, A, H, and M. Figure 20 depicts the evolution of impact stress (σ_{imp}) and impact resistance ($f_{c,imp}$) with time.

At the very beginning of impact, the striker deforms the specimen at a higher strain rate, hence, higher impact resistance is observed. However, the impact resistance decreases as striker velocity approaches zero at $t = \pi/2\omega$. In the meantime, the impact stress increases due to the use of a SDOF system for modeling behavior of specimen. Figure 21 depicts the variations of the impact stress and the impact resistance as a function of the striker velocity.

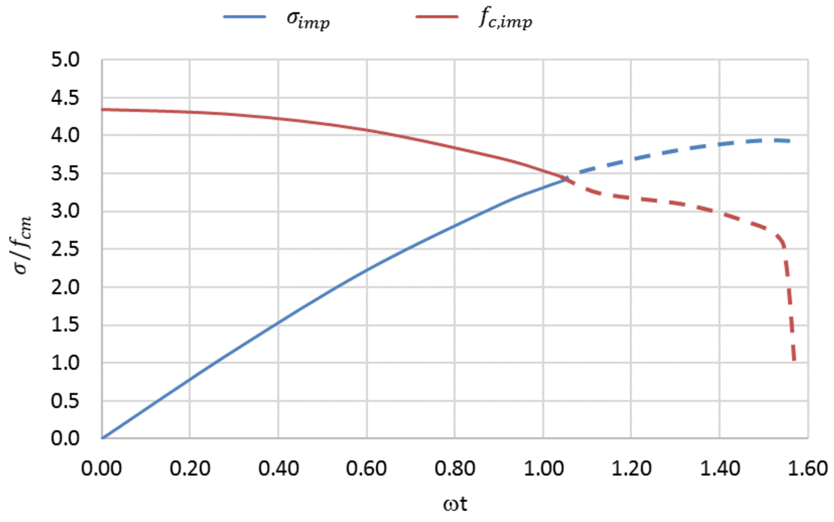

Figure 20, Variation of impact stress and impact strength with time for a typical impactor mass and striker impact velocity with failure at pi/3

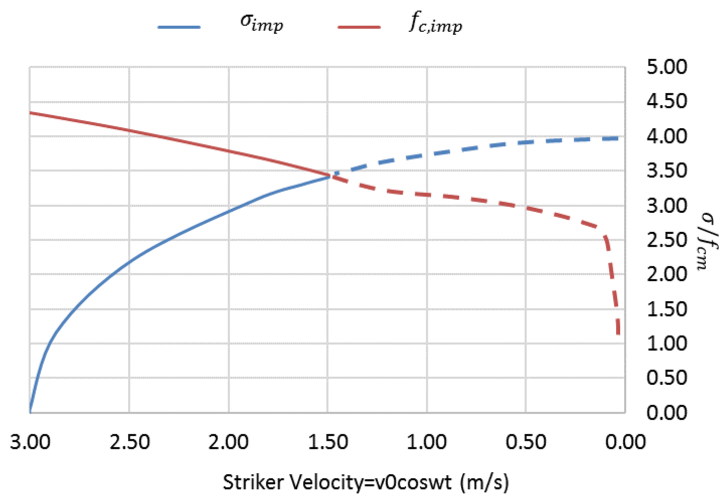

Figure 21, Variation of impact stress and dynamic strength as a function of striker velocity for a typical impactor mass and striker impact velocity for failure at pi/3

Expanding $\sigma_{imp} - f_{c,imp} = 0$, one would obtain:

$$\frac{M \times v_0\,(\dot{\varepsilon}_c)\ \times \omega\,(\dot{\varepsilon}_c)}{A}\sin(\omega t) - \begin{cases} \left(\frac{\dot{\varepsilon}_c}{\dot{\varepsilon}_{c0}}\right)^{1.026\alpha_s}, & \dot{\varepsilon}_c\ \leq 30\ s^{-1} \\ \gamma_s\left(\frac{\dot{\varepsilon}_c}{\dot{\varepsilon}_{c0}}\right)^{\frac{1}{3}}, & \dot{\varepsilon}_c\ \geq 30\ s^{-1} \end{cases} = 0$$

Where,

$$v_0(\dot{\varepsilon}_c) = \frac{\dot{\varepsilon}_c\ \times H}{\cos(\theta)}, \qquad and\ \omega(\dot{\varepsilon}_c) = \sqrt{\frac{k}{M}} = \sqrt{\frac{E_{c,imp} \times A}{M \times H}} = \sqrt{\frac{A\ E_c}{MH}\left(\frac{\dot{\varepsilon}_c}{\dot{\varepsilon}_{c0}}\right)^{0.026}}$$

Entering input parameters such as impactor mass (M), specimen area (A) height (H), modulus of elasticity (E_c) and quasi-static compressive strength (f_{cm}), one can obtain the strain rate $\dot{\varepsilon_c}$ at failure from which impact velocity, impact incident energy and impact strength can be obtained. The above equation is rewritten in terms of v_0 and solved using fsolve function in MATLAB as detailed in Appendix A.

From an energy perspective, the strain energy (absorbed energy) at the moment of failure i.e. at $t = \pi/3\omega$ is equal to the strain energy for rupture. The absorbed energy is a fraction of the incident impact energy (75 % for $t = \pi/3\omega$) at the moment of failure.

$$\frac{\mathrm{E_{absorbed}}}{\mathrm{E_{impact}}} = 75\%\ \text{for failure at}\ \theta = \pi/3$$

For the purpose of facilitating the experiment design, dynamic response of specimen for different quasi-static compressive strengths are plotted against strain rate in Figure 22. On this diagram, the dashed lines represent a parameter related to impactor mass and specimen geometry. Finding this parameter enables one to find the associated impact strength, and strain rate the diagram. This parameter is a multiplication of impactor mass by ratio of area to height of the specimen (M*H/A).

These dashed line are calculated based on the following relationship from Section 4.1.2. the stress at the moment of failure t can be calculated by:

$$\sigma_{imp}(\dot{\varepsilon}) = \frac{M \times v_0\,(\dot{\varepsilon}_c)\ \times \omega\,(\dot{\varepsilon}_c)}{A}\sin(\omega t) = \frac{M \times sin(\omega t)}{A} v_0\,(\dot{\varepsilon}_c)\ \times \omega\,(\dot{\varepsilon}_c)$$

Therefore,

$$\sigma_{imp}(\dot{\varepsilon}) = \sqrt{\frac{M \times H}{A}}\ \sqrt{\frac{E_c}{\dot{\varepsilon}_{c0}{}^{0.026}}}\tan(\omega t)\,\dot{\varepsilon_c}^{1.013}$$

As it can be seen the stress at failure is a function of strain rate and depends on the impactor mass, specimen geometry and properties.

Stress at failure is plotted against strain rate for different values of M*H/A. Now, plotting the specimen resistance (Section 4.2.1) against strain rate on the same figure, one could obtain the intersections of stress developed in the specimen and the resistance of the specimen. These intersections are, in fact, failure points.

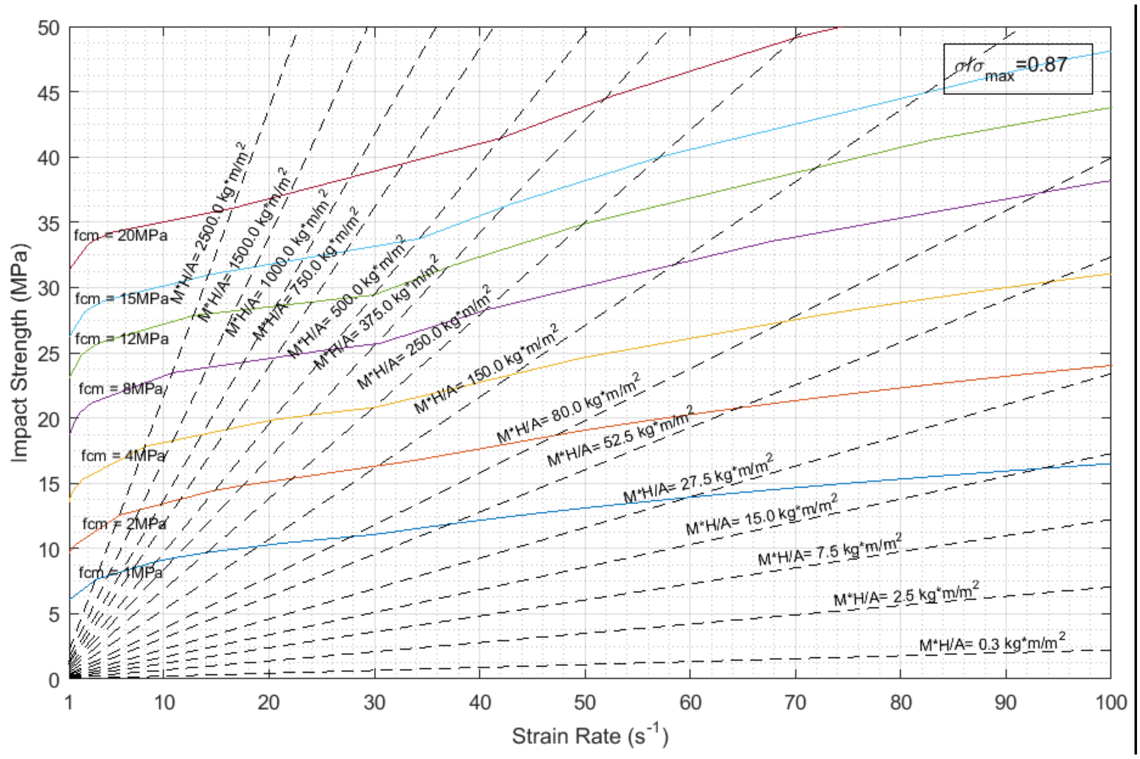

Figure 22, Impact strength for the achievable strain rates based on CEB 1990

As the diagram indicates M*H/A should decrease to achieve higher strain rates. This will lead to higher impact energies. For this purpose, multiple scenarios can be considered.

First, to achieve the maximum strain rate, the impactor mass can be decreased while increasing impact velocity. This scenario is limited due to the minimum available impact weight that is 5 kg and the maximum velocity that is 4 m/s. Furthermore, the impactor mass must be at least ten times more than the equivalent mass of the specimen in order for the quasi-static assumption to hold.

Second, the specimen height can be decreased. On one hand, this approach decreases H/D ratio and may pose difficulties with friction on the end surfaces and misleading strength enhancement. On the other hand, smaller specimen height ensures adequate reflections of the stress wave (minimum 3 times) for reaching stress equilibrium.

Third, the specimen area can be increased, which might create fabrication problems. One should bear in mind that the specimen area and quasi-static compressive strength will determine the maximum force during impact, which should be always less than 89 kN which is the striker load measurement capacity.

This parametric study has been performed in MATLAB (Appendix A) with different specimen sizes, various static compressive strengths, available impactor masses and possible impact velocities.

Assuming a compressive strength of 8 MPa for the material and impactor masses between 5 to 14 kg, Table 4 lists the achievable strain rates, necessary incident energy and peak forces for different geometries based on Figure 22. It is obvious that a cylindrical specimen would be suitable for our experiment in terms of the variables discussed earlier. However, a 40-mm cube specimen has been selected based on availability of molds and other mentioned laboratory constraints.

Table 4, Specimen geometries, their dimensions and relevant parameters based on CEB (1990)

Specimen Geometry #	*Dimensions* (m)	H/A (m/m^2)	$M*\frac{H}{A}$ (kg/m)	$\dot{\varepsilon}_{available}$ (s^{-1})	$f_{c,imp}$ (MPa)	V_imp (m/s)	*Peak Force* (kN)
Cylinder 1	D=0.06, H=0.12	42	212-594	24-48	25-32	6-12	90
Cylinder 2	D=0.05, H=0.075	38	191-534	25-50	24-30	4-8	59
Cylinder 3	D=0.05, H=0.05	25	127-357	31-70	25-34	3-7	67
Cylinder 4	D=0.04, H=0.04	32	160-446	27-55	25-32	2-4	40
Cube 1	L=0.04, W=0.04, H=0.04	25	125-350	32-72	26-34	3-6	54.4

4.3.3 Instron Dynatup drop-weight impact machine

In addition to general information provided about drop-weight impact machines, Instron Dynatup (model 9250 HV) is further presented based on its operations manual.

Instron Dynatup (model 9250 HV) has an adjustable falling weight, which can be dropped from a maximum height of 1.25 m reaching a maximum striker impact velocity of 5 m/s. Nevertheless, with spring-assisted acceleration, it can reach a maximum speed of 20.4 m/s.

The specimen is placed on a steel platen which supports the specimen during impact. The velocity measuring system uses a flag on the drop-weight to commence data acquisition and to record striker impact velocity when it passes through photo-diode emitter/detector assemblies. Instron Dynatup has an anti-bouncing system and that prevents multiple impacts on the specimen.

Instron dynatup has been calibrated in 2015[2]. Striker calibration certificate indicates that the striker force measurement accuracy meets or exceeds $\pm 3\%$ of the reading. The crosshead lifting load cell accuracy is within $\pm 2\%$.

Table 5-Table 8 provide detailed information about the specifications of the machine.

Table 5, Operational specifications for Instron drop tower impact tester (model 9250 HV)

Drop-weight Energy Range	J
Light	2.6 to 826
Medium	4.6-985
Heavy	25-1603
Striker impact velocity	**m/s**
Free fall (maximum drop height of 1.25m)	5
Free fall (minimum drop height of .05 m)	
Spring assisted acceleration	20
Drop-weight Ranges	**kg**
Light (weight set: 1x0.5kg, 2x1kg, 1x2kg, 2x5kg)	2.7-14.7
Medium (weight set increments: : 1x0.5kg, 2x1kg, 4x2kg, 3x5kg)	4.7-23.7
Heavy (weight set increments : 1x0.5kg, 2x1kg, 4x2kg, 4x5kg, 4x9kg)	24.2-80.5

[2] Instron dynatup has been calibrated in 2015. However, only calibration certificates of 2014 were accessible and could be provided during preparation of this report.

Measurement of drop-weight (Electrical with strain gauge load cell)	
Load cell full-scale Load cell maximum capacity Load cell accuracy	90.7 kg 136 kg +/- 2% of the actual load
Instrumented Striker	Hemispheric head with diameter of 16 mm and capacity of 89 kN.
Test setup and start	Test panel or PC
Status Display	Digital display of height, energy, velocity, frame status messages on PC and Test panel status lights
Drive speed	1600 mm/min
Drive speed accuracy	+/- 0.1% steady state
Velocity detector display accuracy	+/- 0.25% of the actual
Velocity accuracy	+/- 2% of the set value
Position Transducer	Optical encoder
Position accuracy	Equal or less than +/-0.02mm or +/-0.05mm of the displaced reading
Position repeatability	+/-0.015mm
Force transducer type	Strain gauge[3]

Table 6, Data acquisition for Instron drop tower impact tester (model 9250 HV)

PC control and analysis package	9250HV standard
A/D convertor resolution	12 bits per channel
Sampling rate	Up to 1.7 MHz in 7 ms (Optional 4.1 MHz in 2ms)
Data points	Standard 8192 points per channel for 2 channels Optional: simultaneous sampling of 8192 points per channel for 1, 2, or 4 channels
Bandwidth	500 kHz
Acquisition time	Standard: 7-100 ms Optional: 2-100 ms
Trigger methods	Flag with photo detector cell load trigger
Number of data channels	2 channels (optional 4 channels) Channel 1: standard striker or piezoelectric striker Channel 2: other signal source

Table 7, Shock absorbers for Instron drop tower impact tester (model 9250 HV)

Shock absorbers	Max. Velocity (m/s)	Max. Drop mass (kg)	Color code
Light weight	14	14.5	Green
Medium weight	9.5	23.6	Blue
Heavy weight	5	81.5	Red

[3] No information could be obtained from Instron manuals about the force transducer. After contacting Instron calibration office, they confirmed that the force transducer contains most likely a strain gauge. They provided a procedure to verify. The procedure is shared with the responsible of Instron Machine at UCL. No response has been obtained at the moment of preparing this report.

Super Heavy weight	8.8	81.5	Violet

Table 8, Drop tower base options (model 9250 HV)

Base Options for maximum specimen size	Width x depth x height
S1 base unit	483 mmx 508 mm x 533 mm
S2 base unit	838 mm x 686 mm x 584 mm
S3 base unit	1143 mm x 686 mm x 584
Support pedestal base height	400 mm

4.3.4 Modifications for Instron Dynatup drop-weight impact machine

Instron Dynatup has a hemispherical striker head (tup insert) used for puncture tests of composite materials. In order to distribute the impact force uniformly, a rigid cylindrical steel head (tup insert) with a flat end has been designed. This flat end will avoid application of a point load for which stress concentrations up to a depth equal to the width of specimen can be twice than that of the average stresses– Saint Venant's Principle (Beer, 2016). The details of this new tup insert are shown in Figure 23.

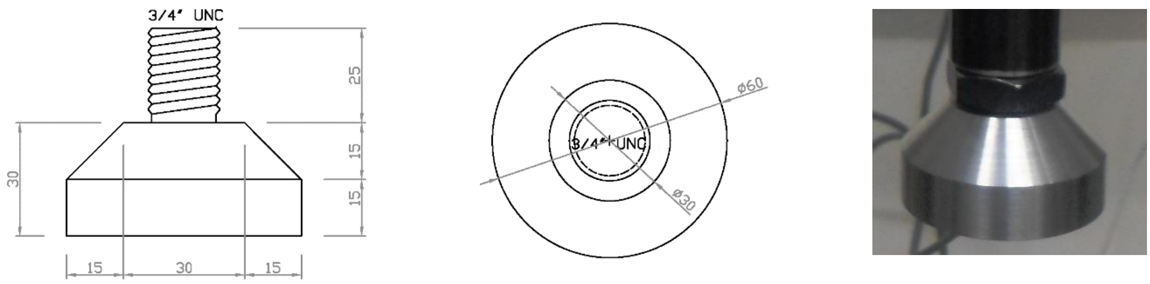

Figure 23, New striker (tup insert) details

This new striker head has a diameter of 60 mm which is large enough to cover the diameter of a cubic specimen of dimensions 40 mm x 40 mm x 40 mm. it has an estimated weight of 0.518 kg[4] and is made of high grade steel (42CrMo4). The whole weight of striker as well as its head is approximated as 1.446 kg[5]. This weight should be added to the available drop-weights starting from 2.7 to 14.7 kg, so as to obtain range of adjustable impactor masses.

Furthermore, the machine base is modified so as to accommodate a cubic specimen of 40mm x 40mm x 40mm and a future cylindrical specimen of 55 mm in diameter. The base material is ST52-3 with a thickness of 20 mm.

Metallic pins are used to prevent lateral instability of the specimen and possible damage to machine. These holding pins are placed on the impact anvil to surround the specimen without confining it tightly

[4] The mass of striker head is estimated based on density of high grade steel (7830 kg/m3) and its dimensions since it was not available for measurement at the moment of writing this report.
[5] The striker mass was measured and it was equal to 0.928 kg.

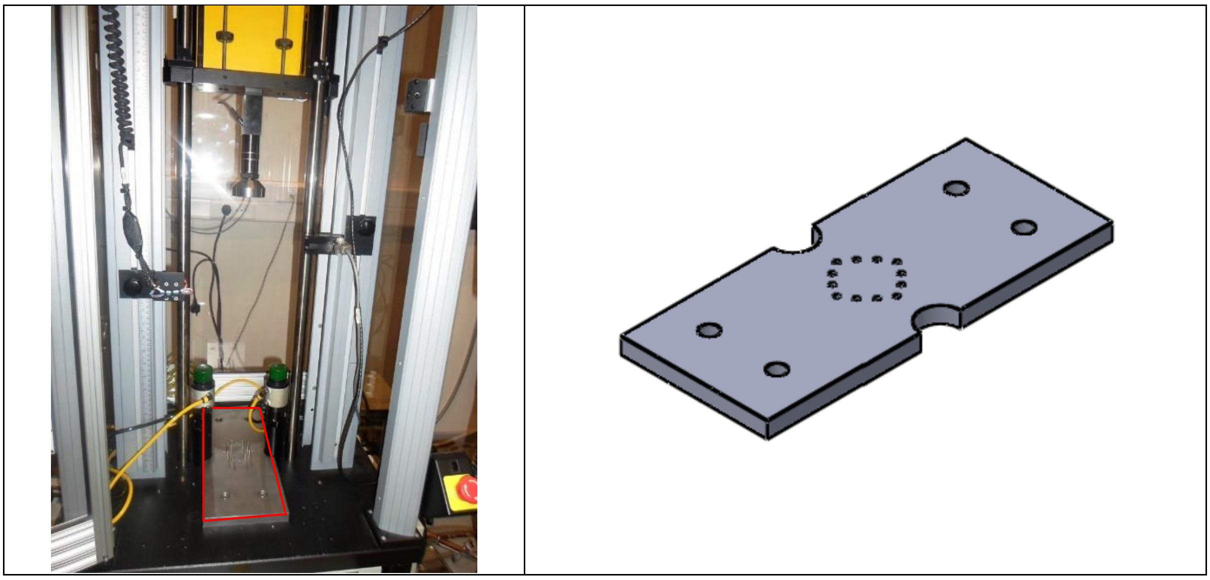

Figure 24, Schematic view of the new impact base

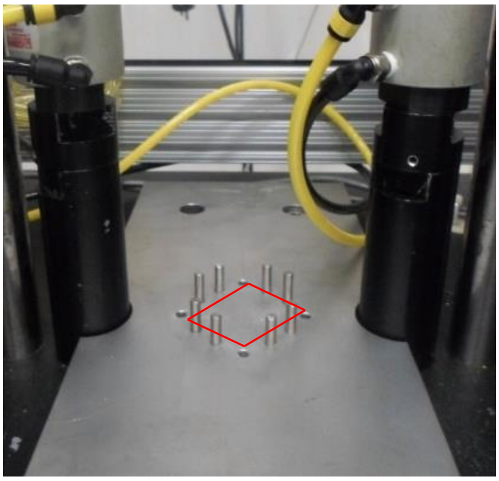

Figure 25, Schematic view of the holding pins and specimen placement.

These pieces were fabricated by mechanic workshops at UCL. Detailed drawings of these modifications are provided in Appendix C.

Experimental program

5.1 Material

A synthetic rock, formulated at UCL, is used in these studies to ensure the homogeneity of the specimen and avoid any impacts it might have (Cho et al., 2003). This synthetic rock is later tested to find the quasi-static properties and it will simplify the analysis since it is isotropic and contains no foliation and planes of weaknesses, a common cause of strength anisotropy in rocks (Prasad, 1994). The results of this study will pave the way toward characterizing the dynamic behavior of natural rock.

- *Composition of synthetic rock*

Synthetic rock consists of 1-part cement and 4 parts of sand proportioned by mass mixed at a water-cement ratio of 0.75.

Table 9 provides the quantities of materials to be mixed at one time in a typical batch of synthetic rock with 14% excess for making 24 prismatic specimens of 40 mm x 40 mm x 160 mm. Graded Standard sand with tap water are used in the preparation of the mix.

Table 9, Composition of a typical batch

Cement	2465 g
Sand	9882 g
Water	1852 mL

- *Apparatus used for material preparation*

1. Weighing devices
2. Glass graduates
3. Specimen molds

   Each mold contains three compartment of 160 mm x 40 mm x 40 mm. The parts of the mold when assembled hold together tightly. They are made of a hard metal. The sides are sufficiently rigid to prevent spreading/warping. The interior faces of the molds are plane surfaces.
4. Metal pan

   A watertight, clean, damp, metal pan is used to mix the material inside.
5. Tamper,

   A moist wooden block with no apparent absorption and a cross-section of 40 mm x 60 mm is used as a guide for the compaction mass of 5 kg. The tamping face is flat and at right angles to the direction of compaction.
6. Trowels
7. Scoops
8. Straight-edge

- *Preparation of the batch of the synthetic rock*

The batch is mixed by hand in a metal pan with a bricklayer's trowel. The batch is of such a size to leave about 14 % excess after molding the test specimens. The batch had a volume of 0.007 m3.

$$Batch\ Volume = 8 * 3 * 0.16 * 0.04 * 0.04 * 1.14 = 0.007\ m3$$

The batch is mixed according to the following procedure:

- Mixing the cement, and fine aggregate without addition of water until they are thoroughly blended.
- Adding water in increments, and mixing without interruption until the synthetic rock is homogeneous in appearance

- *Placement and compaction of synthetic rock*

The mix is placed into the molds using scoops while being compacted by hand. Then, the prismatic specimens are compacted in one layer by 2 blows of 5-kg weight from a height of 3 cm[6].

$$Compaction\ Energy = No.of\ Blows * M * g * H = 3\ J$$

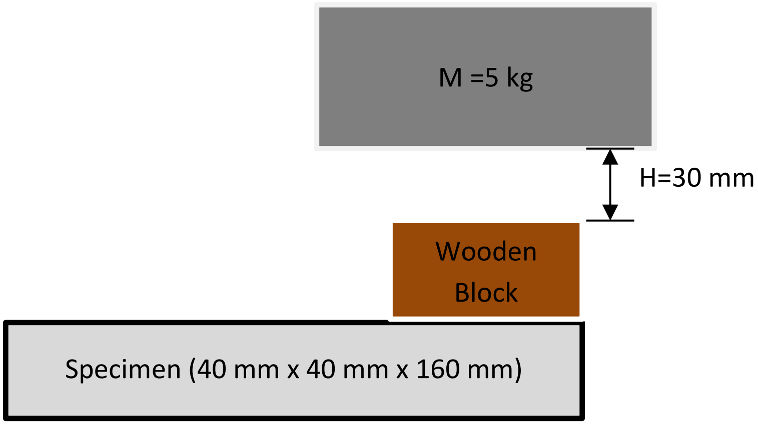

Figure 26 Schematic illustration of compaction process

Finally, the surface is smoothened using a straight-edge. Extreme care should be exercised in the smoothening of the specimen surface, since multiple specimen were discarded with uncorrectable surface irregularities.

- *Temperature and humidity*

The air in the vicinity of the mixing slab, the dry materials, and equipment is room temperature. The specimens were placed in a ventilated moist room at a temperature of 20 °C and relative humidity of 99% (Figure 27). They are cured for one day in the molds, then stripped and kept in the same moist room until tested.

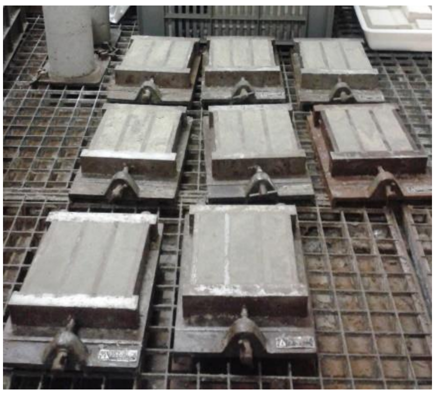

Figure 27, Specimens placed in the moist room

[6] Particular attention should be paid to the compaction energy. Multiple specimens were discarded due to excessive scatter in their final densities. Although the available compaction mass is difficult to manipulate, the batch cast and compacted on 7/06/2016 has resulted in an almost uniform density for all specimens

5.2 Specimens

- *Specimen preparation*

Prismatic specimens are cut with a cutting machine (blade thickness=2.3 mm) to obtain 40-mm cubic specimen 18-24 hours before commencement of test. No water is used in the cutting process so that moistening of the specimen could be avoided[7].

The specimen surfaces are corrected using a sand paper. The specimens are wrapped with three layers of thin transparent plastic sheet to prevent any damage from the fragmentation of synthetic rock during impact.

- *Specimen labeling*

The following labeling convention is adapted so that no two specimens coming from the same bar are tested under the same test conditions.

The specimens are numerated based on their location on each prism. The last digit in the specimen ID indicates how far the specimen is located with respect to one end of the bar as depicted in Figure 28. The remaing digits indicate the prismatic specimen number from which the specime is cut. Specimen # 83 means that it is cut from bar # 8 and it does not from the far ends of the bar.

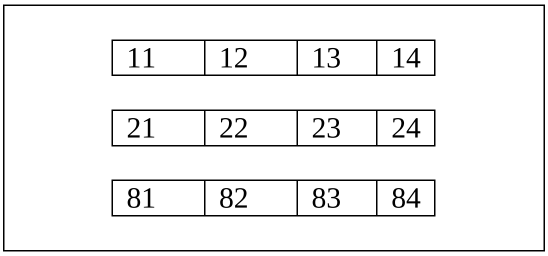

Figure 28, Specimen labeling based on their location

The specimen is marked on the top side to ensure that they are later loaded in the direction of compaction.

- *Specimen area measurements*

Initially, it was thought that obtained cube specimens would have a cross-sectional area of 40 mm x 40 mm after being cut from the prismatic specimen. However, it was later found after performing impact tests that that there are shortcomings in the cutting operation, hence leading to different cross-sectional areas.

In order to account for these variations in cross-sectional areas of specimens, areas of thirty-three 40-mm cubes of ten prismatic specimens were measured since the original specimens were not available. The average area and standard deviation of each specimen location is used in normalizing striker force measurements to stress (Section 6.2.1).

	Location # 1	Location # 2	Location # 3

[7]Initially, water was used in the cutting process and moistened specimen were oven-dried. However, these specimens were discarded since probable impact of oven-drying was feared to affect the specimen resistance.

L (mm)	42.57 (0.91) [8]	41.13 (0.96)	42.72 (0.62)
W (mm)	40.09 (0.10)	40.09 (0.10)	40.14 (0.16)
H (mm)	39.61 (0.17)	39.53 (0.18)	39.45 (0.19)
$Area\ (mm^2)$	1706.48 (39.9)	1649.21 (39.86)	1715.00 (26.45)

5.3 Quasi-static tests

These quasi-static compressive strength of the synthetic rock is determined using 40-mm cube specimens**.**

A modulus of elasticity (E) equal to 1.5 GPa, a cross-sectional area of 1600 mm2 is assumed so as to determine the required machine force rate,

$$\dot{F} = E * A * \dot{\varepsilon}_{quasi-static} = 1.5 * 10^9 * 1600 * 10^{-6} * 30 * 10^{-6} = 72\,N/s \sim 70\ N/s$$

- *Test specimens*

A total number of 3-5 specimens were tested for each batch to observe reproducibility of the results.

- *Testing machine*

Testing machine is a Zwick apparatus with a maximum force capacity of 270 kN. ISRM (1983) requires at least the top platen be spherically seated since the application of load may result in some deviations from the plane of parallelism which needs to be compensated for.

In Zwick apparatus, the upper bearing is spherically seated. It has a hardened metal block firmly attached at the center of the upper head of the machine as required by ("ASTM C109 / C109M - 16a Standard Test Method for Compressive Strength of Hydraulic Cement Mortars (Using 2-in. or [50-mm] Cube Specimens)," n.d.)

The block is closely held in its spherical seat, but is free to tilt in any direction. The diagonal of the bearing surface is slightly greater than the diagonal of the face of the cube to facilitate accurate centering of the specimen. Furthermore, a hardened metal bearing block is used beneath the specimen to minimize wear of the lower platen of the machine.

5.4 Drop-weight impact tests

Knowing the available impactor masses, and the specimen geometry, one can obtain the necessary impactor velocities using $f_{c,imp} - \dot{\varepsilon}$ diagram of Section 4.3.2 for conducting tests.

The striker impact velocity and mass can be used to determine the impact energy supplied to the specimen. This energy should be controlled to avoid damage to the machine and to ensure failure of specimen with adequate strain rate.

Modulus of toughness of a material indicates its energy absorption capacity and it equals the area under the stress strain diagram. Based on quasi-static uniaxial compressive strength of synthetic rock, it is found that modulus of toughness for synthetic rock is equal to 73.1 kJ/m^3 (Section 6.1). For our theoretical specimen dimensions, the amount of absorbed energy is 4.68 J under quasi-static loading.

[8] The value in parenthesis is the standard deviation (SD) of the measured quantity.

Assuming no strength enhancement, one can find a lower bound for the absorbed energy while the CEB (1990) givens the upper bound for the impact energy.

Some trial tests were performed starting from low impact energies as low as the quasi-static energy absorption capacity of the specimen. It is found that the striker rebounded or caused limited damage to the specimen leading to the conclusion the impact energy can be increased without damaging the machine.

In order to have sufficient strain at failure, the choice of failure moment at $\pi/3\omega$ (Section 4.3.2) seems reasonable. It results in a slow-down velocity of 50%. Using $f_{c,imp} - \dot{\varepsilon}$ diagram of Section 4.3.2, the drop-weight test parameters are listed in Table 10.

Table 10, Design combinations of impactor mass (M) and striker impact velocity (v0) for failure moment at π/3ω

$M\ (kg)$	$E_{incident}\ (J)$	$E_{abs}\ (J)$	$V_{imp,design}\ (m/s)$	$\dot{\varepsilon}\ (s^{-1})$	$\sigma\ (MPa)$
6.146	57.8	43.3	4.3	54.2	29.8
8.146	50.6	38.0	3.5	44.1	27.8
11.146	43.7	32.7	2.8	35.0	25.7
14. 646	40.0	30.0	2.3	29.0	24.3

The energy absorption predictions by CEB (1990) indicates that the absorption can be as high as 9.25 times as that of the quasi-static static one. The impact strength can be as high as 4.3 times as that of the quasi-static one.

Since exact impactor masses, and possible impact velocities were based on the Instron catalogue, the impact velocities were modified to adapt to actual machine conditions. It is found that the machine cannot exceed 4 m/s without spring-assistance. Actual combinations of impactor mass (M) and striker impact velocity (v0) with $t = \pi/3\ \omega$ are listed in Table 11 for tests on 23/06/2016

Table 11, Actual combinations of impactor mass (M) and striker impact velocity (v0) with failure moment at π/3ω used for tests on 23/06/2016

$M\ (kg)$	$V_{imp,real}\ (m/s)$	$E_{inc,real}\ (J)$
6.146	4.0	49.2
8.146	3.5	49.9
11.146	3	50.2
14. 646	2.4	42.2

The expected ranges of strain rate are approximately from $30\ to\ 55\ s^{-1}$. In order to have lower strain rates, it is decided to change the failure moment definition. Tests were performed at $t = 0.4\pi/\omega$ so that that one would have a velocity slow-down of 70% at the failure moment. $f_{c,imp} - \dot{\varepsilon}$ diagram of Section 4.3.2 was modified for $t = 0.4\pi/\omega$. Drop-weight test parameters for $t = 0.4\pi/\omega$ are listed in Table 12.

Table 12, Design combinations of impactor mass (M) and striker impact velocity (v0) for failure moment at 0.4π/ω

$M\ (kg)$	$E_{incident}\ (J)$	$E_{abs}\ (J)$	$V_{imp,design}\ (m/s)$	$\dot{\varepsilon}\ (s^{-1})$	$\sigma\ (MPa)$
6.1	31.8	28.8	3.2	24.9	24.0
8.1	31.1	28.1	2.8	21.3	23.7
11.1	30.3	27.4	2.3	18.0	23.3

14. 6	30.0	26.8	2.0	15.5	23.0

Actual combinations of impactor mass (M) and striker impact velocity (v0) with $t = 0.4\pi/\omega$ are listed in Table 13 for tests on 24/06/2016

Table 13. Actual combinations of impactor mass (M) and striker impact velocity (v0) with failure moment at 0.4π/ω used for tests on 24/06/2016

$M\ (kg)$	$V_{imp,real}\ (m/s)$	$E_{inc,real}\ (J)$
6.146	3.3	33.5
8.146	2.8	31.9
11.146	2.4	32.1
14. 646	2.0	29.3

A total number of 3-5 specimens making a test lot are used for each mass-velocity combination to confirm reproducibility of the results[9]. It is tried to have at least three different specimen locations (Section 5.2) in each test lot.

Test results

6.1 Quasi-static test results

Table 14 provides the results of uniaxial compressive strength tests for synthetic rock used in tests drop-weight tests. Detailed stress-strain diagrams are provided in Appendix D.

The platen displacement is corrected and used to plot the stress-strain diagrams. The quasi-static modulus of elasticity, in this report, is the slope of secant at 30-80% of the peak stress (rectilinear part of the stress-strain diagram).

Table 14, Quasi-static properties of the synthetic rock

Casting Date: 07/06/2016, Test Date: 23/06/2016	Batch # SR1
Static uniaxial compressive strength (f_{cs})	6.9 (0.33)MPa
Modulus of elasticity (E)	449.3 (50) MPa
Density (ρ)	1751 (31) kg/m^3
Bar wave velocity ($\sqrt{E/\rho}$)	506.7 m/s

Since the initial force rate is calculated based on an assumed modulus of elasticity (1.5 GPa) and cross-sectional area, the actual strain rate is calculated as follows:

$$\dot{\varepsilon} = \frac{\dot{\sigma}}{E} = \frac{\dot{F}/A_{avg}}{E_{avg}} = \frac{70/1690.23}{449.3} = 92 \times 10^{-6}\ s^{-1}$$

Thus, the applied strain rate is almost three times higher than the quasi-static strain rate defined by CEB 1990.

[9] It is important to verify steel striker head and adjustable impactor masses are tightened firmly after each finishing each test.

However, this strength is assumed as the quasi-static strength of synthetic rock for subsequent calculations of dynamic increase factor.

6.2 Drop-weight test results

6.2.1 Unfiltered stress time-history

The instrumentation placed at striker records the force which is later normalized by the average area of each specimen location as discussed in Section 5.2. Stress time-histories are provided in Figure 29 andFigure 30. The stress signals show a considerable amount of noise.

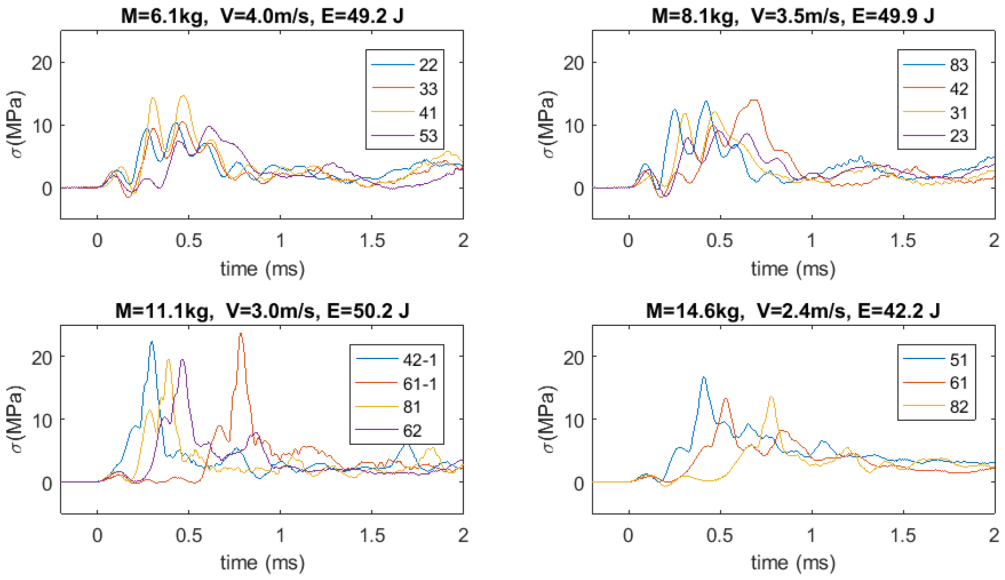

Figure 29, Unfiltered stress time-history for specimen tested on 23/06/2016[10]

[10]Specimen # 42-1 and Specimen # 42 do not come from the same prismatic bar.
Specimen # 62-1 and specimen 62 do not come from the same prismatic bar.

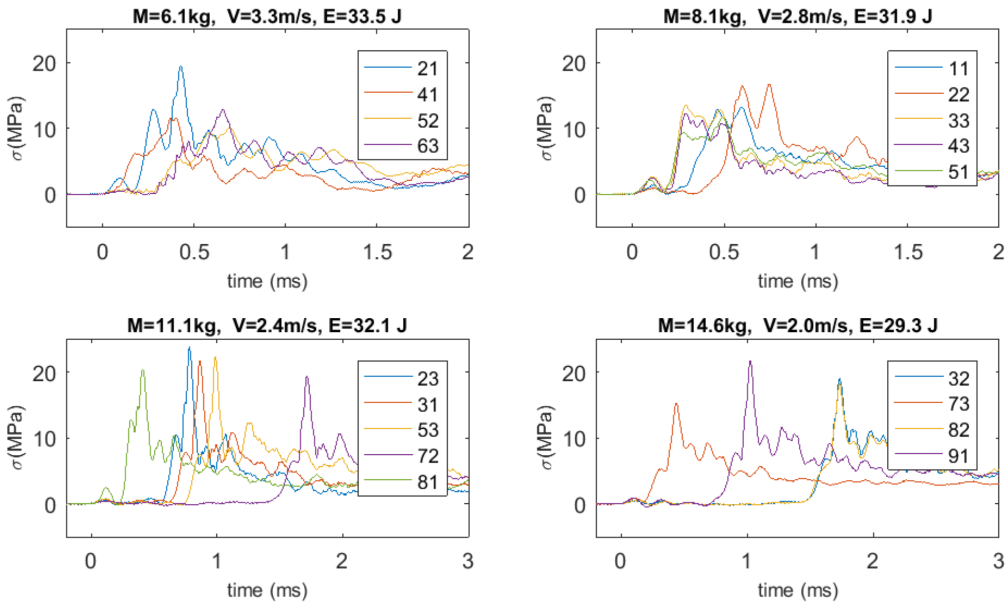

Figure 30, Unfiltered stress time-history for specimen tested on 24/06/2016

6.2.2 FFT and smoothing of stress time-histories

For the purpose of using the striker force signals, they should be smoothened and normalized. Care must be exercised so that the smoothing does not attenuate the striker signal excessively. Therefore, a Fourier transformation of the stress time histories is performed by a script written in MATLAB (Appendix B) to reveal the nature of the noise present in the striker signals.

Fourier transform converts the time domain representation of a signal into frequency domain.

$$F(t) = \sum_{i=0} A_i \sin(2\pi f_i t) + B_i \cos(2\pi f_i t)$$

A continuous function of time can be represented as sum of sinusoids. This property is extended to discrete functions using Euler's formula as discrete Fourier transform (DFT).

$$x(n) = \frac{1}{N} \sum_{k=0}^{N-1} \mathbf{X}(k)\ e^{-j(2\pi /N)nk}$$

An inverse Fourier transform is used to recover the original time domain representation,

$$\mathbf{X}(n) = \sum_{n=0}^{N-1} x(n)\ e^{-j(2\pi /N)nk}$$

The impact force resembles a half sine pulse for a ductile-brittle failure. However, frequency spectrum does not contain a single frequency (Figure 31). The frequency is spread over a wide range due to the fact that the signal is actually a combination of a half sine pulse, and unit step functions (Cain, 1986) (Figure 32).

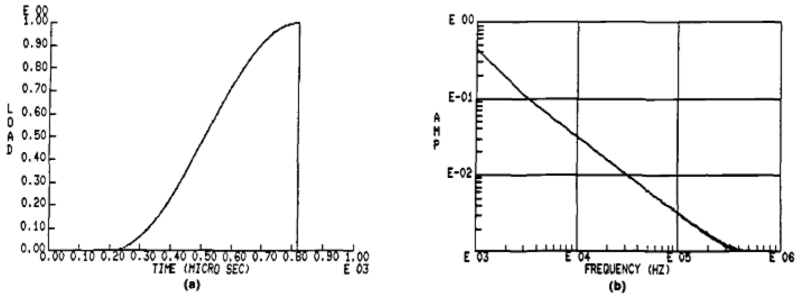

Figure 31, Time-history (a) and frequency spectra (b) for a material with ductile-brittle failure characteristics (Cain, 1986)

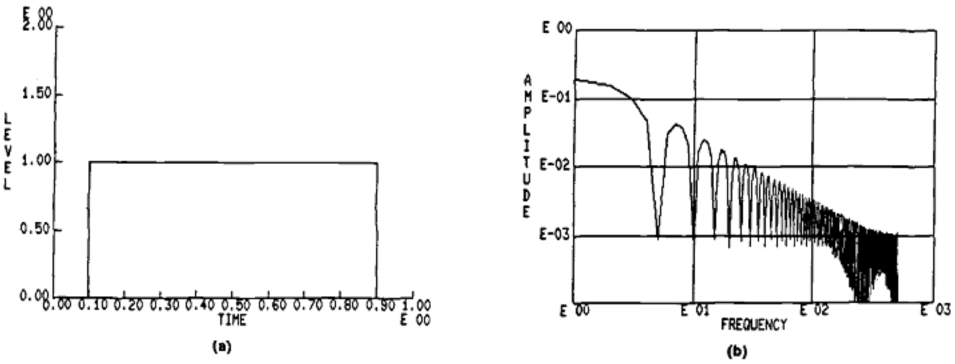

Figure 32, Time-history of the boxcar function (a) and the frequency spectrum (b) (Cain, 1986)

Based on the frequency content observed, a symmetric moving average filter was used with a window size large enough to remove the observed noise frequency. For example, a window size of 47 points (0.172 ms) is used to remove frequency content above 6 kHz for the stress time-history in Figure 33. This frequency is called the cut-off frequency.

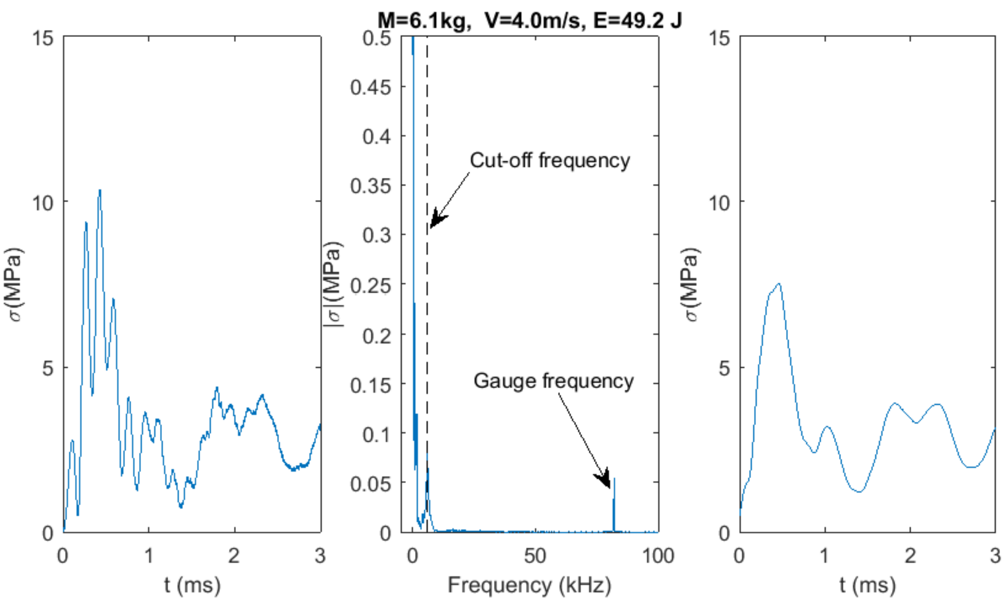

Figure 33, Time domain representation, frequency spectrum and the smoothed signal of a typical stress-time signal

In this symmetric moving average filter, striker signal is averaged on small sections comprising a number of data points equal to the ratio of noise period to data acquisition time step.

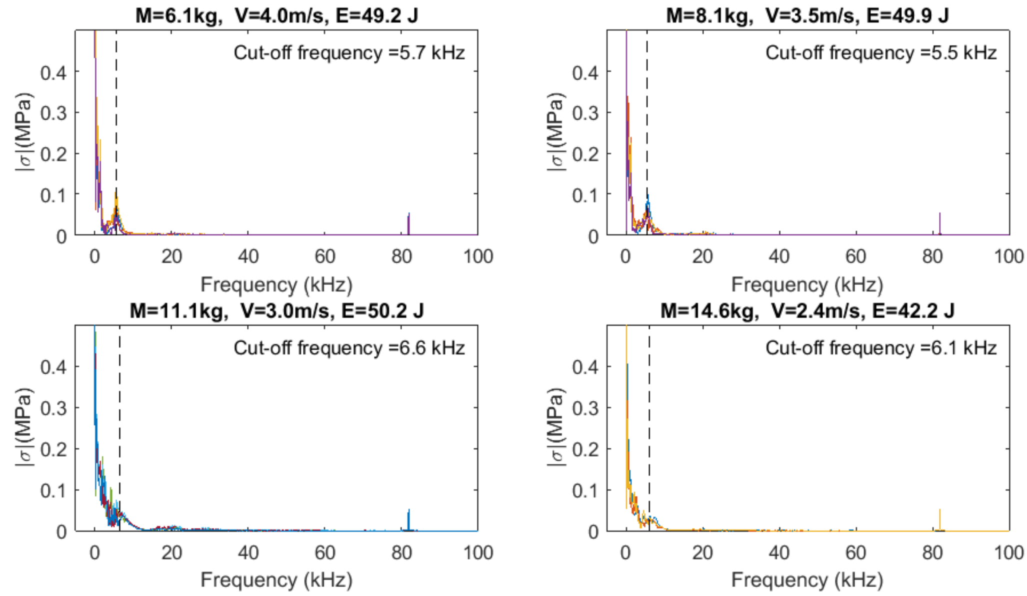

Figure 34, Fourier transformation of the stress time-history for specimen tested on 23/06/2016

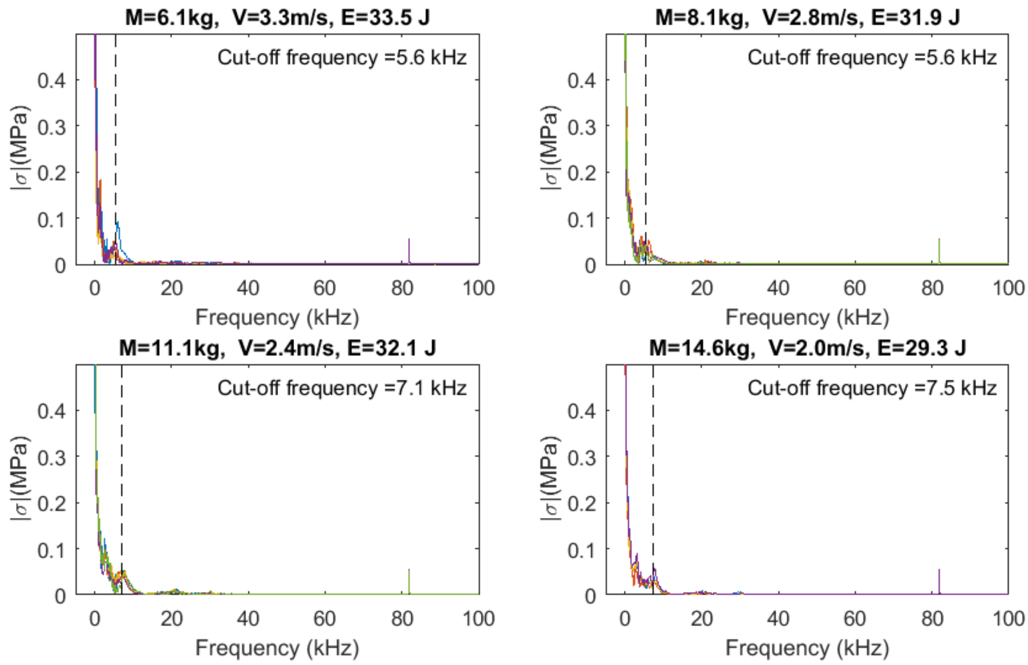

Figure 35, Fourier transformation of the stress time-history for specimen tested on 24/06/2016

Figure 36 depicts typical stress time-history curves before and after smoothing according to the noise frequency observed in Figure 34. It is obvious that the choice of the smoothing algorithm is critical for interpreting stress time-histories.

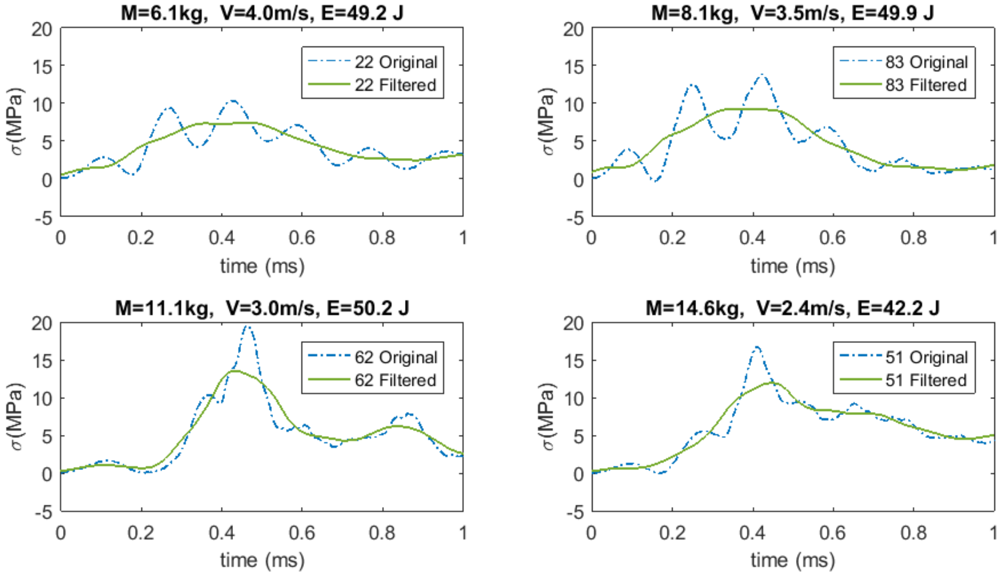

Figure 36, Typical stress time-history signals (23/06/2016) before and after smoothing

6.2.3 Smoothed stress time-history

After smoothening the stress time-histories, it is observed that the signals contain an initial peak and prolonged section before the sharp rise. The former is treated as an inertial force (Refer to Section 7.2). and the latter is considered as a consequence of slight height difference between specimens[11] or slight displacement of the velocity detector.

In order to eliminate the initial peak and prolonged section, the stress time-histories curves are synchronized and plotted at a stress value of 1.8 MPa (3kN). The synchronized curves of each test lot are superimposed to plot their trend. The trend is the mean of y-coordinates of the synchronized curves. Then, the synchronized curves are shifted on the x-axis such that the extension of a secant passing through the synchronization value and another arbitrary value on the curve intersect the x-axis at zero.

[11] The zero elevation was set once at the beginning of test for the first specimen.

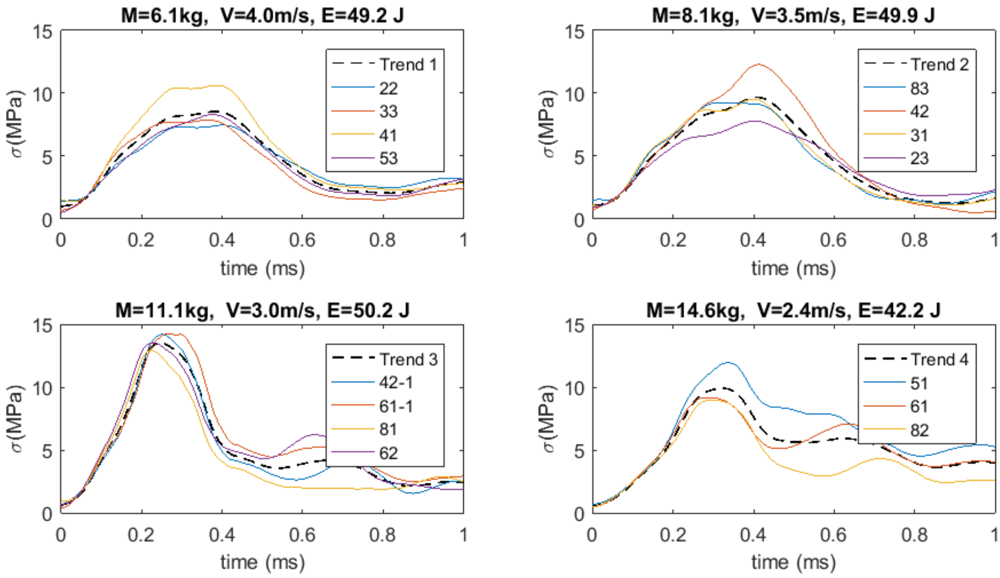

Figure 37, Stress time-history curves for specimens tested on 23 Jun 2016

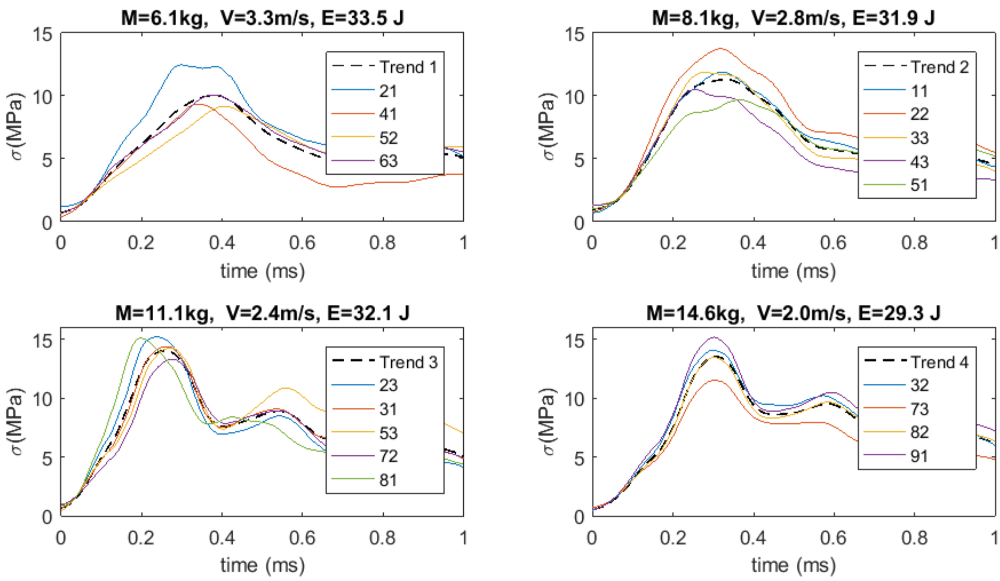

Figure 38, Stress time-history curves for specimens tested on 24 Jun 2016

6.2.4 Comparison of stress time history with time response of a SDOF system

The evolution of impact stress with time can be plotted using a SDOF system as discussed in Section 4.1.2.

$$\sigma_{imp} = \frac{M v_0 \omega}{A} \sin(\omega t)$$

Where

σ_{imp}: impact stress

M: impactor mass

$\omega = \sqrt{k/M}$: natural frequency of specimen calculated using specimen stiffness (k) and impactor mass (M).

The experiment stress time histories are plotted together with the time response of their respective SDOF elastic systems in Figure 39 and Figure 40.

Tests were performed for two different failure moments of $t = \pi/3\omega$ and $t = 0.4\pi/\omega$. The designed $\sigma_f\ /\sigma_{max}$ for these two failure moments are 87% and 95% respectively. However, as it can be observed in Figure 39 and Figure 40, the specimens have failed between 35-65% of possible peak impact stress. This is attributable to overestimation of the strength of synthetic rock by CEB (1990).

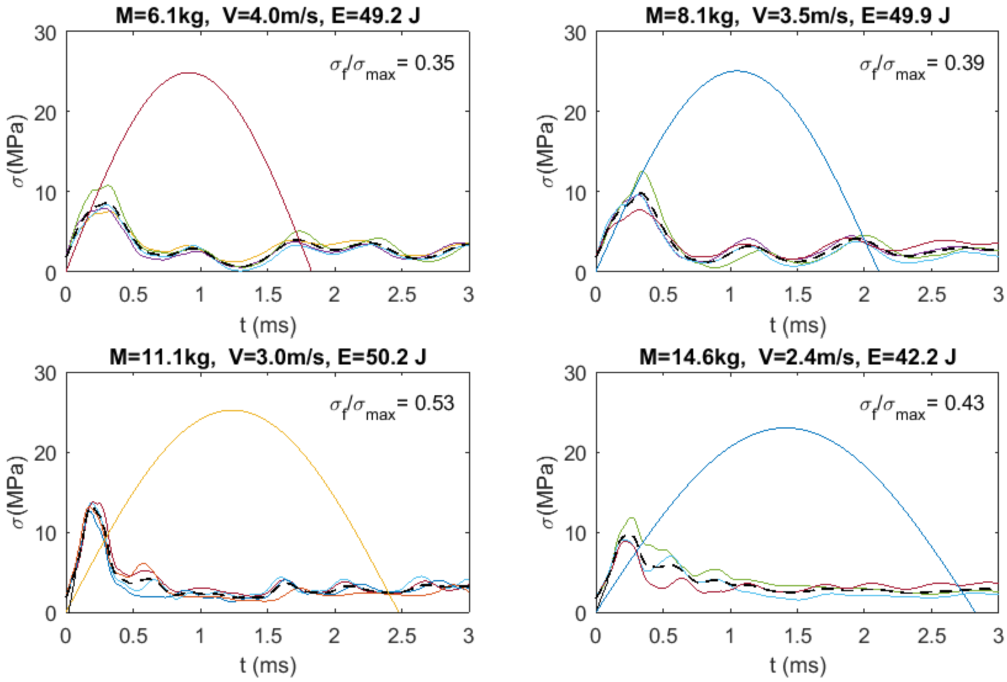

Figure 39, Stress time-history curves with time response of their respective SDOF elastic systems for specimens tested on 23/06/2016

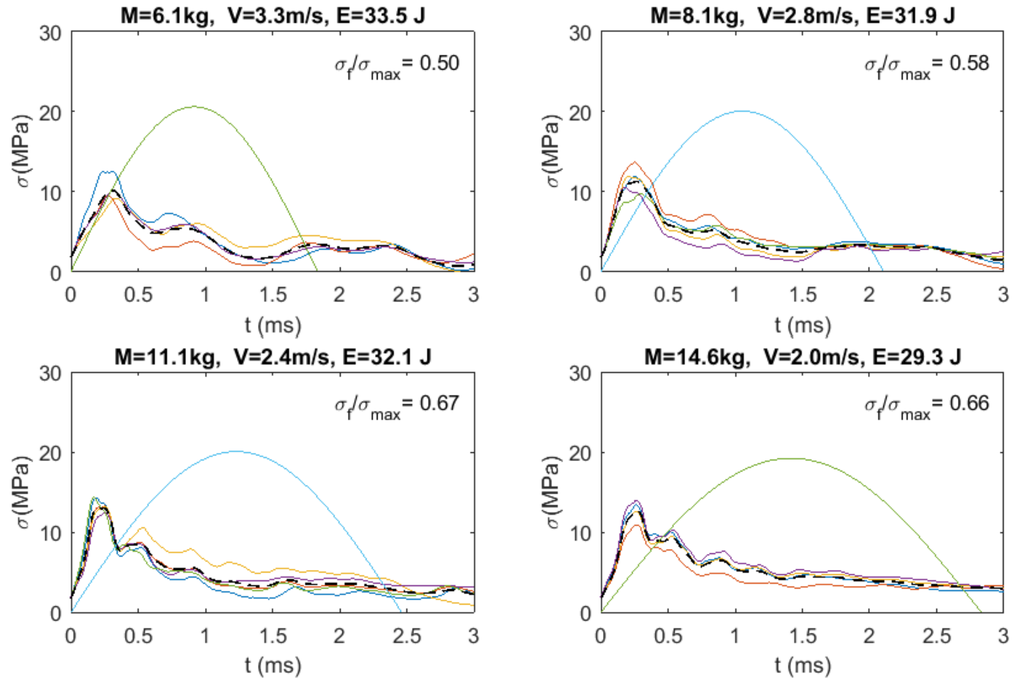

Figure 40, Stress time-history curves with time response of their respective SDOF elastic systems for specimens tested on 24/06/2016

6.2.5 Smoothed stress-strain diagrams

An approach similar to smoothening of stress time-histories is used to smoothen, synchronize and shift the stress-strain curves. Trend curves are plotted for superimposed stress-strain curves of each test lot Strain is calculated based on striker deflection information as follows:

$$\varepsilon = \frac{d(t_f) - d(t_0) + d_{shift}}{39.53 - d(t_0) + d_{shift}}$$

Where,

ε: strain

$d(t_f)$:striker displacement at failure

$d(t_0)$: striker displacement at time zero

d_{shift}: distance representing the intersection of a secant on the smoothed curves passing through the synchronization value and an arbitrary point on the smoothed curve with x-axis. The objective is to remove the initial curvilinear section of curves.

Stress-strain diagrams for tests on 23/06 and 24/06 are provided in Figure 41 and Figure 42. The superimposed trends of these tests are provided in Figure 43.

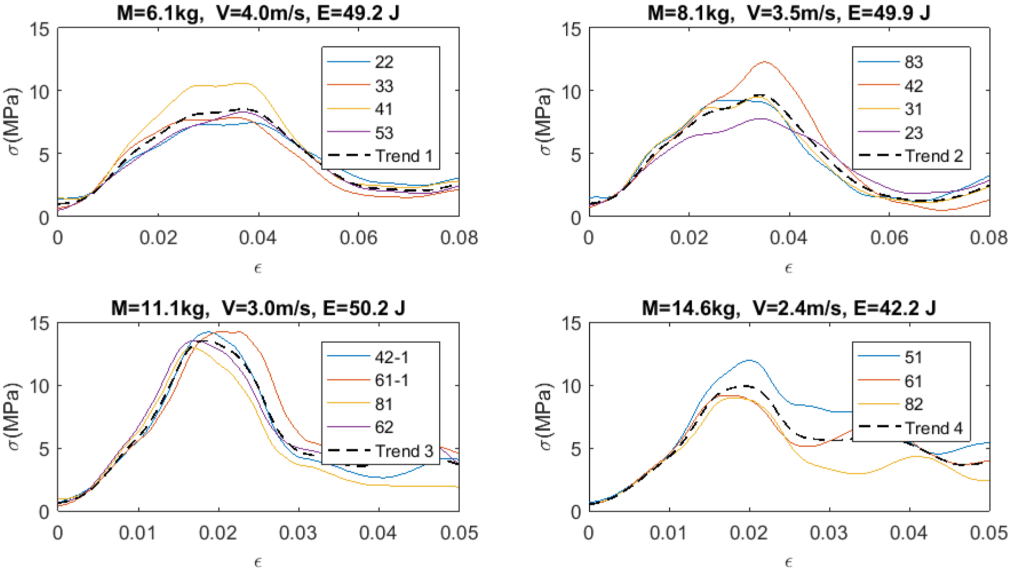

Figure 41, Stress-strain diagrams for specimens tested on 23 Jun 2016

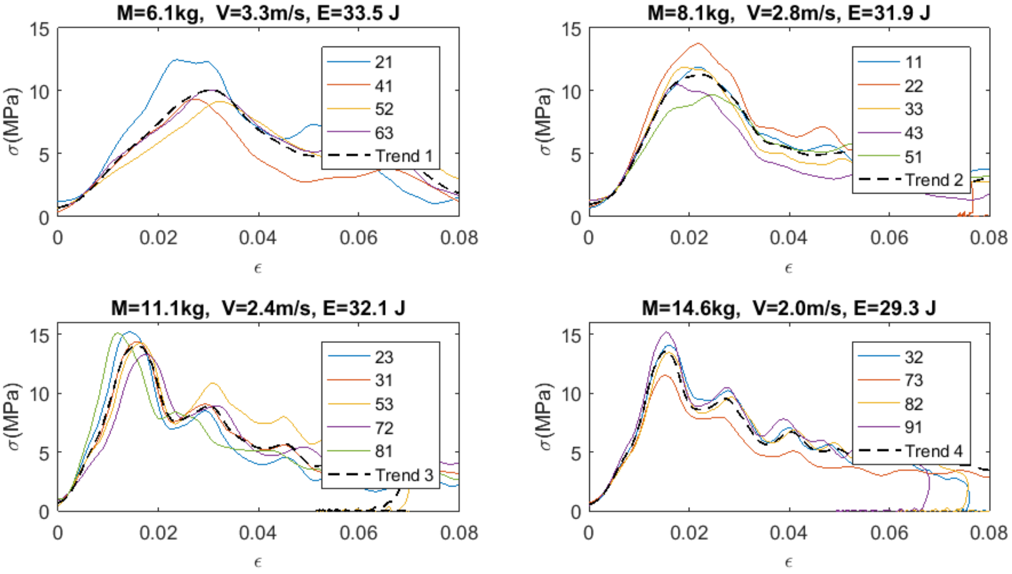

Figure 42, Stress-strain diagrams for specimens tested on 24 Jun 2016

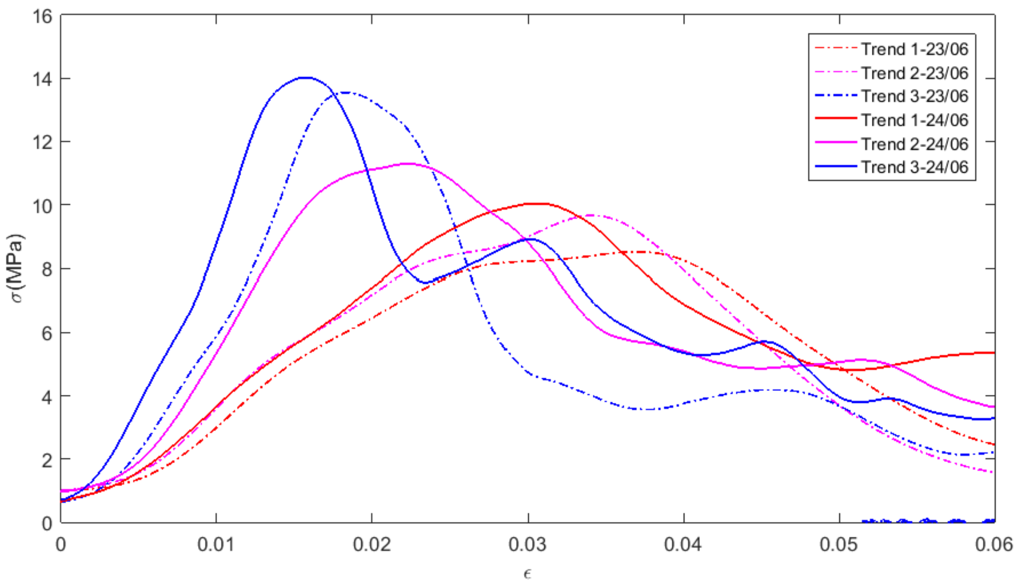

Figure 43, Superimposed trends for stress-strain diagrams with two energy levels: 50 J (dashed-dotted line) and 32 J (solid line)

Analysis of test results and discussion

7.1 Dynamic increase factor

Drop-weight impact tests were performed at approximately two different levels of incident impact energy 50 J and 32 J corresponding to two failure moments of $t = \pi/3\omega$ and $t = 0.4\pi/\omega$. The designed σ_f / σ_{max} for these two failure moments are 87% and 95% respectively. However, as it can be observed in Section 6.2.4, the specimens have failed between 35-65% of possible peak impact stress. This is attributable to overestimation of the strength of synthetic rock by CEB (1990).

As discussed in Section 4.2.1, the ratio of impact to quasi-static compressive strength is referred to as dynamic increase factor (DIF). Variations of DIF with strain rate is usually used to characterize dynamic behavior of materials.

Impact strength is obtained by averaging the peak stresses from stress time-histories of each test lot (Section 6.2.3). Strain rates are calculated averaging the velocity of striker (Section 4.1.3) at the moment of peak stresses.

Figure 44 depicts how the peak stress and striker velocity at failure are identified on their time histories. A script is written in MATLAB to perform these calculations as detailed in Appendix B.

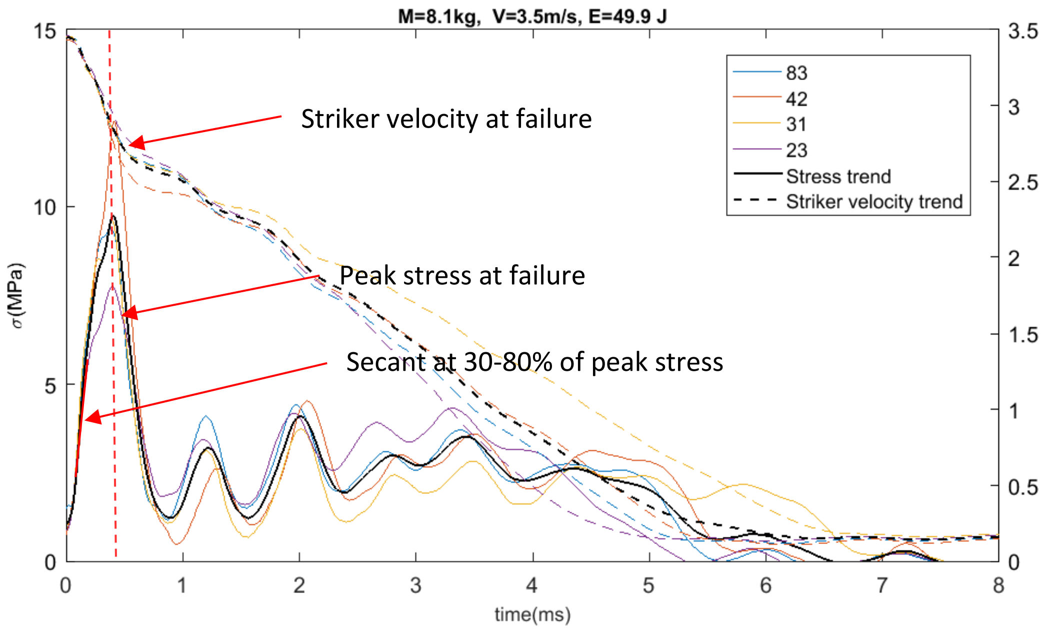

Figure 44, Identifying peak stress and striker velocity at failure on a typical stress (solid line) and velocity time history (dashed line)

As it can be seen in Figure 45, dynamic increase factor decreases with higher strain rates contradicting the initial assumptions using CEB (1990) in Section 4.2.

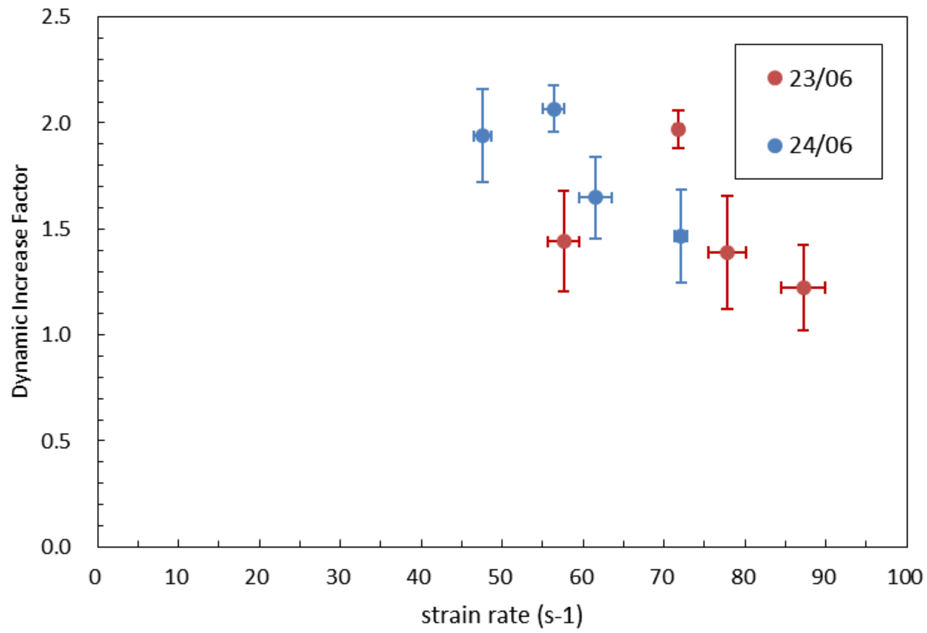

Figure 45, Dynamic increase factor as a function of strain rate calculated using failure velocity

In order to further investigate such behavior, DIF is also plotted against average stress-rate. Since stress is directly obtained from striker force measurements, it is less prone to probable velocity measurement errors. The stress rate for each curve is the slope of the secant on the curve between 30 to 80 percent of the peak force as depicted in Figure 44. A script is written in MATLAB to perform these calculations as detailed in Appendix B.

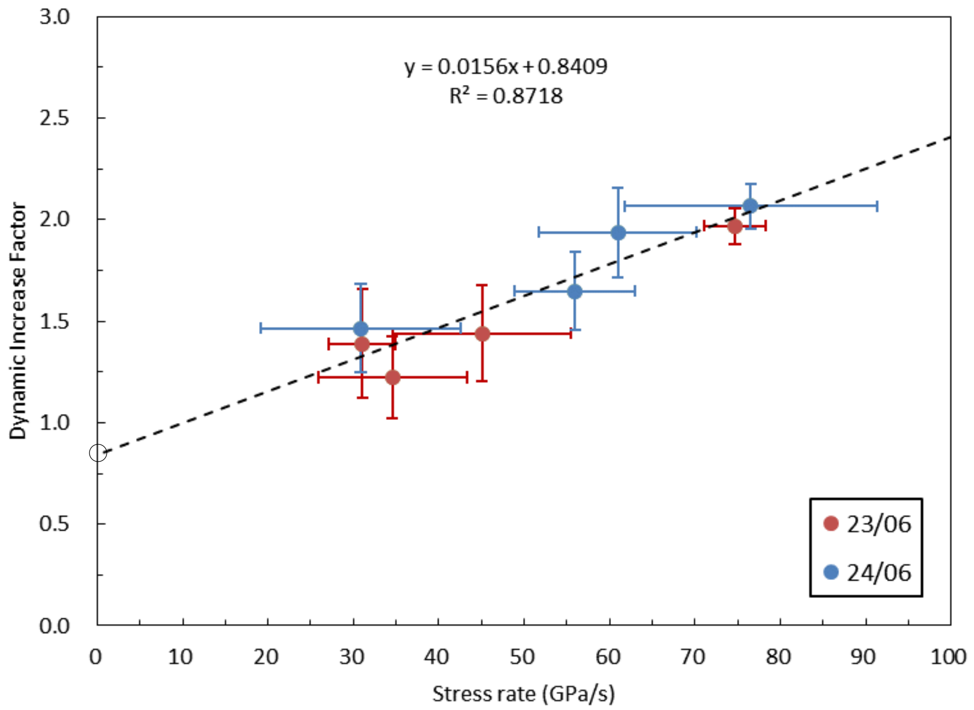

Figure 46, Dynamic increase factor versus stress rate[12]

As it can be seen, the dynamic increase factor is linearly increasing with the stress rate (Figure 46). A linear fit is used to establish the relationship between stress rate and dynamic increase factor.

$$DIF = f_{c,imp}/f_{cm} \quad = 0.0156\,\dot{\sigma}_c + 0.8409 \qquad for\ 30\ GPs/s < \dot{\sigma}_c \le 80\ \ GPs/s$$

Converting the range of stress rates to strain rate by quasi-static modulus of elasticity, one would obtain a rather high range of strain rates from $65 - 180\ s^{-1}$, which is close to the pile driving strain rates ($1 - 100\ s^{-1}$).

Variations of dynamic increase factor according to this linear fit and CEB 1990 are plotted in Figure 47. For CEB (1990), strain rates are converted to stress rates using the elastic modulus of elasticity of synthetic rock. It can be seen that the linear fit for synthetic rock provides much lower strain rate sensitivity for the observed interval of stress rates.

[12] Error bars are placed at 1 standard deviation from the mean value

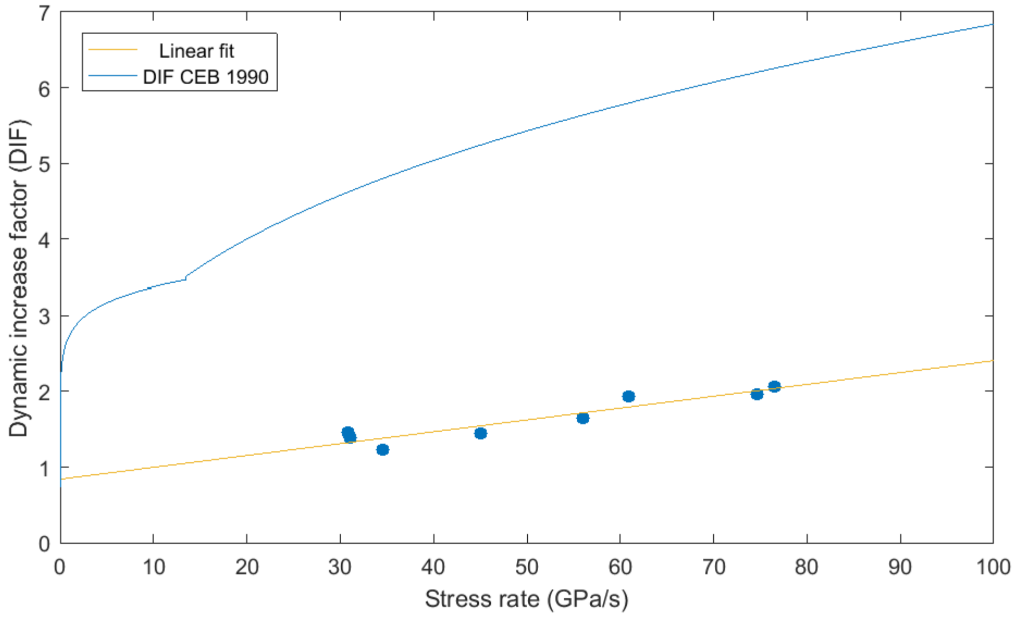

Figure 47, Variation of DIF according to CEB (1990) and linear fit for synthetic rock

The question that, now, rises is that how stress rates and peak forces are related to test parameters such as impactor mass and velocity and why the DIF is decreasing with higher strain rates.

The results of 14.1-kg impactor mass are removed in the following discussion so that two distinct energy levels of 50 J (tests on 23/06/2016) and 32 J (tests on 24/06/2016) could be ensured.

Figure 48 depicts that the stress rate increases with higher impactor masses, and lower impactor velocities at the same energy level. This is against the fact that higher impactor velocities should result in higher strain rates.

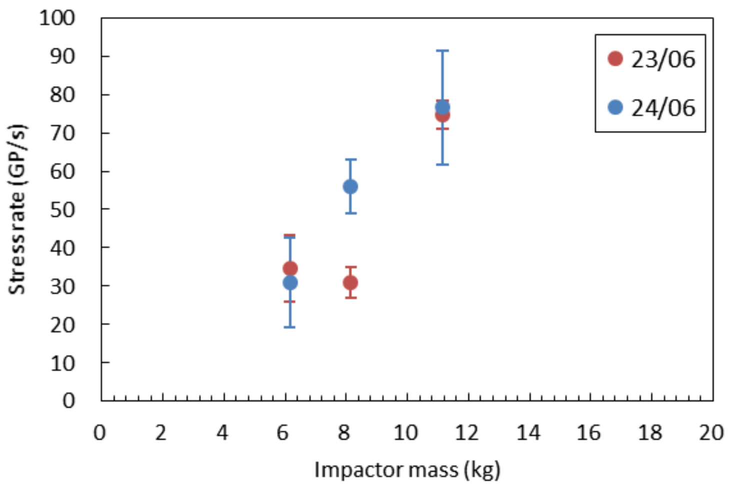

Figure 48, Measured stress rate versus impactor mass for two different energy levels: 50 J (red) and 32 J (blue)

Similarly, DIF increases with higher impactor masses as shown in Figure 49.

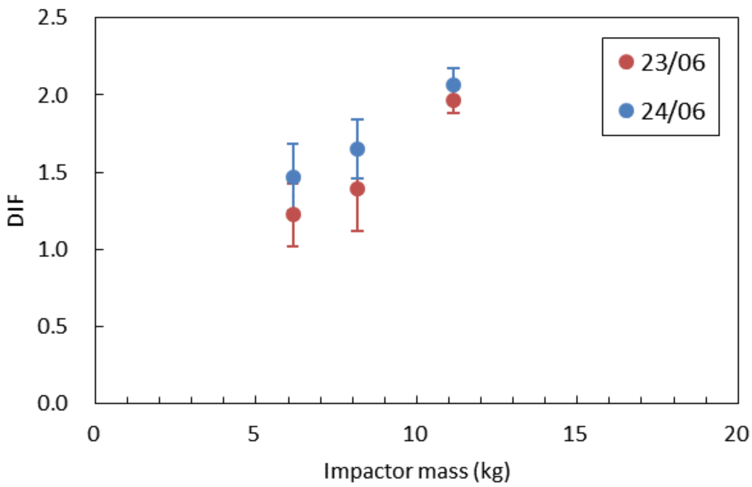

Figure 49, Dynamic increase factor versus impactor mass for two different energy levels : 50 J (red) and 32 J (blue)

At the same time, the peak strain (Figure 50) and energy absorption (Figure 51) decrease with higher impactor masses.

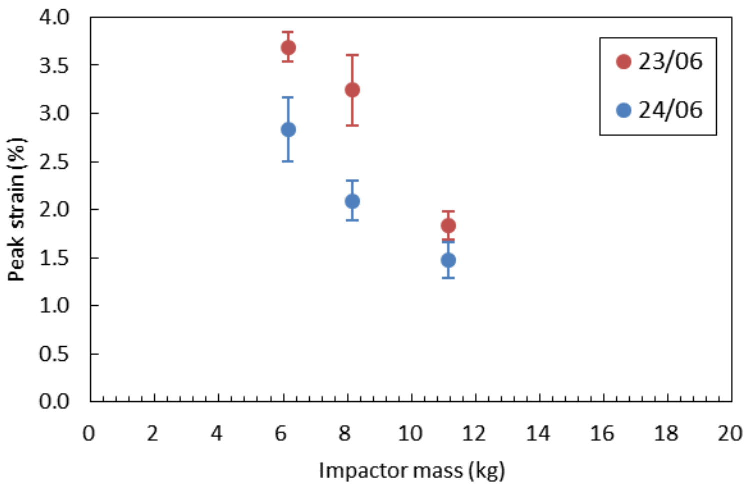

Figure 50, Variation of peak strain with impactor mass for two different energy levels: 50 J (red) and 32 J (blue)

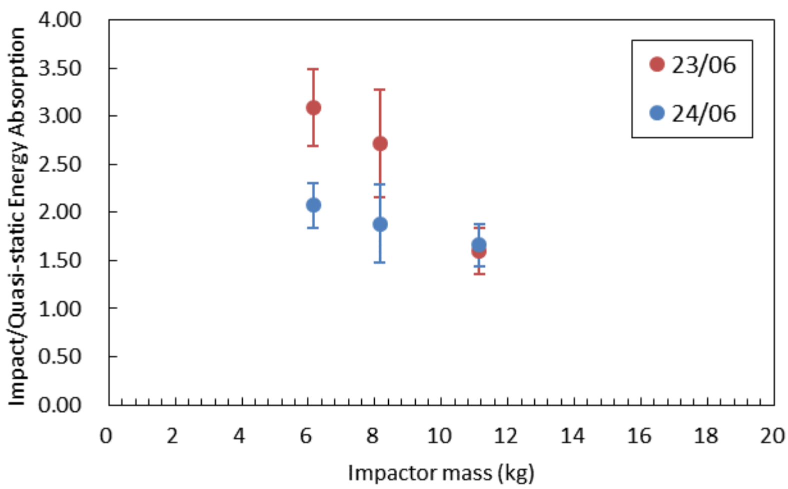

Figure 51, Variations of Absorbed Energy/Impactor Energy against impactor mass at two different energy levels : 50 J (red) and 32 J (blue)

Figure 52 Figure 53 show the variations of strain rate and stress rate with the incident impact energy. It can be seen that for the same energy levels, high impactor masses result in high stress rates and low strain rates.

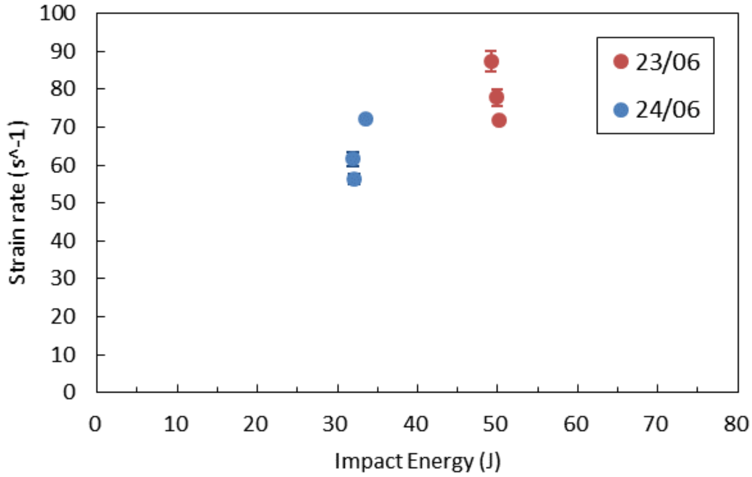

Figure 52 : Variation of strain rate with incident impact energy for two different energy levels: 50 J (red) and 32 J (blue)

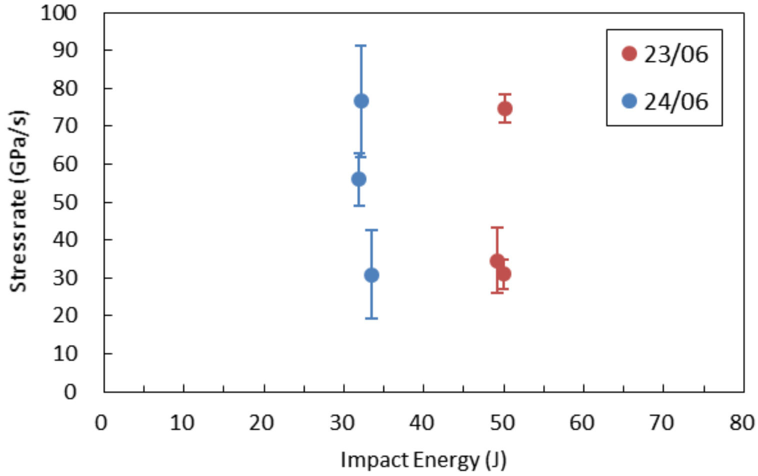

Figure 53 : Variation of stress rate with incident impact energy for two different energy levels: 50 J (red) and 32 J (blue)

Furthermore, lower impact energy surprisingly results in higher peaks and stress rates. As it can be seen in Figure 54, the peak stress increases sharply with 11.1 kg impactor mass.

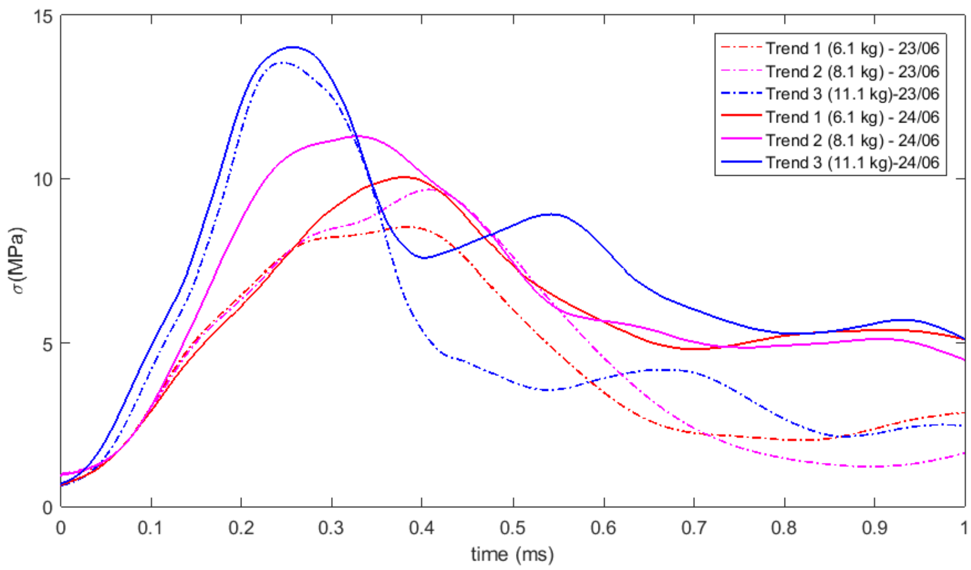

Figure 54, Superimposed trends for stress time-histories with two energy levels: 50 J (dashed-dotted line) and 32 J (solid line)

This behavior is suspected since stress time-histories for large impactor masses have very high signal-to-noise ratio of approximately 200% (Figure 37 and Figure 38). It is feared that the spike in the signals is the origin of this behavior.

That is why it is decided to further characterize the stress-time histories in terms of oscillations, equilibrium and frequency response of system in order make sure the observed behavior is not related to system shortcomings.

7.2 Load oscillations

The striker signals (load-time record) contain a considerable amount of superimposed oscillation imputable to different sources such as inertial acceleration, test system ringing and mechanical axial loads (Saxton et al., 1974). These oscillations are comparable in size to the signal produced by the mechanical resistance of the specimen. An understanding of these sources is essential in interpreting the obtained results.

First oscillation on the striker signal should be considered as a result of inertia. Inertial forces last for the very first moments of the impact event bringing the specimen from rest to striker velocity.

System ringing is a result of stored elastic energy, release of fracture energy and reflection of stress waves. Each of these oscillations are discussed as follows.

- **Inertial acceleration loads**

At the very beginning of impact, the stationary specimen absorbs energy to reach the same velocity as the striker. Since the force transducer at the striker has a limited frequency, it can't capture the continuity of stress, thus, recording an initial peak which is not reflecting the true mechanical response of the specimen. (Saxton et al., 1974) (Figure 55).

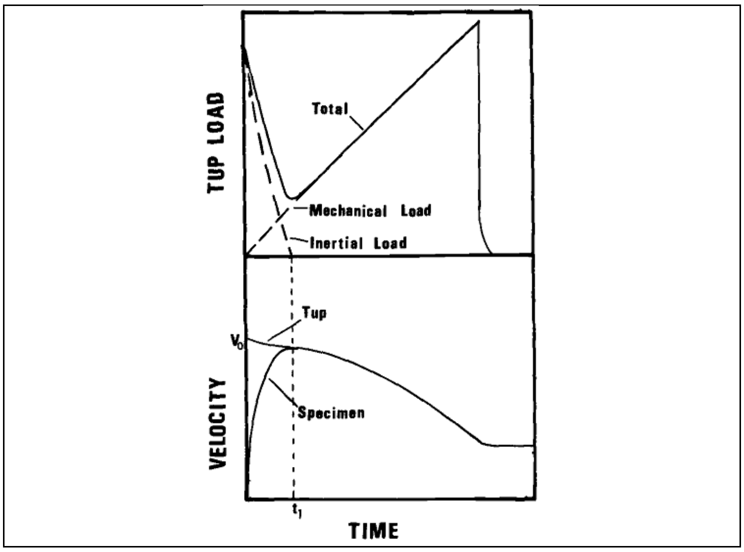

Figure 55, schematic of the load-time and velocity-time behavior actually experienced by striker and specimen an impact

The apparent magnitude (P_I) of the size of oscillations can be predicted based on a model developed by (Ireland, 1974). They have estimated that this inertial oscillation is actually proportional to the stress wave that travels along the specimen and the striker upon impact.

$$P_I \propto \frac{Z_1 Z_2}{Z_1 + Z_2} V_{imp}$$

Where,
$P_I = inertial\ force$
$Z_i = C_{Di}\rho_i$
$C_{Di} = dilation\ sound\ speed$
$\rho_i = density$
$V_{imp} = initial\ tup\ velocity$
Since $Z_1 \gg Z_2$, $P_I = Z_2 = V_{imp}$

$$P_I = \rho_{spec} C_{spec} A_{spec} * V_{imp}$$
$$or$$
$$\sigma_{inertia} = \rho_{spec} C_{spec} V_{imp}$$

The above equation gives a good approximation of initial inertial oscillations as listed in Table 15.

Table 15, Estimation of inertial oscillations

V_{imp} (m/s)	$Inertial\ Stress\ (Mpa)$
1	0.9
2	1.8
3	2.7
4	3.5

To control the inertial effects, it is recommended to decrease impact velocity in order to avoid failure in the zone which is masked by inertial effects. As it can be observed in unfiltered stress time histories (Section 6.2.3) the initial oscillation diminishes significantly as the impact velocity is decreased.

- **Test system ringing**

System ringing is as a result of reflection of stress waves in the striker and specimen.

For the specimen, assuming that the first mode of vibration of a fixed-fixed bar, the natural frequency can be calculated by:

$$f_n = n\frac{C}{2H}, n = 1 \rightarrow f_1 = 6\ kHz, T_1 = 0.164\ ms$$

Where,

C: Bar wave speed

H: Specimen height

T: Characteristic time

Presence of higher modes are improbable as it can be observed from the FFT analysis containing no significant frequency content above 8 kHz. Furthermore, the subsequent stress wave reflections in the specimen might have very negligible impact on the striker recordings. During impact, the specimen (very low specific impedance) is sandwiched between two materials with relatively high impedances. Therefore, the striker acts like a fixed support, to which transmitted stress is negligible.

Therefore, it is more probable that the present oscillations come from the compliance and vibrations of the drop-weight assembly. A detailed diagram of the drop-weight assembly is provided in Figure 51.

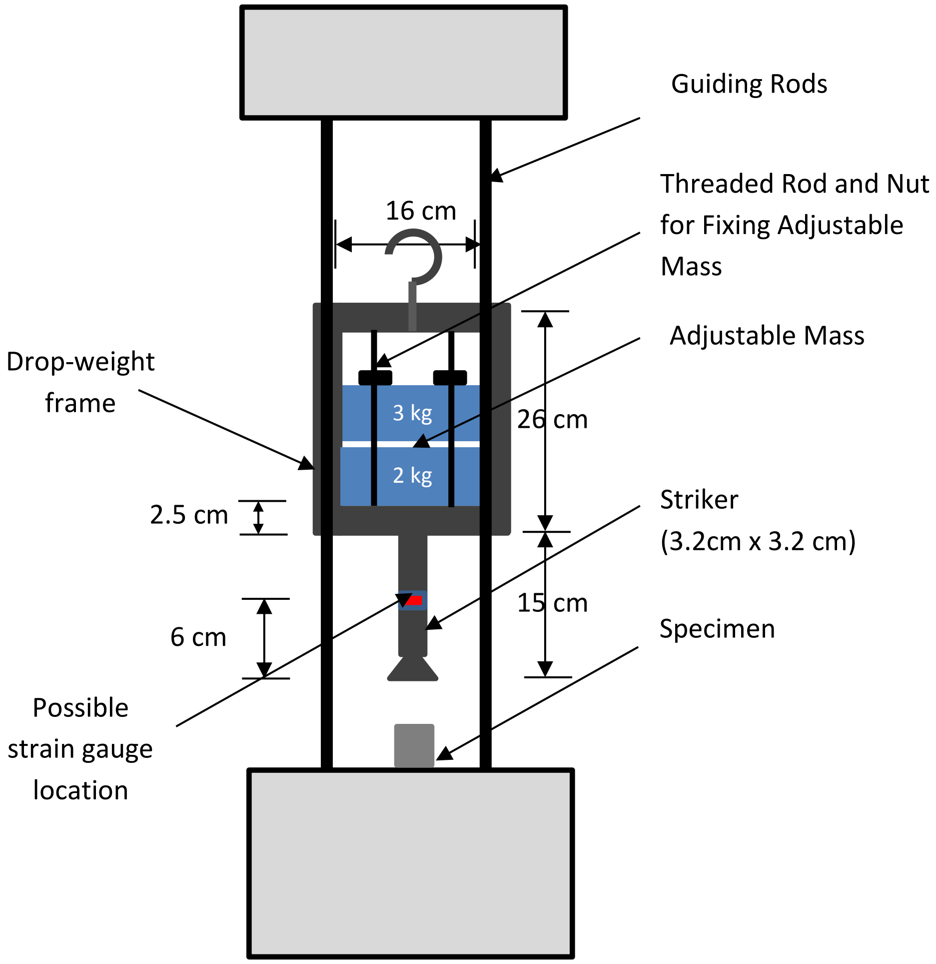

Figure 56, A schematic illustration of drop-weight frame, striker and specimen.

The striker may excite the fundamental natural frequency of the bottom of drop-weight frame which acts as a hypothetical fixed-fixed beam. For the calculation of natural frequency, dimensions are approximated from available photos since the machine is not accessible at the moment of preparing this report.

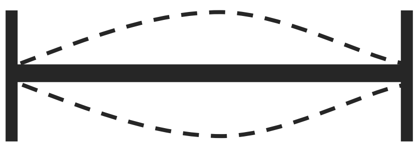

Figure 57, (a) Vibration of a fixed-fixed beam at its fundamental mode (b) with possible adjustable mass

The natural frequency of a fixed-fixed beam (Rao, 2007) is:

$$f_1 = \frac{1}{2\pi} 4.73^2 \sqrt{\frac{EI}{A\rho L^4}}$$

where,

$E\ (GPa) = 210$, modulus of elasticity of the drop-weight frame

$b\ (m) = 0.025$, section height

$h\ (m) = 0.075$, section width

$L(m) = 0.16$, beam length

$\rho(kg/m^3) = 7830$, beam density

$A(m^2) = bh$, beam cross-sectional area

$I = \frac{1}{12}bh^3$, moment of inertia of the beam section

Using the above relation, one obtains a natural frequency of 5.2 kHz, which is close to the noise frequencies observed in the frequency domain of striker signals with lower impactor masses.

As the adjustable weight increases, the natural frequency of bottom of drop-weight also increases since the height and flexural rigidity of the hypothetical beam increases. However, if the nuts holding the adjustable weight loosen after an impact, the final response of drop-weight bottom is the response of a fixed-fixed beam in the middle of which an adjustable weight is attached. That may be why the noise becomes more and more obscure by increasing the adjustable mass. This possibility could not be further investigated since the exact dimensions of adjustable masses were not available or could not be estimated.

Looking from a different perspective, the specimen is exciting the striker-drop-weight assembly at 6 kHz. By increasing the adjustable weight, the natural frequency of the drop-weight assembly approaches the excitation frequency resulting in resonance. Resonance can be observed with impact masses of 11.1 and 14.6 kg where the noise to signal ratio exceeds 200%.

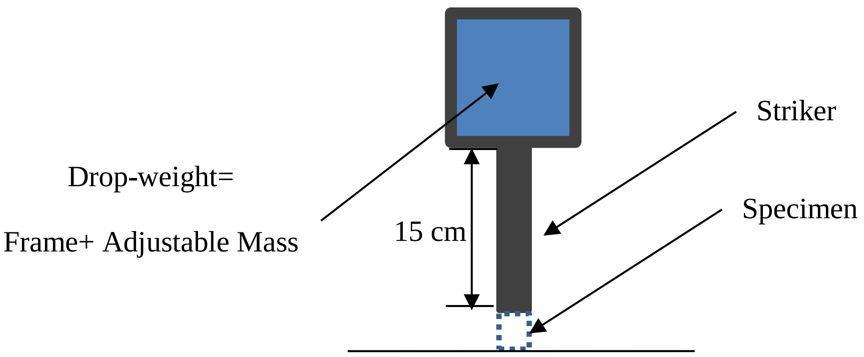

Figure 58, Axial vibrations of striker drop-weight assembly

Furthermore, there is a possibility of axial vibrations of striker attached to a mass (Figure 58). In such a case, this would be similar to the vibrations of a fixed or free bar attached to a mass. Before and after failure of specimen, the bar can be treated as fixed and free respectively.

Table 16 depicts the frequency equations and natural frequencies for longitudinal vibrations of bars with different boundary conditions.

Table 16, Natural frequencies for longitudinal vibrations of bars with different boundary conditions (Rao, 2007)

End conditions of the bar	Frequency equation	Natural frequencies of vibration
Case 1: Fixed-attached mass 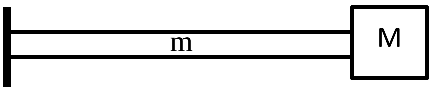	$\alpha \tan(\alpha) = \beta$	$f_n = \frac{1}{2\pi}\frac{\alpha_n C}{l}, n = 1, 2, 3, \ldots$
Case 2: Free-attached mass 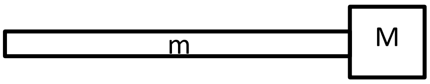	$\tan(\alpha) = -\alpha\beta$	$f_n = \frac{1}{2\pi}\frac{\alpha_n C}{l}, n = 1, 2, 3, \ldots$

In order to calculate the wave speed in the striker assuming $G = 210\ GPa, \rho = 7830\ kg/m^3$ for the striker material, one would obtain $C = \left(\frac{210*10^9}{7830}\right)^{0.5} = 5179\ m/s$.

Table 17 lists the natural frequencies of the drop-weight assembly for different masses assuming end conditions of case 1 and 2 in addition to the frequency impact load (f_{imp}).

Table 17, Natural frequencies of striker-drop-weight assembly according to cases 1 and 2.

Total Mass (kg)	M (kg)	m (kg)	f_{imp}	Case 1-f1 (kHz)	Case 2-f1 (kHz)
6.1	4.70	1.45	0.28	2.9	13.7
8.1	6.70	1.45	0.24	2.5	14.4
11.1	9.70	1.45	0.21	2.1	15.1
14.6	13.20	1.45	0.18	1.8	15.6

It seems that hypothetical fixed-fixed beam can simulate the noise observed. And there is a very high probability of resonance with 11.1-kg and 41.6 kg impactor masses.

7.3 Equilibrium of stresses

One of the major problems in rapid loading of brittle materials such as impact testing is to ensure that stress equilibrium is achieved in the specimen before failure. Figure 59 depicts time-to-failure for the tests on 23/06 and 24/06.

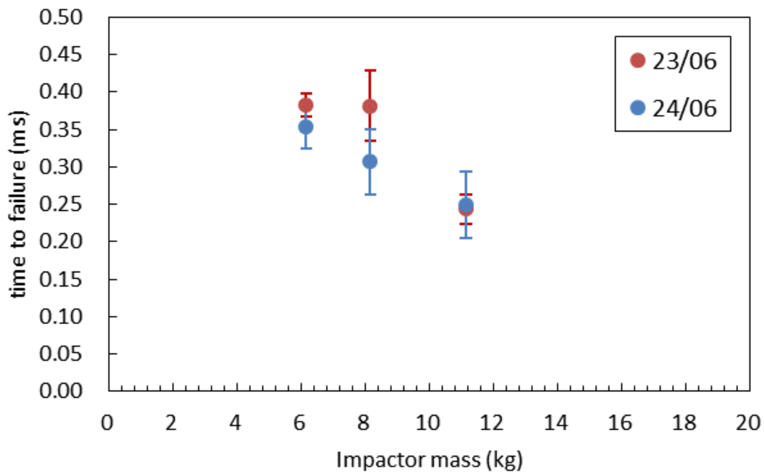

Figure 59, Time-to-failure versus impactor mass for two different levels of impact energy

Stress equilibrium is highly suspected although the mass ratio (μ) requirement of quasi-static analysis (Section 4.1.2) are respected. Mass ratio (μ) ranges from 54 to 130.

Lack of stress equilibrium results in domination of stress wave propagation effects. An apparent strength gain of the material can be observed and explained in terms of large propagating plastic wave fronts in the specimen (Dioh et al., 1995).

After comparing time-to-failure with the characteristic time (2H/C=0.16 ms) of the elastic waves through the specimen, one finds that only one stress wave reverberation has occurred before failure in the best case. The time-to-failure is so short that it does not allow for the build-up of stresses (3 reverberations) in the specimen because it was assumed that the synthetic rock specimen could resist higher stresses with longer time-to-failures according to CEB (1990).

It can be seen that the mass ratio does not seem a sufficient for ensuring stress equilibrium. Referring to literature, failure in the specimen can occur in two ways depending on the impact velocity.

At low impact velocities, the deformation of the specimen is initially elastic, governed by the propagation of elastic waves within the specimen. As subsequent reflections take place, the stress at each point within the specimen increases resulting in failure once strength is exceeded. The initial failure may consequently start at any point in the specimen depending on the magnitude of the loading pulse. At higher impact velocities, and for a loading pulse having a small rise time, the initial stress attained at the front face of the specimen (plastic wave) will exceed the strength thus, creating a non-uniform distribution of stresses (Johnson, 1987).

In order to ensure that the initial stress wave does not exceed the elastic limit, one can use the Young's relation:

$$\frac{v_0}{C} < \varepsilon_Y \qquad or \qquad \rho C v_0 < \sigma_y$$

For a compressive strength (assuming no strain rate dependency) $\sigma_y = 7$ MPa , density $\rho = 1751\, kg/m^3$, $wave\ speed\ C = 507\ \ m/s$, maximum allowable impact velocity is $v_0 = 7.9\, m/s$ without creating plastic wave front upon impact.

It should be noted that the impact velocity should much smaller (to be determined by trial tests) since there is risk of plastic wave fronts after each stress wave reverberations in the specimen.

In addition, reducing height-to-diameter rations (H/D) ratios can ensure sufficient number of reverberations. However, frictional effects should be accounted for.

Finally, it can be concluded that lower impact energy levels with higher impactor masses are necessary to ensure stress equilibrium.

7.4 Frequency response of test system

One of the problems associated with sampled data is the possibility of aliasing, which is due to limited frequency response of system. It affects the apparent load-time record by causing attenuation and extended duration of load-time signal as depicted in Figure 60 . This occurs when the system is not taking enough samples per unit of time (sampling rate) to reflect the true behavior of measured parameter.

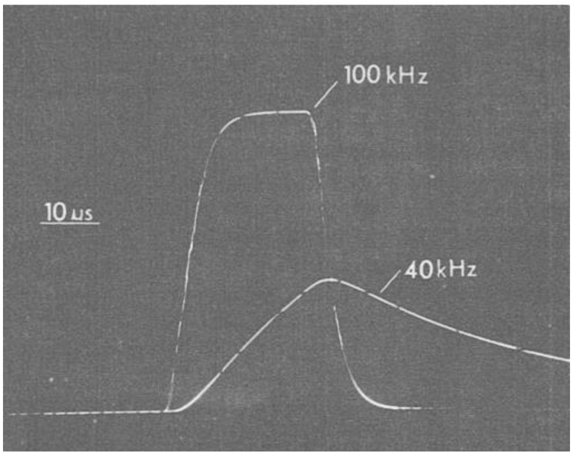

Figure 60, Response of the impact instrumentation to a square wave generator input at system frequency settings of 40 and 100 kHz (Saxton et al., 1974)

To avoid such problems, the Nyquist criterion is applied for accurate definition of the data. Based on this criterion, the sampling rate should be twice the highest frequency present in the data. In practical terms, harmonic content above one half of the sampling frequency should be negligible (Cain, 1986).

For the impact tests, the system has recorded 8181 points per 20 ms (273 points/ms), thus, the sampling frequency is 273 kHz.

As Fourier transforms indicate, the highest frequency content related to impact is approximately 10 kHz which is less than half of the sampling rate (136.5 kHz). Therefore, it can be concluded that the load-time record has not been affected by possible limitations of system frequency response.

Sometimes, it is easier to work with the rise time of a signal instead of frequency. The rise time of a system frequency response is defined as the time necessary for the signal to rise from 10% to 90% of the signal (Ireland, 1974).

$$T_R\ (micros):=\frac{0.35}{273\ kHz}=1.3\ \mu s$$

In terms of rise time, the signal rise time should be at least two times greater than the system rise time. $t_w > 2\ t_r$

Observing the unfiltered time histories of stress, one would find that the smallest rise time is around 33 μs. Thus:

$$33\ \mu s > 2 * 1.3\ \mu s$$

It is noteworthy that the frequency content at 83 kHz comes probably from the limited transducer channel band width or the strain gauge frequency about which no information could be obtained.

7.5 Remarks

It is observed that DIF and stress rates increase with higher impactor masses. At 11.1-kg and 14.6 kg impactor masses, very sharp spikes are present in the stress time histories. This apparent strength gain is doubted to be due to system shortcomings.

The sources of oscillations in stress time-histories were studied. No distortion of stress time-histories as a result of limited frequency response of system can be observed.

Moreover, the impact duration is not sufficiently long for the build-up of stresses and reaching equilibrium. Lack of equilibrium and plastic wave front propagation in the specimen can also increase the impact strength (Dioh et al., 1995).

Short impact durations are imputable to high impact energy owing to overestimation of the strength of synthetic rock strength using CEB (1990). The results obtained in this study can serve as a basis for approximately synthetic rock strength in future experiments.

Finally, it is most probable that the sharp spike in the stress time-histories are due to bending resonances of the test system frame. Thus, stress-strain diagrams are not elaborated further to calculate the dynamic modulus of elasticity of synthetic rock. Further experiments with different impactor masses are needed to confirm this conclusion.

To avoid resonance and increase time-to-failure to reach equilibrium, the following recommendations are made:

1) Use of a material with lower specific impedance (such as aluminum) for the striker head can change the resonant frequency of the test system (Warnet and Reed, 1999). Current steel striker head (tup insert) presents very high rigidity resulting in stress waves of high amplitude distorting the signal. Similar literature confirms problems related to steel strikers (Wu et al., 2015).
2) Use of pulse shaping techniques such as placing a softer material, such as cupper at the interface of specimen and striker head can decrease the excitation frequency on the striker. These techniques are usually used for SHPB test (Li et al., 2009) , some of which can be applied to drop-weight impact tests.
3) Use of instrumented base, which records the stresses in the specimen during impact is an alternative when the striker signals contain too much noise (Radford et al., 2003).

The following modifications are recommended in the design of experiment:

- Using cylindrical specimens to ensure axisymmetric distribution of stresses.
- Improving the compaction procedure for synthetic rock so that the amount of compaction work could be more precise.
- Reducing height-to-diameter rations (H/D) ratios to less than one to ensure sufficient number of reverberations and accounting for frictional effects by use of different types of lubricants on the end faces.
- Use of molds for casting the specimen and using it directly without resorting to cutting operations.
- Use of heavy drop weights 24.2-80.5 kg with lower impactor velocities ($< 2\ m/s$).

Conclusions

Prediction of soil resistance to driving (SRD) is an essential parameter in pile foundation installation. Pile driving in indurated formations involves high strain rates. It is believed that rock strength increases with strain rate. In order to observe and quantify such behavior, an experiment has been designed using a drop-weight test system and a synthetic rock developed at iMMC of UCL.

After reviewing Hoek-Brown failure criterion for modeling mechanical behavior of rocks under quasi-static loading, it became obvious that strain rate sensitivity of its parameters such as uniaxial compressive strength is the basis of any study on the dynamic characterization of rock. For this purpose, it was decided to study the dynamic uniaxial compressive strength of rock.

Experimental techniques for dynamic characterization of materials were reviewed. Drop-weight test systems are not very popular among the researcher due to the difficulties associated with signal-to-noise ratio, inertia and machine resonance. Nevertheless, their instrumented striker renders them very attractive for this study. This instrumented striker can be used for a variety of geometries and materials without even without instrumenting them.

The impact dynamics was studied. A SDOF system was used to predict the impact stresses. CEB (1990) was used to approximate the synthetic rock strength. Optimal mass-velocity combinations were found for reaching failure in the specimen with adequate strain rates. In order to facilitate obtaining mass-velocity combinations, $f_{c,imp} - \dot{\varepsilon}$ diagrams were developed to read the achievable strain rates (thus, velocity and impact energy) and impact strength directly for an arbitrary specimen geometry and dimensions based on CEB (1990). Based on this diagram, a parametric study was used to select the optimal specimen dimensions.

An Instron Dynatup machine (model HV 9250) was modified with a new anvil and striker head to accommodate the selected specimen geometry and dimensions.

A synthetic rock previously formulated at UCL was used in fabricating the specimens. The specimens were tested at an age of 16 ± 1 days. Quasi-static compressive strength tests were performed for comparison with the impact compressive strength. Drop-weight impact tests were performed.

The stress time-histories were highly distorted due to noise. A discrete Fourier Transform was performed to observe the stress time-histories in the frequency domain. A symmetric moving average filter was used to smoothen the observed noise without adversely distorting the signal with respect to the specimen reaction.

A linear relationship between impact strength and stress rate is observed within an interval of 30-80 GP/s. The constitutive model developed is compared with that of CEB 1990. The linear relationship shows far less strain-rate sensitivity of compressive strength of synthetic rock comparing to that of CEB 1990.

However, the observed behavior was suspected since the high DIF’s and stress rates were associated only with 11.1-kg and 14.6-kg impactors. The stress time-histories for these to impactor masses contained very sharp spikes. Besides, the Fourier transform of the signals shows that the noise is easily noticeable with 6.1-kg and 8.1-kg impactor masses while it is less noticeable with higher impactor masses (11.1-kg and 14.6 kg).

As a consequence, the obtained stress time-histories were carefully studied from several perspectives so as to account for various factors, which may lead to false results. These factors include inertial effects, possible limited frequency response of system, system ringing and equilibrium of stresses.

It was concluded that sharp spikes in the stress time-histories are most probably due to bending resonances of the test system frame and the stress equilibrium is not achieved owing to overestimate approximation of synthetic rock strength based on CEB (1990).

Further experiments with different impactor masses are needed to confirm this conclusion. Removing the 11.1-kg and 14.6 kg test results, a dynamic increase factor of approximately 1.3 can be observed for 6.1-kg and 8.1-kg drop weights at an average stress rate of 33 GPa/s.

Finally, some recommendations are made for improving the experiment design to avoid resonance, to ensure equilibrium of stresses and to minimize the experiment errors associated with the fabrication and preparation of specimens.

APPENDIX A

MATLAB script for parametric study of the mechanical model

A.1 Finding failure points

```
%*****************************************************************************
%% Input
%*****************************************************************************
global D H A rho m edot_c0 edot_c f_cm E_c0 theta
theta=pi/3; % Desired failure point
D=0.04; H=0.04; A=D*D; % Area of the cross section
rho=1751; % Density
m=A*H*rho; % Specimen mass
E_c0=449.347e6; % Quasi-static modulus of elasticity
M=[6.146    8.146   11.146  14.646]; % Impactor mass in kg
f_cm=[1,2,4,8,12,15,20]; % specimen quasi-static compressive strength in MPa
alpha_s=1./(5+9.*f_cm./10); gamma_s=10.^(6.156.*alpha_s-2); % fib model code 1990
parameters
edot_c=30e-6;% Quasi-static strain rate

%*****************************************************************************
%% Using fsolve to find failure points
%*****************************************************************************
for k=1:length(f_cm)
    for i=1:length(M)
        myfun1 = @(v0)
[(cos(theta).*(v0./H)./edot_c0).^(1.026.*alpha_s(k)).*f_cm(k).*10^6.*A-
M(i).*v0*sin(theta).*(A.*E_c0./(H.*M(i))*(cos(theta).*v0./(H.*edot_c0)).^0.026).^0.
5];
        x0 = [0; 100];
        x1(:,i) = fsolve(myfun1,x0);v1(i,k)=max(x1(:,i));
        x0 = [0; 100];
        myfun2 = @(v0)
[gamma_s(k).*(cos(theta).*(v0./H)./edot_c0).^(1/3).*f_cm(k).*10^6.*A-
M(i).*v0*sin(theta).*(A.*E_c0./(H.*M(i))*(cos(theta).*v0./(H.*edot_c0)).^0.026).^0.
5];
        x2(:,i)= fsolve(myfun2,x0);v2(i,k)=max(x2(:,i));
            if cos(theta).*v1(i,k)/H<=30
                v0(i,k)=v1(i,k);
            else
                v0(i,k)=v2(i,k);
```

```
            end
        ep_dot(i,k)=v0(i,k)/H*cos(theta); % strain rate in s^-1

omega(i,k)=(A.*E_c0./(H.*M(i))*(cos(theta).*v0(i,k)./(H.*edot_c0)).^0.026).^0.5;%
Natural frequency of SDOF sytem in rad/s
sigma(i,k)=sin(theta)*M(i).*v0(i,k).*omega(i,k)./A/10^6;% Impact Strength in MPa
E0_incident(i,k)=1/2*M(i)*v0(i,k)^2; % Incident impact energy in J
E0_absorbed(i,k)=1/2*M(i)*v0(i,k)^2-1/2*M(i)*(v0(i,k)*cos(theta))^2;% Absorbed
impact energy J
E0_incident_s(i,k)=E0_incident(i,k)/(A*H)/10^3; % specific incident energy kJ/m3
E0_absorbed_s(i,k)=E0_absorbed(i,k)/(A*H)/10^3; % Modulous of toughness in kJ/m3
    end
plot(ep_dot(:,k),sigma(:,k),'o-','markersize',5) % plotting impact strength (MPa)
against strain rate (s^-1)
str = {'fcm = ' num2str(f_cm(k)) 'MPa'}; % labeling each curve with quasi-static
strength
    text(ep_dot(length(M),k), sigma(length(M),k),['fcm = ' num2str(f_cm(k))
'MPa'],'horizontalAlignment', 'left','fontsize',8);
    mylegend{k} = ['fcm = ' num2str(f_cm(k)) ' MPa' num2str(D) 'x' num2str(H)]; %
    xlabel('Strain Rate (s^{-1})')
    ylabel('Impact Strength (MPa)')
    hold on
    grid on
    grid minor
    axis([1 100 0 50])
end

%*****************************************************************************
%% Annotations
%*****************************************************************************

dim = [0.59 0.6 .3 .3];
str=['\sigma/\sigma_{max}=' num2str(sin(theta),'%.2f')];
annotation('textbox',dim,'String',str,'FitBoxToText','on');
legend(mylegend,'location','eastoutside')

%*****************************************************************************
%% Output
%*****************************************************************************
Impact_velocity=v0;
Impact_Energy= E0_incident;
Strain_rate=ep_dot;
Impact_strength=sigma;
Absorbed_Energy=E0_absorbed;

output=[Impact_Energy,Absorbed_Energy,Impact_velocity,Strain_rate,Impact_strength,
omega/(2*pi*1000)]
```

A.2 Plotting σ_{imp}–$\dot{\varepsilon}$ curves for different M*H/A.

```
%*****************************************************************************
%% Input
%*****************************************************************************

    mass=[.01,.1,.3,.6,1.1,2.1,3.2,6,10,15,20,30,40,60,100]; % Impactor masses (M)
    velocity=.01:50; % Desired range of impactor Velocity
    st=cos(theta)*velocity'/H; % Desired range of strain rates


%*****************************************************************************
%% Plotting stress strain-rate curves for different M*H/A.
%*****************************************************************************
    for kk=1:length(mass)
        for ii=1:length(velocity)
```

```
omega_c(ii,kk)=(A.*E_c0./(H.*mass(kk))*(cos(theta).*velocity(ii)./(H.*edot_c0)).^0.
026).^0.5;% Natural frequency of SDOF system in rad/s
        sigma_c(ii,kk)=sin(theta)*mass(kk).*velocity(ii).*omega_c(ii,kk)./A/10^6; %
Stress in the specimen in MPa
        end
    end
        plot(st,sigma_c,'k--')

%************************************************************************
%% Labeling each stress strain-rate curve with its M*H/A
%************************************************************************

for kk=1:length(mass)
        myfun3 = @(x)
[sin(theta)*mass(kk).*x.*H/cos(theta).*(A.*E_c0./(H.*mass(kk))*(x./(edot_c0)).^0.02
6).^0.5./A/10^6+50/100.*(x-100)];
        x0 = [0; 200];
        % Finding the intersection of stress strain-rate curve with an arbitary
linear line y=50/100.*(x-100)in order to place labels.
        % This line is selected base on axis values.
        st_text(:,kk) = fsolve(myfun3,x0); % x-coordinate of label
        sigma_text(kk)=-50/100.*(st_text(1,kk)-100)% y-coordinate of label
        str=['M*H/A= ' num2str(mass(kk)*H/A,'%.1f') ' kg*m/m^{2}']; % label
description
        h1(kk)=text(st_text(1,kk),sigma_text(kk),str,'horizontalAlignment',
'right','verticalAlignment', 'bottom','fontsize',8);
        slope(kk)=atan(sigma_text(kk)/st_text(1,kk))*180/(pi); % labe rotation
        set(h1(kk),'Rotation',slope(kk));
    end
```

APPENDIX B

MATLAB script written for analyzing data from Instron IMPULSE software

B.1 Data Management

Each test sheet was renamed according to the following dating format:

"Date23_06Mass6_3266Velocity4_0000Specimen22"

This format includes the recorded test date, impactor mass, impactor velocity and specimen ID. Then, each test sheet obtained through IMPULSE software was imported into MATLAB as a numeric matrix.
The matrix "mydata" contains individual test matrices placed side by side. Each matrix is a actually a test lot that is obtained under similar test parameters such as impact velocity and mass. Each test matrix contains seven columns each representing a measured or calculated parameter obtained through IMPULSE software.

Col1	Col2	Col3	Col4	Col5	Col6	Col7
Index	Time	Raw Data A/D Counts	Load	Energy	Velocity	Deflection

```
%% Input ****************************************************************************

mydata= [Date23_06Mass6_3266Velocity4_0000Specimen22, Date23_06Mass6_3266Velocity4_0000Specimen33,
Date23_06Mass6_3266Velocity4_0000Specimen41, Date23_06Mass6_3266Velocity4_0000Specimen53];
M=6.146; V=4; Area= [1649.21 1715.00 1706.48 1715.00];
```

```
*************************************************************************
```

B.2 Calling test lots and colums of numeric matrices from the global test results matrix

A for-loop is used for calling each test lot from the global test results matrix. The time, force, etc arrays are extracted from numeric matrix of each individual test.

```
%% Calling and plotting each test lot from the global test results matrix
% Secondary parameters are calculated by Instron IMPACT software.
%*****************************************************************%

[m,n]=size(mydata);
time=zeros(m,n/7);force=zeros(m,n/7);stress=zeros(m,n/7);
velocity=zeros(m,n/7);deflection=zeros(m,n/7);energy=zeros(m,n/7);

for ii=1:n/7;
    data=mydata(:,(1+(ii-1)*7:7+(ii-1)*7)); % Extracting extracting each test
    lot from the global matrix
    time(:,ii)=data(:,2); % Calling time array
    force(:,ii)=data(:,4); % Calling force array
    stress(:,ii)=data(:,4)./Area(ii)*1000; % Calling stress array
    energy(:,ii)=data(:,5); % Calling absorbed energy array
    velocity(:,ii)=data(:,6); % Calling tup velocity array
    deflection(:,ii)=data(:,7); % Calling specimen deflection

end
```

B.3 Fourier Transform

The following script was written in order to obtain frquency spectrum of load time history.

```
%%FFT*************************************************************************

 [m,n]=size(mydata);

 for ii=1:n/7;

 data=mydata(:,[1+(ii-1)*7:7+(ii-1)*7]);

 L(ii)=length(data);
 Y(:,ii) = fft(data(:,4)./Area(ii)*1000);
 P2 = abs(Y(:,ii)/L(ii));
 P1 = P2(1:L/2+1);
 P1(2:end-1) = 2*P1(2:end-1);

 Duration(ii)=data(end,2)-data(1,2); % time step
 Fs(ii)=(L(ii)-1)/(Duration(ii)); %sampling_frequency
 f = Fs(ii)*(0:(L(ii)/2))/L(ii);

 plot(f,P1)
 title(' Frequency Spectrum of Load Time History')
 xlabel('frequency (kHz)')
 ylabel('|\sigma|(MPa)')
 hold on

 end
%%*********************************************************************
```

The written script was used to transform a known time domain signal in to frequency domain. The signal was created by a function:

$$y(t) = 2 * \sin(t) + \sin(10 * t)$$

Where

y: Amplitude in MPa

t: Time in milliseconds

Figure 61 depicts a time domain representation of this signal. It contains a low and a high frequency.

The function contains two frequencies at:

$$f_1 = \frac{1}{2\pi} = 0.16\ kHz, \qquad f_2 = \frac{10}{2\pi} = 1.6\ kHz$$

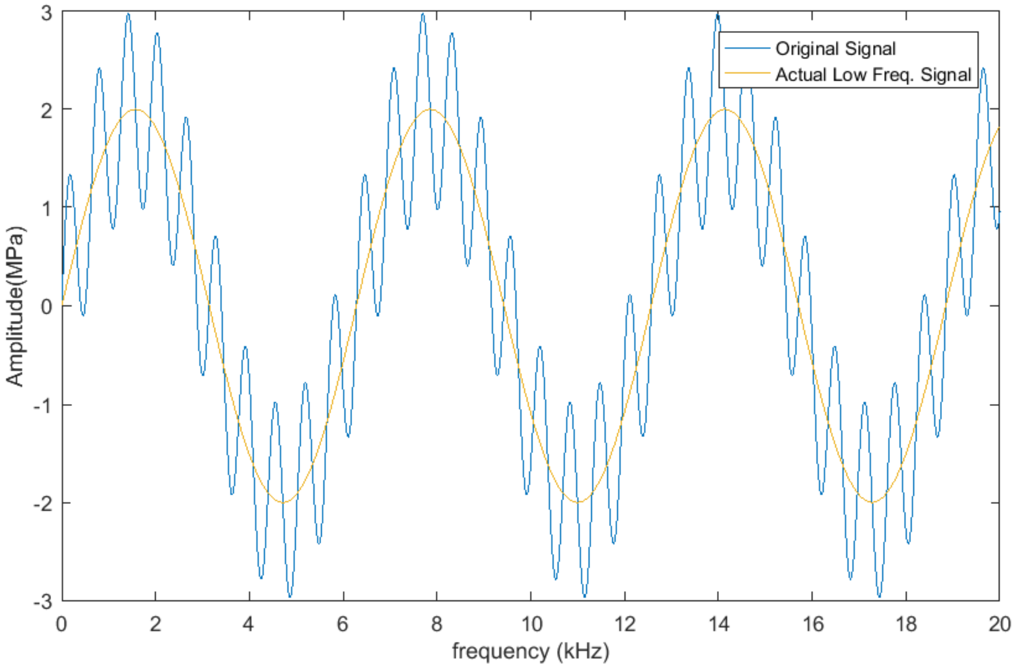

Figure 61, Time domain representation

Figure 62 is the frequency representation of this signal. It clearly displays the frequency content of the signal.

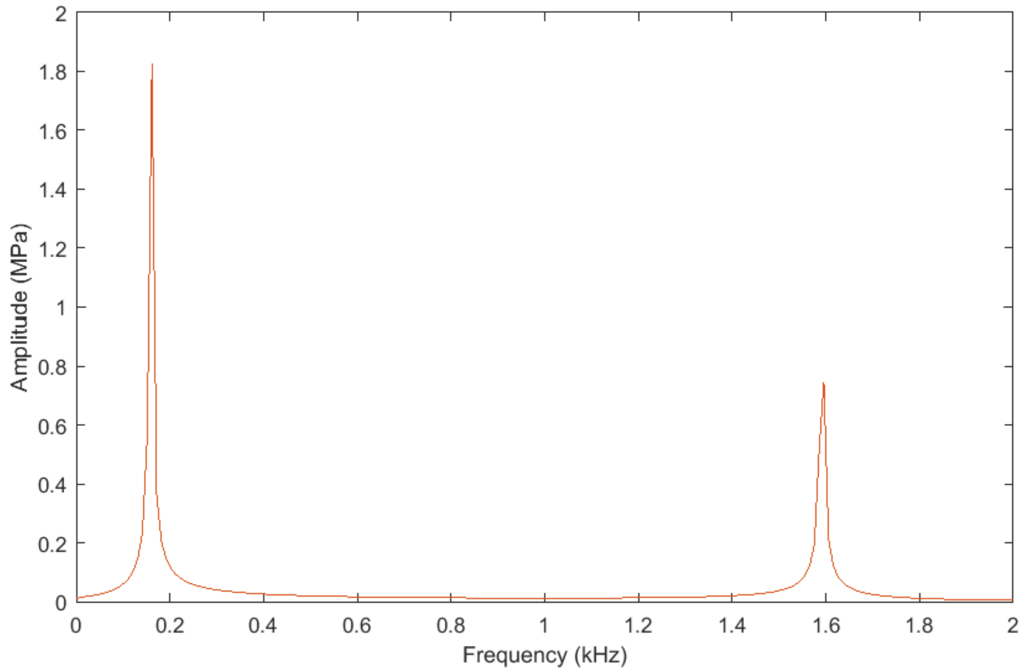

Figure 62, Frequency representation

B.4 Moving Average Filter Design

A centered moving average filter was used to remove the noise (high frequency content) at 1.6 kHz in the previous section. The only concern is the loss of information for period equal to half of the noise period, which is short enough to be extrapolated graphically.

The filtered curve matches very well with the original low content frequency.

```
%% Enter Parameters ****************************************************************
f_noise=1.6; % Noise Frequency in kHz


%% Calling and plotting each test lot from the global test matrix
******************************************************************

%% Moving Average Filter Design and Plot
******************************************************************

T_noise=1/f_noise; % Noise period in ms
t_step=time(2,1)-time(1,1); %sampling_time_step
N=T_noise/t_step; %Number of points used for moving average
N_odd=ceil((N+1)/2)*2-1; % Rounding the number of points to the next odd number
NN=(N_odd-1)/2; % Number of points on each side of centered moving average
[row,col]=find(time==0); % Finds the index number for t=0
force_smooth=zeros(m,n/7); % Preallocating for smoothes force matrix
stress_smooth=zeros(m,n/7);


 for kk=(NN+1):(length(force)-NN-1);
  force_smooth(kk,:)=mean((force((kk-NN:kk+NN),:)));
```

```
 stress_smooth(kk,:)=mean((stress((kk-NN:kk+NN),:)));
end
plot(time,force_smooth);
```

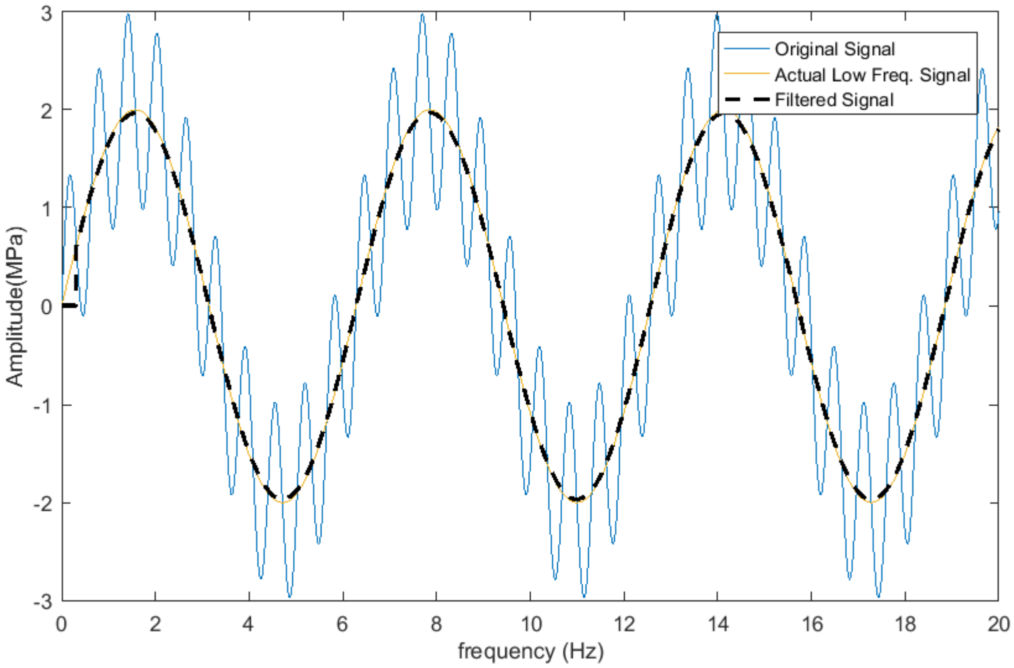

Figure 63, Filtering high frequency content

B.5 Plotting the elastic curve

```
%% Plotting the elastic curve
%*****************************************************************%
E=341e6; L=.04;A=.04*.04;
f=1/(2*pi)*(E*A./(L*M))^.5 % Hz
t_e=0:.001:(1/f*1000); V=velocity(1:1)
F_e=1/1000*M*V*2*pi*f*sin(2*pi*f*t_e/1000);
```

B.6 Synchronization of curves

The force time history curves are synchronized at a force value of y_syn=3 kN which is large enough to eliminate the initial peak and prolonged section.

```
%% Synchronization, Identifying peak force, time, velocity and deflection at
failure
y_sync=3;
force_peak=max(force_smooth); stress_peak=max(stress_smooth);
A=zeros(1,length(force_peak)); v_failure=zeros(1,length(force_peak));
t_new=zeros(m,n/7);
[row,col]=find(time==0); % Finding the index for t=0

for mm=1:length(force_peak)
[c0(mm) indice0(mm)]=min(abs((force_smooth(:,mm)-force_peak(mm)))); % finding the
index for peak force
[c1(mm) indice1(mm)]=min(abs((force_smooth(row(mm):indice0(mm),mm)-y_sync))); %
finding the index for synchronization force

v_failure(mm)=velocity(indice0(mm),mm);
t_failure(mm)=time(indice0(mm),mm)-time(indice1(mm)+row(mm),mm);
d_failure(mm)=deflection(indice0(mm),mm)-deflection(indice1(mm)+row(mm),mm);
e_failure(mm)=energy(indice0(mm),mm);
```

```
t_new(:,mm)=time(:,mm)-time(indice1(mm)+row(mm),mm);
d_new(:,mm)=deflection(:,mm)-deflection(indice1(mm)+row(mm),mm);

end

% Plot desired curves,

plot(t_new,stress_smooth);

% plot(d_new,stress_smooth);
```

B.7 Plotting trends and shifting synchronized time history curves

The curves which are synchronized at y_sync are superimposed in order to plot their trend. These synchronized curves are then shifted a distance t_shift and d_shift on the x-axis. This distance represents the intersection of x-axis with a secant on the smoothed curves passing through y_sync and y_slope. The objective is to remove the initial curvilinear section of curves.

```
%*****************************************************************%
%% Plotting the trend curve
%*****************************************************************%
force_mean=zeros(length(force),1);force_sdt=zeros(length(force),1);
[row,col]=find(time==0); % Finds the index number for t=0
indice_new=row'+indice1; % Refer to section 6 for indice1
[a,b]=max(indice_new);
x=zeros(1,n/7);y=zeros(1,n/7);z=zeros(1,n/7);
for gg=1:(length(force)-a+200)
    for ff=1:n/7
        x(ff)=force_smooth(indice_new(ff)-1-200+gg,ff);
        y(ff)=velocity(indice_new(ff)-1-200+gg,ff);
        z(ff)=deflection(indice_new(ff)-1-200+gg,ff);
        w(ff)=stress_smooth(indice_new(ff)-1-200+gg,ff);
    end
        force_mean(gg+a-200,1)=mean(x);
        force_sdt(gg+a-200,1)=std(x,0);
        velocity_mean(gg+a-200,1)=mean(y);
        deflection_mean(gg+a-200,1)=mean(z);
        stress_mean(gg+a-200,1)=mean(w);

end

% Plot desired curves: force_mean, stress_mean, etc.

plot((t_new(:,b),stress_mean,'--k','linewidth',1);



%*****************************************************************%
%% Shifting the synchronized curves
%*****************************************************************%
y_slope=4;
[c2, indice2]=min(abs((force_mean(row(b):indice0(b))-y_slope)));
t_shift=(time(indice2,b)-time(indice1(b),b))*y_sync/(y_slope-y_sync);
d_shift=(deflection(indice2+row(b),b)-
deflection(indice1(b)+row(b),b))*y_sync/(y_slope-y_sync);

% Shifting and plotting synchronized curves: force_mean, stress_mean, etc.

% Plot desired curves

plot(t_new+t_shift,stress_smooth);
```

B.8 Calculating stress rate, strain rate, plotting stress-strain diagrams and the rectilinear section of stress time history.

The linear section of the curves lies mostly between 30-80% of the peak. Thefore, the slope of secant between these to points is used for calculating stress rate. In order to verify the behavior of curve, it is also plotted in this interval (t_slope).

```
%*****************************************************************%
 %% Stress Rate
%*****************************************************************%
t_slope=zeros(m,n/7);
t_interval=zeros(1,length(force_peak)); F_interval=zeros(1,length(force_peak));
for hh=1:length(force_peak)
[C0(hh) DD(hh)]=min(abs((force_smooth(:,hh)-force_peak(hh))));
[C1(hh) index1(hh)]=min(abs((force_smooth([row(hh):DD(hh)],hh)-
.3*force_peak(hh)))); % finding the index for 30% of peak
[C2(hh) index2(hh)]=min(abs(force_smooth([row(hh):DD(hh)],hh)-.80*force_peak(hh)));
% find the index for 80% of the peak
t_interval(hh)=time(index2(hh)+row(hh),hh)-time(index1(hh)+row(hh),hh); % time
interval between 30-80 of peak force
F_interval(hh)=force_smooth(index2(hh)+row(hh),hh)-
force_smooth(index1(hh)+row(hh),hh); % force interval between 30-80% of peak force
stress_interval(hh)=stress_smooth(index2(hh)+row(hh),hh)-
stress_smooth(index1(hh)+row(hh),hh); % stress interval between 30-80% of peak
force
d_interval(hh)=deflection(index2(hh)+row(hh),hh)-deflection(index1(hh)+row(hh),hh);
% Displacement interval between 30-80% of peak force
H_specimen(hh)=39.53-deflection(indice1(hh)+row(hh),hh)+d_shift; % Corrected
specimen height after removing the displacement up to y_sync
strain_interval(hh)=d_interval(hh)/H_specimen(hh)
t_slope(:,hh)=time(:,hh)-time(index1(hh)+row(hh),hh);% time interval between 30-80%
of peak force
I_s(hh)=row(hh)+index1(hh); I_e(hh)=row(hh)+index2(hh);
% plot(t_slope([I_s(hh):I_e(hh)],hh),force_smooth([I_s(hh):I_e(hh)],hh)); %
plotting the secant at 30-80% of peak.

plot((d_new(:,hh)+d_shift)/H_specimen(hh),stress_smooth(:,hh))% plotting stress-
strain diagram
 hold on
end

% plot((d_new(:,b)+d_shift)/39.53,stress_mean,'--k','linewidth',1);


force_rate=F_interval./t_interval; % MN/s - kN/ms
stress_rate=stress_interval./t_interval; % GPa/s - kPa/ms
E_modulus=stress_interval./strain_interval*10^-3; % GPa
cal_strain_rate=stress_rate*10^9/(449.347e6); % calculated strain rate assuming a
constant modulus of elasticity.
strain_rate=v_failure./(H_specimen/1000);% calculating strain rate at failure
```

B.9 Calculating stress rate, strain rate, plotting stress-strain diagrams and the rectilinear section of stress time history.

Failure is defined as the point when maximum stress is reached.

```
%*****************************************************************%
%% Identifying peak force, time, velocity and deflection at failure
%*****************************************************************%


for mm=1:length(force_peak)
```

```
v_failure(mm)=velocity(indice0(mm),mm);
t_failure(mm)=(time(indice0(mm),mm)-time(indice1(mm)+row(mm),mm))+t_shift; % Refer
to section 6 and 7
d_failure(mm)=(deflection(indice0(mm),mm)-
deflection(indice1(mm)+row(mm),mm))+d_shift; % Displacement at failure, refer to
section 6 and 7
e_failure(mm)=energy(indice0(mm),mm); % Energy at failure, refer to section 6 and 7

end
```

APPENDIX C

Drawings for INSTRON Dynatup Modifications

C1 - Striker head (tup insert) details

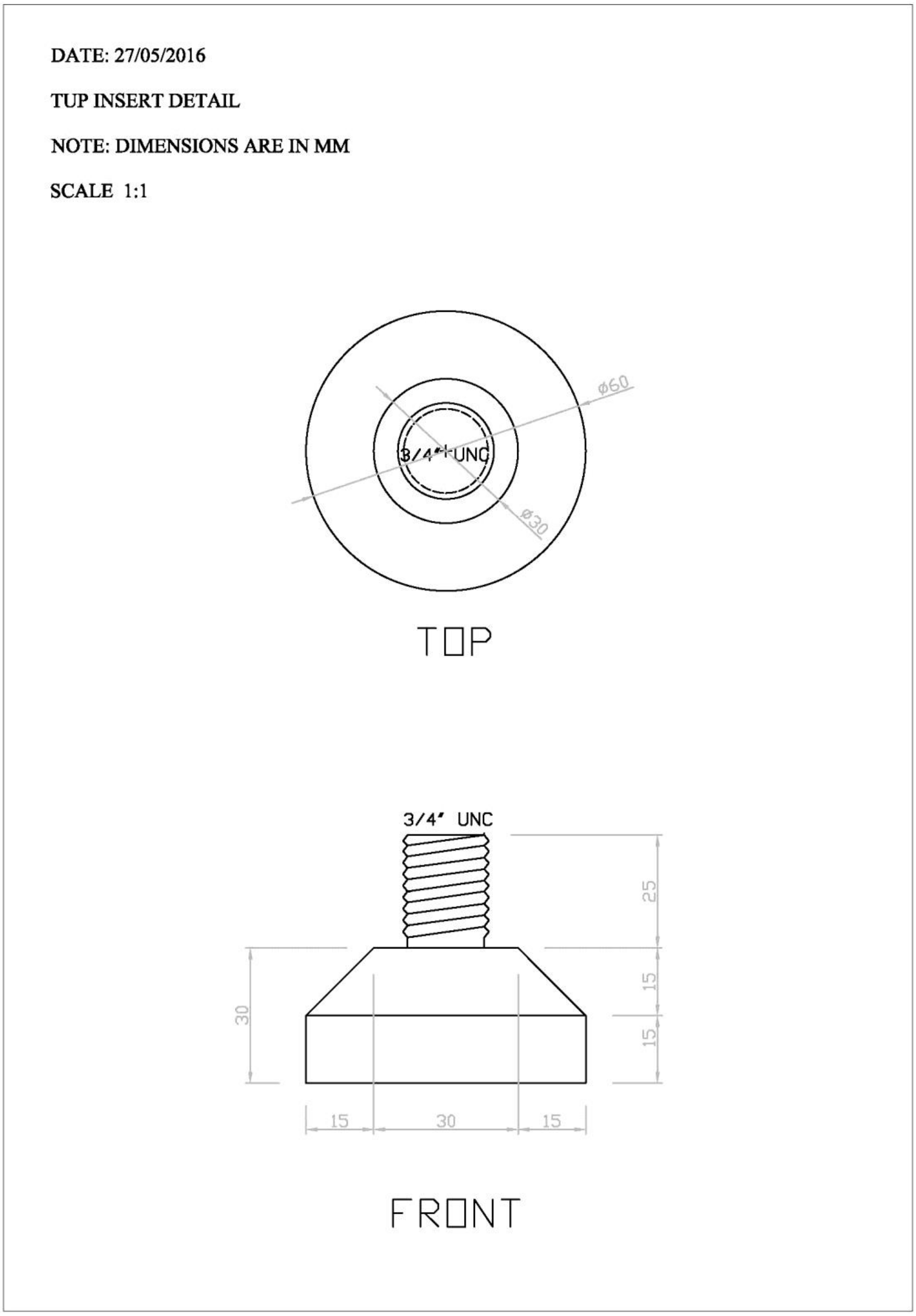

C2 - Machine base details

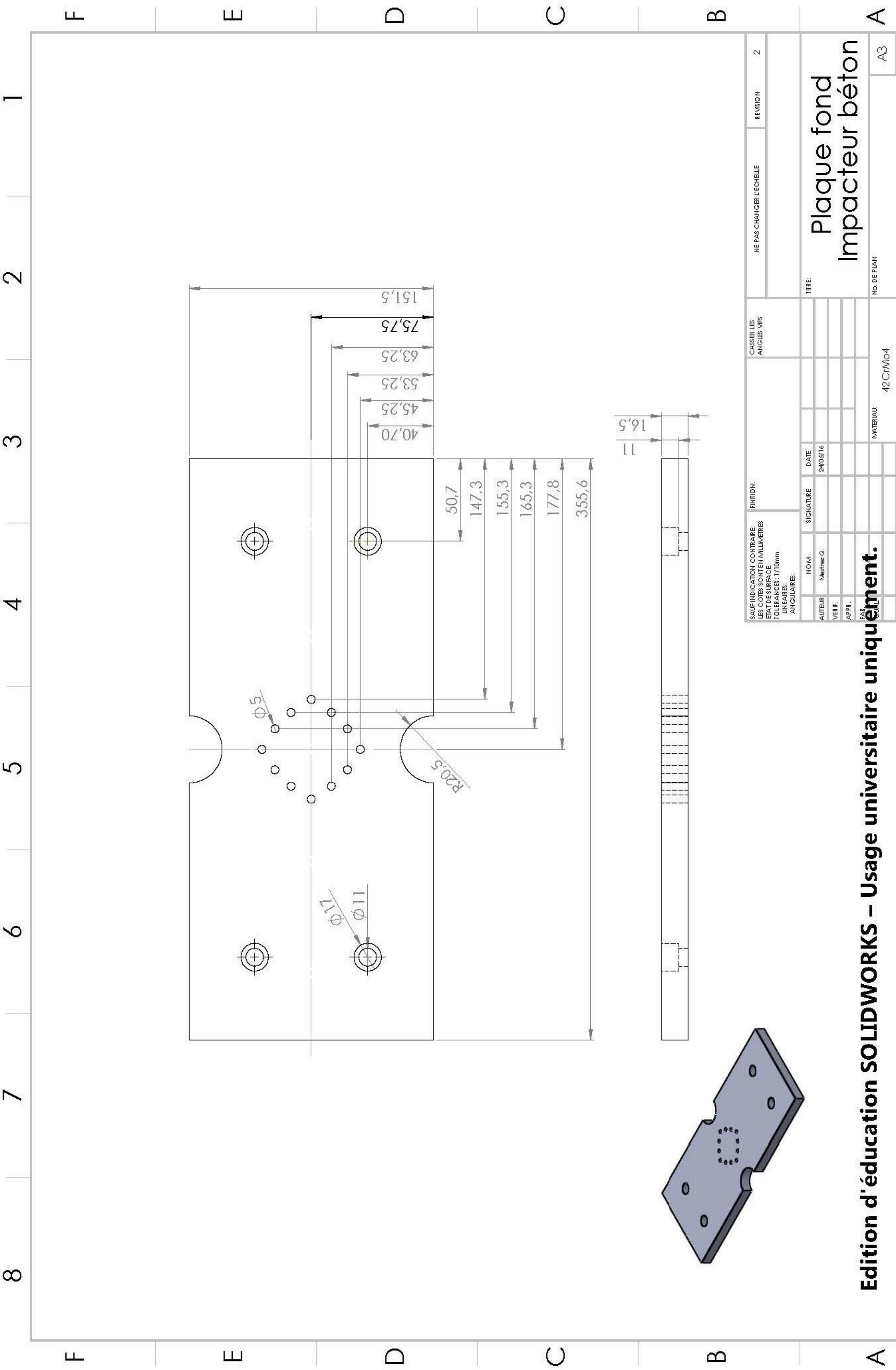

APPENDIX D

Tests Description :	Quasi-static compressive strength of synthetic rock
Specimen Age	16 days
Casting Date:	7/06/2016
Test Date	23/06/2016
Force Rate	70 N/S
Technician	Quentin Mestrez
Tested by:	Mustafa Jafari
Machine Name	Zwick 250 kN
Calibration Date	Unavailable

SP #	F_{max}	*Area (mm2)*	*UCS (MPa)*	δ *(mm)*	$\epsilon(\%)$[13]	*E(MPa)*	$MT(kJ/m^3)$
11	11.32	1706.5	6.6	0.62	1.57	523.6	59.46
52	11.37	1649.2	6.9	0.82	2.08	421.4	85.97
53	11.47	1715.0	6.7	0.70	1.77	419.7	63.81
91	12.55	1706.5	7.4	0.75	1.9	432.7	83.08
Average	11.68	1694.3	6.9	0.72	1.83	449.3	73.1
SD	0.59	30.3	0.33	0.08	0.21	50	13
SD/Avg %	5.0	1.8	4.8	11.6	11.75	11.1	18.3

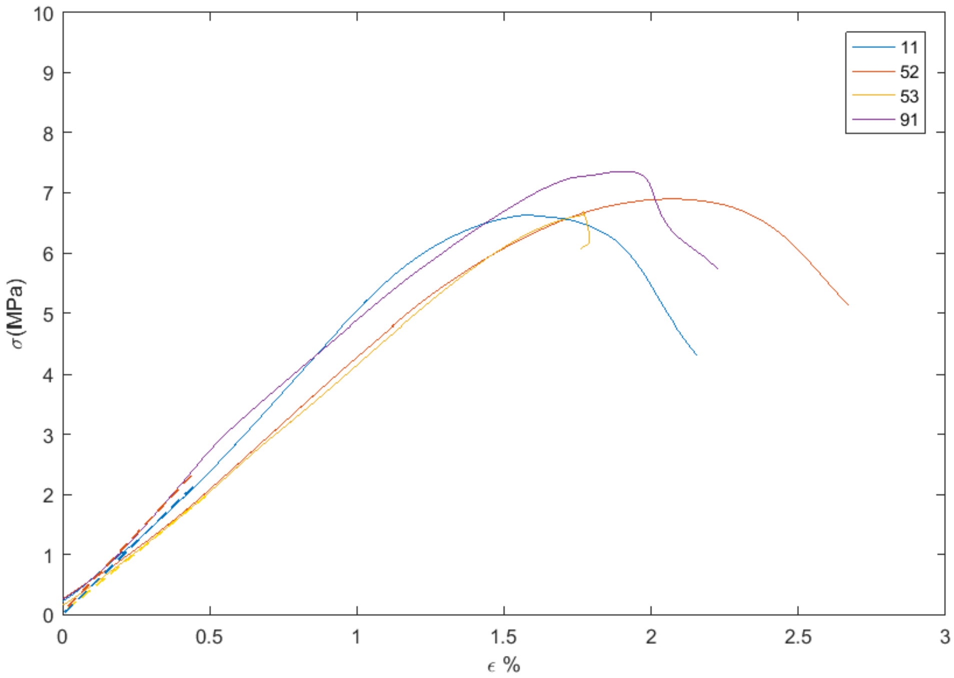

[13] The average height of the specimen is 39.53 mm.

Specimen No.	Failure Pattern
11	
52	
53	
91	

APPENDIX E

References

Aldridge, T.R., Carrington, T.M., Jardine, R.J., Little, R., Evans, T.G., Finnie, I., 2010. BP Clair phase 1–Pile driveability and capacity in extremely hard till. Frontiers in Offshore Geotechnics II 477.

ASTM C109 / C109M - 16a Standard Test Method for Compressive Strength of Hydraulic Cement Mortars (Using 2-in. or [50-mm] Cube Specimens) [WWW Document], n.d. URL http://www.astm.org/Standards/C109 (accessed 7.6.16).

Aymerich, F., Marcialis, P., Meili, S., Priolo, P., 1970. An instrumented drop-weight machine for low-velocity impact testing. WIT Transactions on The Built Environment 25.

Balachandran, B., Magrab, E.B., 2008. Vibrations. Cengage Learning.

Beer, F., 2016. Statics and mechanics of materials. McGraw-Hill Higher Education.

Board, T.R., 2011. Structural Integrity of Offshore Wind Turbines: Oversight of Design, Fabrication, and Installation. Transportation Research Board, Washington, D.C.

Cain, P.J., 1986. Digital filtering of impact data, in: Instrumented Impact Testing of Plastics and Composite Materials. ASTM International.

Cho, S.H., Ogata, Y., Kaneko, K., 2003. Strain-rate dependency of the dynamic tensile strength of rock. International Journal of Rock Mechanics and Mining Sciences 40, 763–777. doi:10.1016/S1365-1609(03)00072-8

CEB, F.M., 1990. CEB-FIB Model Code 1990 Design Code. Bulletin d'Information 195.

Cotsovos, D.M., Pavlović, M.N., 2008. Numerical investigation of concrete subjected to compressive impact loading. Part 1: A fundamental explanation for the apparent strength gain at high loading rates. Computers & Structures 86, 145–163. doi:10.1016/j.compstruc.2007.05.014

Dioh, N.N., Ivankovic, A., Leevers, P.S., Williams, J.G., 1995. Stress wave propagation effects in split Hopkinson pressure bar tests, in: Proceedings of the Royal Society of London A: Mathematical, Physical and Engineering Sciences. The Royal Society, pp. 187–204.

Field, J.E., Walley, S.M., Proud, W.G., Goldrein, H.T., Siviour, C.R., 2004. Review of experimental techniques for high rate deformation and shock studies. International Journal of Impact Engineering, Fifth International Symposium on Impact Engineering 30, 725–775. doi:10.1016/j.ijimpeng.2004.03.005

Grote, D.L., Park, S.W., Zhou, M., 2001. Dynamic behavior of concrete at high strain rates and pressures: I. experimental characterization. International Journal of Impact Engineering 25, 869–886.

Hamdi, S., others, 2016. Pipe pile driving into rock. UCL.

Harris, C.M., Piersol, A.G., 2002. Harris' shock and vibration handbook. McGraw-Hill New York.

Hoek, E., Carranza-Torres, C., Corkum, B., 2002. Hoek-Brown failure criterion-2002 edition. Proceedings of NARMS-Tac 1, 267–273.

Ireland, D., 1974. Procedures and Problems Associated with Reliable Control of the Instrumented Impact Test, in: DeSisto, T. (Ed.), Instrumented Impact Testing. ASTM International, 100 Barr Harbor Drive, PO Box C700, West Conshohocken, PA 19428-2959, pp. 3-3–27.

Johnson, K.L., 1987. Contact Mechanics, Reprint. ed. Cambridge University Press, Cambridge Cambridgeshire; New York.

joo Kim, D., Sirijaroonchai, K., El-Tawil, S., Naaman, A.E., 2010. Numerical simulation of the Split Hopkinson Pressure Bar test technique for concrete under compression. International Journal of Impact Engineering 37, 141–149. doi:10.1016/j.ijimpeng.2009.06.012

Jr, W., Timoshenko, S.P., Young, D.H., 1990. Vibration Problems in Engineering. John Wiley & Sons.

Kelly, S.G., 2012. Mechanical vibrations: theory and applications. Cengage Learning.

Kessler, M.R., 2004. Advanced Topics in Characterization of Composites. Trafford Publishing.

Lajtai, E.Z., Duncan, E.J.S., Carter, B.J., 1991. The effect of strain rate on rock strength. Rock Mech Rock Engng 24, 99–109. doi:10.1007/BF01032501

Li, X.B., Zhou, Z.L., Hong, L., Yin, T.B., 2009. Large diameter SHPB tests with a special shaped striker. ISRM News J 12, 76–79.

Meyers, M.A., 1994. Dynamic Behavior of Materials. John Wiley & Sons.

Plaxis manual, P., 2015. Plaxis Material Models and Plaxis Reference Manuals. The Netherlands.

Radford, D.D., Walley, S.M., Church, P., Field, J.E., 2003. Dynamic upsetting and failure of metal cylinders: Experiments and analysis. Journal de Physique IV - Proceedings 110, 6. doi:10.1051/jp4:20020704

Ramesh, K.T., 2008. High Rates and Impact Experiments, in: Sharpe, W.N. (Ed.), Springer Handbook of Experimental Solid Mechanics. Springer US, Boston, MA, pp. 929–960.

Rao, S.S., 2007. Vibration of Continuous Systems. John Wiley & Sons.

Reid, S.R., Zhou, G., 2000. Impact Behaviour of Fibre-reinforced Composite Materials and Structures. CRC Press.

Saxton, H.J., Ireland, D.R., Server, W.L., 1974. Analysis and control of inertial effects during instrumented impact testing, in: Instrumented Impact Testing. ASTM International.

Swallowe, G.M., Lee, S.F., 2003. A study of the mechanical properties of PMMA and PS at strain rates of 10-4 to 103 over the temperature range 293–363 K. Journal de Physique IV - Proceedings 110, 6. doi:10.1051/jp4:20020666

Warnet, L., Reed, P.E., 1999. Falling Weight Impact Testing Principles, in: Mechanical Properties and Testing of Polymers. Springer, pp. 66–70.

Wu, M., Chen, Z., Zhang, C., 2015. Determining the impact behavior of concrete beams through experimental testing and meso-scale simulation: I. Drop-weight tests. Engineering Fracture Mechanics 135, 94–112.